

Force-extension of the Amylose Polysaccharide

by

Rudolf van den Berg

A dissertation submitted to the
University of Cape Town
in fulfilment of the requirements for the degree of
Master of Science

M.Sc. Information Technology
Department of Computer Science

December 2009

I know the meaning of plagiarism and declare that all of the work in the document, save for that which is properly acknowledged, is my own.

Abstract

Atomic Force Microscopy (AFM) single-molecule stretching experiments have been used in a number of studies to characterise the elasticity of single polysaccharide molecules. Steered molecular dynamics (SMD) simulations can reproduce the force-extension behaviour of polysaccharides, while allowing for investigation of the molecular mechanisms behind the macroscopic behaviour. Various stretching experiments on single amylose molecules, using AFM combined with SMD simulations have shown that the molecular elasticity in saccharides is a function of both rotational motion about the glycosidic bonds and the flexibility of individual sugar rings. This study investigates the molecular mechanisms that determine the elastic properties exhibited by amylose when subjected to deformations with the use of constant force SMD simulations. Amylose is a linear polysaccharide of glucose linked mainly by $\alpha(1\rightarrow4)$ bonds. The elastic properties of amylose are explored by investigating the effect of both stretching speed and strand length on the force-extension profile. On the basis of this work, we confirm that the elastic behaviour of amylose is governed by the mechanics of the pyranose rings and their force-induced conformational transitions. The molecular mechanism can be explained by a combination of *syn* and *anti*-parallel conformations of the dihedral angles and chair-to-boat transitional changes. Almost half the chair-to-boat transitional changes of the pyranose rings occur in quick succession in the first part of the force-extension profile (cooperatively) and then the rest follow later (anti-cooperatively) at higher forces, with a much greater interval between them. At low forces, the stretching profile is characterised by the transition of the dihedral angles to the *anti*-conformation, with low elasticities measured for all the chain lengths. Chair-to-boat transitional changes of the pyranose rings of the shorter chains only occurred anti-cooperatively at high stretching forces, whereas much lower forces were recorded for the same conformational change in the longer chains. For the shorter chains most of these conversions produced the characteristic "shoulder" in the amylose stretching curve. Faster ramping rates were found to increase the force required to reach a particular extension of an amylose fragment. The transitions were similar in shape, but occur at lower forces, proving that decreasing the ramping rate lowers the expected force. The mechanism was also essentially the same, with very little change between the simulations. Simulations performed with slower ramping rates were found to be adequate for reproduction of the experimental curve.

List of Abbreviations

AFM	Atomic Force Microscopy
CHARMM	Chemistry at Harvard Macromolecular Mechanics
FF	Force Field
MD	Molecular Dynamics
NAMD2	Name of Molecular Dynamics Code
VMD	Visual Molecular Dynamics
SMD	Steered Molecular Dynamics
Fs	femtosecond
ps	picosecond
ns	nanosecond
pN	piconewtons

Contents

1. Introduction	1
1.1. Objectives.....	2
1.2. Thesis Overview.....	3
2. Background and Related Work	4
2.1. Carbohydrates.....	4
2.2. Carbohydrate Conformation	6
2.2.1. Polysaccharide Structure and Conformation	6
2.2.2. Visualisation of Ring Conformations.....	8
2.2.3. Carbohydrate Dynamics	8
2.3. Atomic Force Microscopy	11
2.3.1. AFM Based Polysaccharide Experiments.....	12
2.4. Molecular Dynamics Simulations	16
2.5. Steered Molecular Dynamics.....	17
2.5.1. Steered Molecular Dynamics Simulations	18
3. Simulation Methods	22
3.1. Stretching Simulations.....	22
3.1.1. Simulation Conditions	22
3.1.2. Materials and Computational Methods	23
4. Results and Discussion	26
4.1. Stage I.....	26
4.2. Stage II.....	26
4.3. Stage III.....	35
4.4. Stage IV	35
4.5. The Effect of the Ramping Rate on the Stretching Curve.....	39
4.6. The Effect of Oligosaccharide Length on the Stretching Curve.....	44
5. Conclusions and Future Work	45

6.	References	47
7.	Appendix A.....	53
8.	Appendix B.....	56
9.	Appendix C.....	60
10.	Appendix D.....	66
11.	Appendix E	73
12.	Appendix F	77
13.	Appendix G.....	89

List of Figures

Figure 1: Three-dimensional partial structure of the amylose repeating unit.....	5
Figure 2: A line diagram of a disaccharide showing the ϕ (H1-C1-O1-C _x ') and ψ (C1-O1-C _x '-H _x ') torsion angles.	7
Figure 3: Sample ring structures for amylose shown with a combination of the VMD PaperChain and Licorice visualisation, illustrating the default colour scale for: (a) amylose in chair, (b) in twist-boat and (c) in boat conformation. The colour reflects the puckering amplitude and not necessarily the exact conformation, though there is a high degree of correlation between them.....	9
Figure 4: Three-dimensional structure of a 4-unit amylose oligosaccharide, showing the O1-O4 end-to-end distance (r). The glycosidic linkages are numbered from the non-reducing and to the reducing end of the chain.	24
Figure 5: The force-extension curves produced by stretching simulations of 4, 6, 8, 10 and 16-unit amylose fragments.	27
Figure 6: Comparison between the SMD (a) and AFM (b) [2] force-extension curves for a 4-unit amylose fragment.....	28
Figure 7: Comparison between the SMD (a) and AFM (b) [45] force-extension curves for a 10-unit amylose fragment.....	28
Figure 8: A section of the dihedral angle time series from the stretching simulation of the tetramer, showing transitions to anti conformations that occur during stage II in the force-extension curve.	29
Figure 9: Contoured ϕ , ψ energy surfaces (PMF) for maltose in vacuum as calculated by Kuttel et al [4]. Contours are at 1 kcal/mol intervals above the global energy minimum, to a maximum of 12 kcal/mol. The first contour at 1 kcal/mol is dashed.	29
Figure 10: A section of the dihedral angle time series from the stretching simulation of the 8-unit (a) and 6-unit (b) amylose fragment, showing transitions to anti conformations that occur during stage II in the force-extension curve.	30
Figure 11: A section of the dihedral angles time series from the stretching simulation of the 16-unit (a) and 10-unit (b) amylose fragment, showing transitions to anti conformations that occur during stage II and III in the force-extension curve.	31
Figure 12: Snapshots from the stretching simulation of the tetramer depicted with the PaperChain, Twister and CPK (showing O5) VMD visualisation algorithms. (a) a helical conformation from Stage I and II (138 pN) of the force-extension curve, (b) snapshot from Stage III (444 pN), showing the second residue in a boat conformation (c) the twist-boat conformations from Stage IV (639 pN) and (d) snapshot showing the second and third residues in boat conformations.....	33
Figure 13: The stretching of the 8-unit fragment depicted with the PaperChain, Twister and CPK (showing O5) VMD visualisation algorithms, showing (a and b) a helical conformation from Stage I (138 pN) and II	

(333 pN) of the force-extension curve, (c) the chair-to-boat transitions from Stage III (528 pN) and (d) the chair-to-boat transitions of residue 1 to 7 from Stage IV (1973 pN)..... 34

Figure 14: The force-extension curves produced by stretching simulations of an 8-, 10- and 16-unit amylose fragment at a ramping force of $0.1 \text{ kcal.mol}^{-1}.\text{\AA}^{-1}$ 40

Figure 15: A section of the dihedral angles time series from the stretching simulation of the 16-unit (a) and 10-unit (b) amylose fragment, showing transitions to anti conformations that occur during stage II and III in the force-extension curve. 41

List of Tables

Table 1: The colouring schemes for the puckering distortion as listed in S. Cross et al. [40].	10
Table 2: Interval lengths (ns) and ramping force per increment (pN) used per simulation for each amylose fragment.	25
Table 3: Interval lengths (ns) and ramping force per increment (pN) used to determine the effect of different ramping rates for each amylose fragment.	25
Table 4: The chair-to-boat transitional changes for the stretching of the tetramer at an interval length of 20 ns.	37
Table 5: The chair-to-boat transitional changes for the stretching of the hexamer at an interval length of 20 ns.	37
Table 6: The chair-to-boat transitional changes for the stretching of the 8-unit fragment at an interval length of 20 ns.	37
Table 7: The chair-to-boat transitional changes for the stretching of the 10-unit fragment at an interval length of 20 ns.	38
Table 8: The chair-to-boat transitional changes for the stretching of the 16-unit fragment at an interval length of 40 ns.	38
Table 9: The chair-to-boat transitions of the 8-unit fragment at a ramping force of $0.1 \text{ kcal.mol}^{-1}.\text{\AA}^{-1}$.	42
Table 10: The chair-to-boat transitions of the 10-unit fragment at a ramping force of $0.1 \text{ kcal.mol}^{-1}.\text{\AA}^{-1}$.	42
Table 11: The chair-to-boat transitions of the 16-unit fragment at a ramping force of $0.1 \text{ kcal.mol}^{-1}.\text{\AA}^{-1}$.	42

Chapter 1

1. Introduction

A computer simulation can be defined as a computer program that attempts to simulate a physical model of a particular system. Computer simulations have become an integral part of mathematical modelling of systems in physics, chemistry and biology, to explain the behaviour and to gain insight into the operation of those systems.

Molecular dynamics (MD) is a form of computer simulation wherein atoms in a molecule are modelled as balls which interact according to an energy expression for a period of time, generating information at the microscopic level, including atomic positions and velocities. Simulations of this sort allow researchers to probe the relationship between molecular structure, movement and function.

Generally, molecular systems consist of a vast number of particles. It is therefore virtually impossible to solve the dynamics of such systems analytically. MD simulations are useful, because they circumvent this problem with numerical methods. MD simulations also offer a significant advantage over both experiment and Monte Carlo (another simulation technique) simulations by providing a detailed history of the interactions and dynamics of the individual atoms during the course of the simulation.

These days, with the emerging potential of supercomputers, MD simulations are commonly used to investigate the structure, dynamics and thermodynamics of biological molecules and their complexes. Computational simulations can serve both to supplement experimental data and to provide mechanistic information unobtainable by current experimental methods. The types of biological activity that have been investigated using MD simulations include protein folding, protein stability, conformational changes associated with bio-molecular function, and molecular recognition of proteins, DNA, and membrane complexes [12, 13, 14, 20, 23, 26]. Molecular dynamics (MD) and, in particular, steered molecular dynamics (SMD) can be used to study the unbinding of ligands and conformational changes in bio-molecules [2, 31, 41, 9, 43, 44, 45, 51, 52]. This allows researchers to explore biological processes on time scales accessible to molecular dynamics simulations, currently nano- or microseconds. SMD can also be applied to investigate the molecular mechanisms that determine elastic properties exhibited by molecules subjected to deformations. The elastic properties of a molecule can be determined by analysing the force-extension data produced by constant force SMD simulations.

Carbohydrates are the most abundant class of macromolecule in living organisms. There are four classes of carbohydrate that are of general interest namely, monosaccharides, disaccharides (together known as simple carbohydrates), oligosaccharides and polysaccharides, (together termed complex carbohydrates). Polysaccharides are composed of longer chains of monosaccharide units bound together by glycosidic bonds. Three well known polysaccharides are cellulose, starch and glycogen. Amylose, one of the two components of starch, is one of the most investigated of the carbohydrate polymers. A good understanding of the structure and conformational dynamics of carbohydrates could provide us with a mechanism to alter its properties, with profound implications for biology and medicine, from infection (bacterial pathogens) to immunity (carbohydrate-based vaccines). For example, an understanding of the polysaccharide surface of a bacterium is key in developing modern conjugate vaccines.

Recently, Atomic Force Microscopy (AFM) has become a powerful tool for studying the force driven conformational changes of polysaccharides. Various AFM experiments have been performed on carbohydrate structure and dynamics, particularly for oligo- and polysaccharides in solution, but the structural changes involved in the force-response are difficult to probe experimentally.

Since experimental data on carbohydrates remains limited and with ongoing improvements in computational power, speed and software, computational studies are increasingly used to investigate the conformation and mobility of oligo- and polysaccharides. MD simulations have already provided important qualitative insights on biologically important processes involving carbohydrates such as the hydration of a carbohydrate at the molecular level [12, 13, 14].

Various researchers have studied amylose but there is some disagreement on the conformational transitions responsible for the characteristic features of the force -response curve. Marszalek et al. [31, 41, 50, 53] showed that the elasticity of some polysaccharides is governed by force-induced conformational transitions of the pyranose ring and that the resulting force-extension spectrum produced by these transitions is characteristic of the force-induced flipping of the pyranose rings from their ground-energy chair conformation to the boat-like conformation. In studies performed by Kuttel et al. [51, 52], however, they concluded that the chair to a boat conformational changes are not responsible for the extension of the molecule and proposed a complex helix-ribbon-helix mechanism.

1.1. Objectives

This study will explore the physical conformations and elastic properties of amylose through constant force SMD simulations by stretching amylose strands in vacuum. In each simulation atom O4 on the non-reducing end was fixed, while atom O1 on the reducing end was subjected to a time-dependent spring force in the direction defined by the vector between both atoms. This work serves to establish what effect

the length of the strand and the stretching speed has on the stretching profile and also points towards the minimal strand length required for a polysaccharide model.

The effect of strand length is important to determine how many units are required to effectively simulate an oligosaccharide. The SMD simulation results are compared to experimental data obtained through physical AFM stretching experiments. If the SMD stretching curves correspond to the experimental stretching curves, then the simulations can be used to clarify which conformational transitions contribute to the stretching behaviour. This will provide further data that can be used to resolve ambiguities in the molecular mechanisms involved during polysaccharide stretching. To determine the effect of strand length, stretching simulations were performed on amylose strands of different lengths (4, 6, 8, 10 and 16 units).

It is also important to investigate the effect of stretching speed since previous SMD simulations overestimated the forces necessary to stretch an amylose fragment as compared to AFM measurement. This was attributed to faster ramping rates used in the simulations compared to the experimental ramping rates. Faster ramping rates were found to increase the force required to reach a particular extension of an amylose fragment [57]. The correct stretching speed is therefore vital in producing an accurate polysaccharide model. To establish the effect of the stretching speed on the force curve, additional stretching simulations were performed on the 8-, 10- and 16-unit fragments at a slower ramping rate.

1.2. Thesis Overview

Chapter 2 contains an introduction to carbohydrate composition, structure and conformations, with the emphasis on experimental (AFM) and computational (SMD) methods to characterise carbohydrate conformations.

In Chapter 3, a detailed description of the methods used to perform the SMD simulations is given. The results of the simulations are detailed in Chapter 4. Finally, Chapter 5 contains conclusions and suggestions for future work.

Chapter 2

2. Background and Related Work

Since this study is concerned with the use of computer simulations for exploration of the physical conformations and properties of amylose, it is necessary to have an understanding of both the carbohydrate class of molecules and the general methods employed for molecular simulation.

This section contains an introduction to carbohydrate composition, structure and conformations, focussing on the amylose polysaccharide. The last two sections describe experimental (AFM) and computational (SMD) methods to characterise carbohydrate conformations.

2.1. Carbohydrates

Carbohydrates are organic molecules in which carbon, hydrogen, and oxygen bond together, hence the name 'hydrates of carbon'. Carbohydrates have the general molecular formula $C_x(H_2O)_y$, where x and y are whole numbers that differ depending on the specific carbohydrate.

Carbohydrates have many functions. They are a major source of metabolic energy, in the form of sugars and starches, but also serve as a structural material (cellulose in plants, chitin in animals), a component of the energy transport compound ATP, recognition sites on cell surfaces and one of three essential components of DNA and RNA [42, 48].

All carbohydrates are comprised of saccharide units and are divided into four classes, depending on the numbers of units they contain: monosaccharides (1 unit), disaccharides (2 units), oligosaccharides (up to twenty units) and polysaccharides (more than twenty units). Glucose, galactose and fructose are representatives of the monosaccharides, or simple sugars. Glucose is the primary form of sugar stored in the human body for energy. Fructose is the main sugar found in most fruits. Galactose rarely stands alone but does combine with other simple sugars, notably with glucose to form lactose. All three share the same chemical formula ($C_6H_{12}O_6$), however, they have different structural formulae [48]. Sucrose and lactose are examples of disaccharides, which consist of two monosaccharides linked together by a dehydration synthesis [48]. Oligosaccharides and polysaccharides (complex carbohydrates) are composed of longer chains of monosaccharide units bound together by glycosidic bonds. The number of monosaccharide units present in the chain determines whether it is classified as an oligosaccharide or a polysaccharide [47].

There are three well known polysaccharides namely cellulose, starch and glycogen. These compounds are all polymers of glucose. Cellulose is a structural polysaccharide that plants use as their primary building material. Glycogen is a highly branched starch-like compound used by animals to store energy. Starch is the major carbohydrate reserve in plant tubers and seed endosperm where it is found as granules, each typically containing several million amylopectin molecules accompanied by a much larger number of smaller amylose molecules. Molecules of amylopectin are highly branched networks and are essentially water insoluble. Starch is comprised of glucose monomers that form $\alpha(1\rightarrow4)$ glucose glycosidic linkages. A glycosidic linkage or glycosidic bond is the linkage or bond in the center that links the two glucose units. The $\alpha(1\rightarrow4)$ glycosidic linkage links C1 of the left hand glucose molecule to C4 of the right hand glucose molecule with the oxygen in the alpha position on C₁ (refer to Figure 1). The term 'α' therefore indicates the initial anomeric configuration of the free sugar group.

Amylose is an important food polysaccharide, being the principal component of starch. Amylose molecules (Figure 1) consist mainly of single mostly un-branched chains with 500-20,000 $\alpha(1\rightarrow4)$ -D-glucose units. A few $\alpha(1\rightarrow6)$ branches and linked phosphate groups may be found, depending on the source, but these have little influence on the molecule's behaviour. Amylose generally tends to wind up into a rather stiff single helix [3, 11, 16]. The formation of a helix structure is due to the $\alpha(1\rightarrow4)$ -bonds. Single helical amylose has hydrogen-bonding O2 and O6 atoms on the outside surface of the helix, with only the ring oxygen pointing inwards.

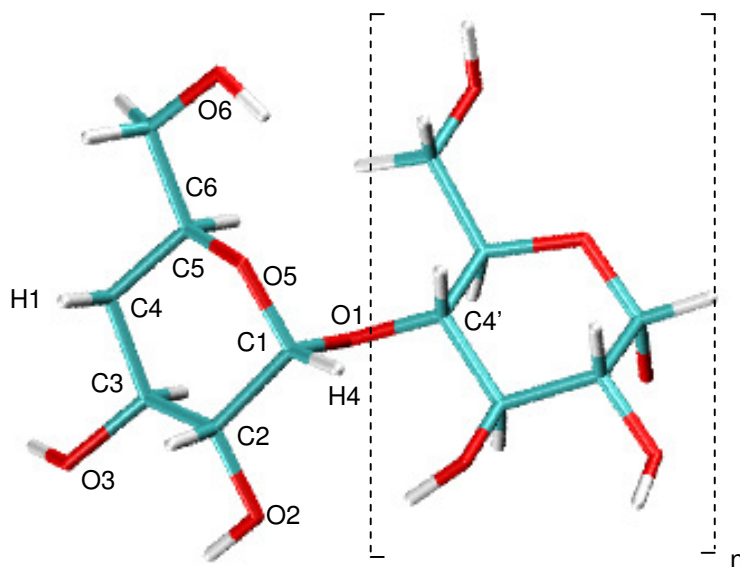


Figure 1: Three-dimensional partial structure of the amylose repeating unit.

2.2. Carbohydrate Conformation

2.2.1. Polysaccharide Structure and Conformation

When characterising bio-molecules it is important to determine the relationship between molecular structure and biological function. Carbohydrates perform diverse biological functions and display exceptional conformational variety and flexibility. In order to understand this relationship one must investigate the mechanics of carbohydrates on a microscopic level.

Most of the well-known polysaccharides, like starch, glycogen, cellulose and the modified polysaccharide, chitin, are polymers of glucose. A linear polymer has several different ways of linking saccharide rings, for example (1→4) and (1→6) linkages (connecting C1 and C4 or C1 and C6 carbon atoms of neighbouring sugar monomers). Compared to polysaccharides with (1→4) linkages, polysaccharides with (1→6) linkages have greater flexibility and more complex conformational behaviour due to the additional bond between neighbouring rings. Starch is a polymer of the α -form of glucose and cellulose is a polymer of β -glucose. Both form (1→4) glycosidic bonds, but starch forms $\alpha(1\rightarrow4)$ linkages and cellulose forms $\beta(1\rightarrow4)$ linkages. This results in very different structures. The position of the bonds and branching patterns are therefore important in the structure and function of the polysaccharides.

This is also the reason why polysaccharides are classified on the basis of their main monosaccharide components and the sequences and linkages between them, as well as the configuration of linkages, the ring size (furanose or pyranose), the absolute configuration (D- or L-) and any other substituents present i.e. certain structural characteristics such as chain conformation and intermolecular associations that will influence the physicochemical properties of polysaccharides [24]. The nature of the glycosidic linkages therefore governs the general characteristics of the polysaccharide chain conformation and flexibility. Polysaccharides are prone to form regular/ordered structures such as single or multiple helices that are stabilised by hydrogen bonds, ionic bridges and also van der Waals interactions, because they have an abundance of hydroxyl, acidic and charged groups.

The most stable arrangement of atoms in a polysaccharide will be that which satisfies both the intra- and inter-molecular forces. Regular ordered polysaccharides, in general, are capable of assuming only a limited number of conformations due to severe steric restrictions on the freedom of rotation of sugar units about the inter-unit glycosidic bonds. There is also a clear correlation between allowed conformations and linkage structure [15].

Conformation refers to the shape of the ring and the positions of the hydroxyl groups and hydrogen atoms in relations to the ring. Carbohydrates don't move around freely, but alternate between several preferred

conformations [17]. The common conformations of the pyranose ring are chair, boat, twist-boat or envelope. Sugar residues have two specific chair conformations, 4C_1 and 1C_4 . The 4C_1 conformation exists when the oxygen ring atom is at the back, the 4-carbon is up and the 1-carbon is down. In the 1C_4 conformation the 1-carbon is up and 4-carbon is down. The boat conformation is an intermediate in the transformation from the 4C_1 to 1C_4 in which 1-carbon has been moved up by rotation around the ring atoms (Figure 3). The flexibility of polysaccharide chains depends on the ease of rotation around the glycosidic oxygen that link together monosaccharides, as the 4C_1 chair conformation of the pyranose ring is comparatively rigid.

Polysaccharide conformation is dominated by the glycosidic linkage conformation. The position and stereochemistry of the linkage governs the extent of interaction between successive sugar residues, which in turn determines the preferred conformations. The glycosidic linkage conformation can be defined by two torsion angles, ϕ and ψ (Figure 2). The ϕ torsion angle describes rotation around the C1-O bond of the acetal link, while the ψ angle describes rotation around the O-C4 bond of the same acetal link, with the glucopyranose ring considered as a rigid rotator. The ϕ and ψ dihedral angles for the $\alpha(1\rightarrow4)$ -linkage for example are defined as:

$$\begin{aligned}\phi &= \text{H1-C1-O1-C4}', \\ \psi &= \text{C1-O1-C4'-H4}'\end{aligned}$$

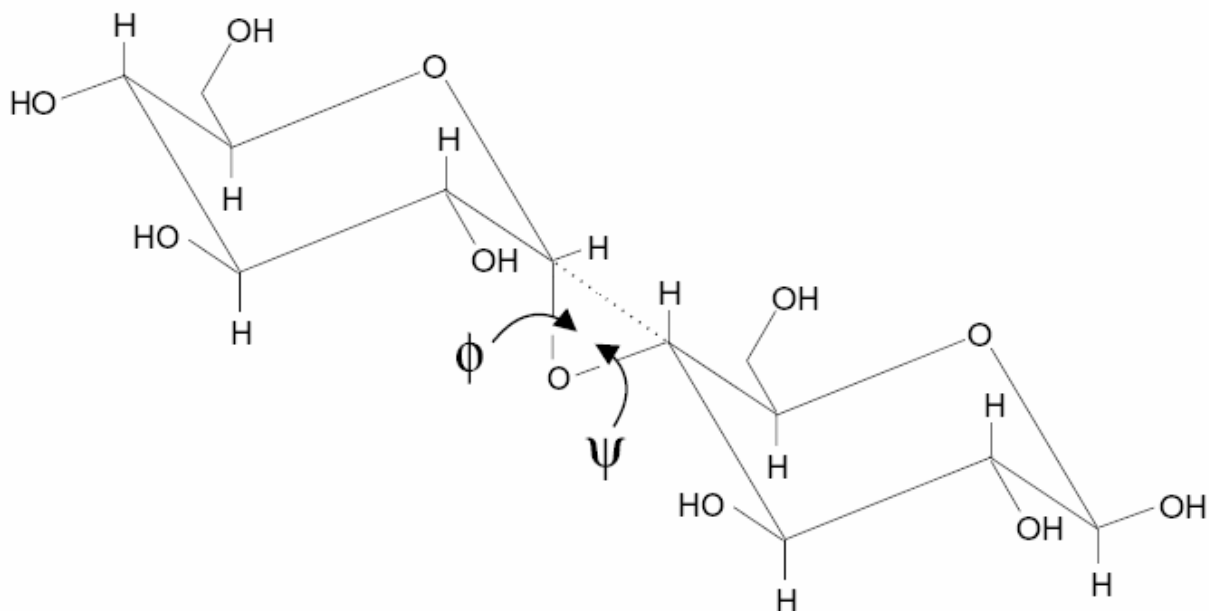


Figure 2: A line diagram of a disaccharide showing the ϕ (H1-C1-O1-C_x') and ψ (C1-O1-C_x'-H_x') torsion angles.

2.2.2. Visualisation of Ring Conformations

Figure 3 shows the ring structures for an amylose tetramer with a combination of the VMD PaperChain and Licorice visualisation, illustrating the default colour scale for the different conformations. The colour reflects the puckering amplitude [40] i.e. the colour scheme differentiates between planar rings and various degrees of pucker. While puckering amplitude is not unambiguously associated with a particular conformation, there is a high degree of correlation between them. The twist-boat conformation, for example, is particularly distorted and therefore dark blue. Table 1 shows the colouring schemes for the puckering distortion.

2.2.3. Carbohydrate Dynamics

The conformation of a carbohydrate in solution can only be described in terms of population distributions in conformational space [25, 27]. This is due to their flexibility and because of this there is no single structure of a carbohydrate in solution. In fact, the type and temperature of the solvent play a big role on the population distributions observed. The flexible nature of oligosaccharide and polysaccharide molecules and the dynamics of their inter-conversion between low energy structures and conformations define its physical and chemical properties in solution.

As mentioned above, conformational changes of oligo- and polysaccharides in solution are primarily due to the rotations about the glycosidic linkages. The flexibility and physics of the glycosidic linkages will therefore define the nature of the conformational changes. At low temperatures the rotations about the glycosidic linkages seems to be localised, in other words, the glycosidic linkages rotate independently of the neighbours [18, 37, 38]. Conformational changes are also possible through the coupled segmental motions of the polymer backbone. These are often referred to as crankshaft motions and involve cooperative motions of two or more sugar residues bonded in sequence [37]. This motion is more likely to occur if hydrogen-bonding spans the glycosidic linkage of a polysaccharide chain.

The dynamic behaviour of carbohydrates can be described in detail by molecular dynamics (MD) simulations. Various theoretical and experimental studies on the physics, mobility and dynamics of oligo- and polysaccharide strands in solution have been performed by researchers making use of MD simulations [21, 22, 32].

Atomic force microscopy (AFM) is another approach to study the elastic properties of oligo- and polysaccharide strands [28]. Elasticity refers to the polymer's resistance to extension. There have been various single-molecule atomic force microscopy experiments that have probed the elastic properties of single polysaccharide strands [29, 30]. This will be discussed in more detail in the following sections.

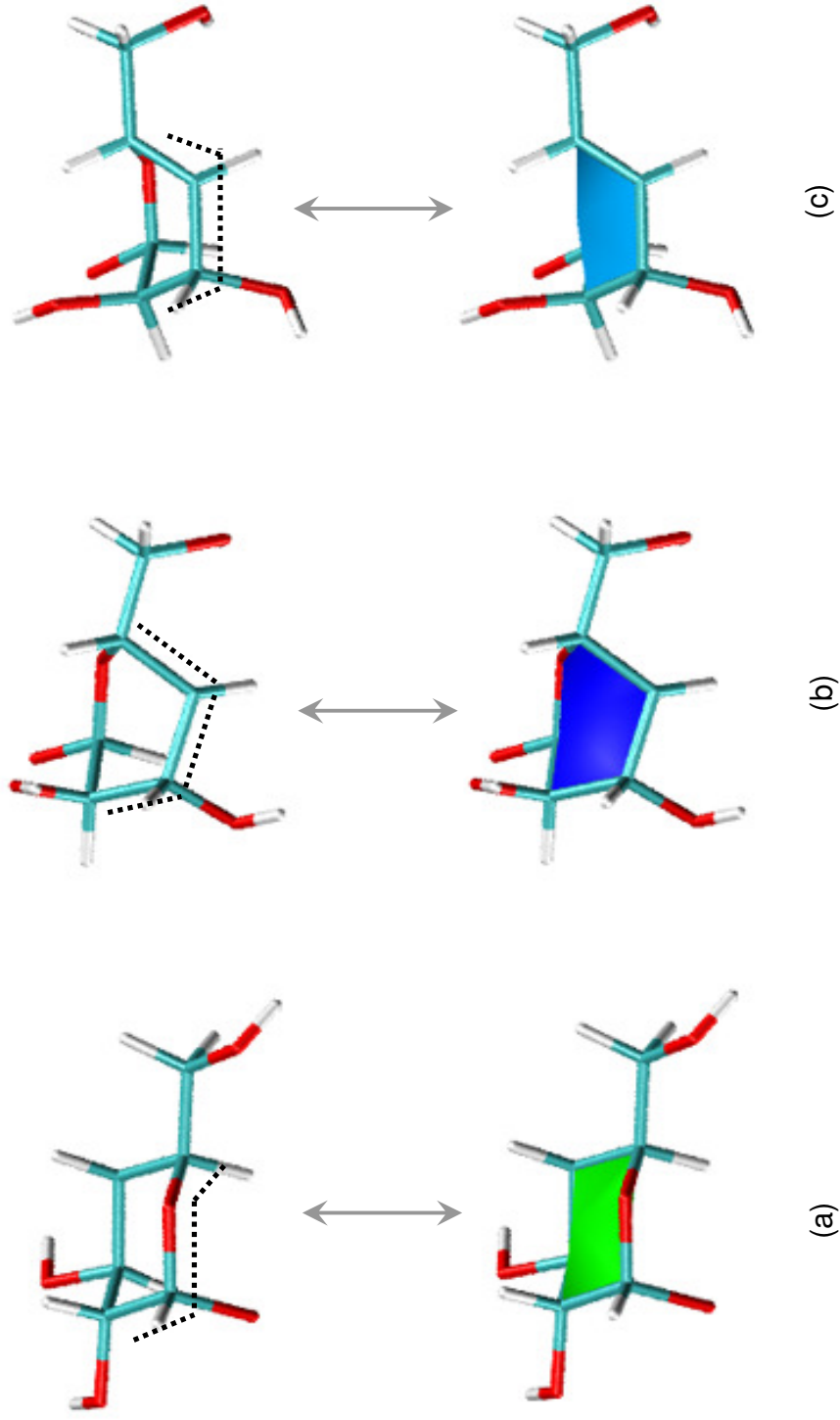


Figure 3. Sample ring structures for amylose shown with a combination of the VMD PaperChain and Licorice visualisation, illustrating the default colour scale for: (a) amylose in chair, (b) in twist-boat and (c) in boat conformation. The colour reflects the puckering amplitude and not necessarily the exact conformation, though there is a high degree of correlation between them.







































Conformer	Cremer-Pople Coordinates			Revised Carbohydra Colours			Colour
	ϕ	θ	Q	R	G	B	
1C_4	0-360	180	0.57	0.0	1.0	0.13	
4C_1	0-360	0	0.57	0.0	1.0	0.13	
$^{1,4}B$	240	90	0.76	0.0	0.0	1.0	
$B_{1,4}$	60	90	0.76	0.0	0.0	1.0	
$^{2,5}B$	120	90	0.76	0.0	0.0	1.0	
$B_{2,5}$	300	90	0.76	0.0	0.0	1.0	
$^{3,6}B$	0	90	0.76	0.0	0.0	1.0	
$B_{3,6}$	180	90	0.76	0.0	0.0	1.0	
1H_2	270	129	0.42	0.88	1.0	0.0	
2H_1	90	51	0.42	0.88	1.0	0.0	
2H_3	150	51	0.42	0.88	1.0	0.0	
3H_2	330	129	0.42	0.88	1.0	0.0	
3H_4	30	129	0.42	0.88	1.0	0.0	
4H_3	210	51	0.42	0.88	1.0	0.0	
4H_5	270	51	0.42	0.88	1.0	0.0	
5H_4	90	129	0.42	0.88	1.0	0.0	
5H_6	150	129	0.42	0.88	1.0	0.0	
6H_5	330	51	0.42	0.88	1.0	0.0	
6H_1	30	51	0.42	0.88	1.0	0.0	
1H_6	210	129	0.42	0.88	1.0	0.0	
1S_3	210	88	0.62	0.0	1.0	0.75	
3S_1	30	92	0.62	0.0	1.0	0.75	
5S_1	90	92	0.62	0.0	1.0	0.75	
1S_5	270	88	0.62	0.0	1.0	0.75	
6S_2	330	88	0.62	0.0	1.0	0.75	
2S_6	150	92	0.62	0.0	1.0	0.75	
1E	240	125	0.45	0.69	1.0	0.0	
E_1	60	55	0.45	0.69	1.0	0.0	
2E	120	55	0.45	0.69	1.0	0.0	
E_2	300	125	0.45	0.69	1.0	0.0	
3E	360	125	0.45	0.69	1.0	0.0	
E_3	180	55	0.45	0.69	1.0	0.0	
4E	240	55	0.45	0.69	1.0	0.0	
E_4	60	125	0.45	0.69	1.0	0.0	
5E	120	125	0.45	0.69	1.0	0.0	
E_5	300	55	0.45	0.69	1.0	0.0	
6E	360	55	0.45	0.69	1.0	0.0	
E_6	180	125	0.45	0.69	1.0	0.0	

Table 1: The colouring schemes for the puckering distortion as listed in S. Cross et al. [40].

2.3. Atomic Force Microscopy

Several experimental techniques based on the application of mechanical forces to single molecules have been applied to study the binding properties of bio-molecules and their response to external mechanical manipulations. These techniques include atomic force microscopy (AFM), optical tweezers, bio-membrane force probe, and surface force apparatus experiments.

AFM is a form of scanning probe microscopy where a small, sharp probe is scanned across the sample to obtain information about the sample's surface. The probe is a tip on the end of a cantilever which bends in response to the force between the tip and the sample. The probe is attached to a piezoelectric scanner tube, which scans the probe across a selected area of the sample surface. Inter-atomic forces between the probe tip and the sample surface cause the cantilever to deflect as the sample's surface topography (or other properties) changes. A laser light reflected from the back of the cantilever measures the deflection of the cantilever, and this information is fed back to a computer [7].

The information gathered from the probe's interaction with the surface can be as simple as physical topography or as diverse as the material's physical properties, magnetic properties, or chemical properties. However, when comparing with SMD simulations we are more interested in the material's physical properties and therefore AFM force curve measurements.

AFM can also record the amount of force felt by the cantilever as the probe tip is brought close to and even indented into a sample surface and then pulled away. Using this technique the long range attractive or repulsive forces between the probe tip and the sample surface can be measured, supplying information on the sample's chemical and mechanical properties like adhesion and elasticity. This procedure typically produces a force–extension graph that provides information on the elasticity and conformational transitions of a molecule obtained by vertically stretching. Force curves typically show the deflection of the free end of the AFM cantilever as the fixed end of the cantilever is brought vertically towards and then away from the sample surface [39].

AFM can stretch biopolymers into important conformations that are inaccessible to other methods of measurement such as NMR spectroscopy and X-ray crystallography. The application of a mechanical force to biological polymers also produces conformations that are different than those that have been investigated by chemical or thermal denaturation. AFM is unique in its ability to apply small (10 pN) and large (1000 pN) stretching forces to individual polymer chains.

Over the last few years, force spectroscopy has become a powerful tool for studying the force driven conformations of proteins, polysaccharides and nucleic acids, and could provide new insights into both structural biology and material sciences.

2.3.1. AFM Based Polysaccharide Experiments

Recently, AFM has been used in many studies to characterise the elasticity of single polysaccharide molecules and has revealed that relatively simple mechanical manipulations can be very informative in probing molecular conformations. Elasticity experiments of single polysaccharide chains using AFM, has shown that stressed sugar rings may be significantly deformed by mechanical forces which can twist and bend their bond angles [8, 9, 10, 29, 31]. Similar studies have shown that sugar rings in a stretched polysaccharide chain can switch their preferred chair conformation to a boat or an inverted chair conformation which suggests that the elasticity of the polysaccharides (e.g., amylose, dextran, pullulan, and pectin) is governed by conformational transitions of the pyranose ring [4, 2].

Various stretching experiments on single amylose molecules using AFM showed that the molecular elasticity in saccharides is a function of both rotational motion about the glycosidic bonds and the flexibility of the sugar rings themselves [8, 9, 10, 31, 41, 46, 49, 50]. Results also indicate that only the α -linked molecules have characteristic plateaus in their force-extension curves, whereas cellulose, an inelastic β -linked molecule, does not. Various researchers attributed these plateaus to transitions of the α -linked glucose rings from the 4C_1 chair to a twist-boat conformation [8, 31, 41, 46, 49, 50].

Marszalek et al. [2, 9] made use of this process in a study to identify the composition of polysaccharide samples at the single-molecule level. They used the resulting force–extension spectra as a measurement of the elasticity of the molecule. Polymer chains exist in a coiled state at zero force, as this maximises their conformational freedom. Extending a relaxed chain generates an opposing force that is predicted from the reduction in entropy. This effect is known as entropic elasticity. The freely jointed chain (FJC) or the wormlike chain (WLC) models can be used to describe the elasticity of polymers [9].

According to the FJC model, a polymer is modelled as a chain of equal, independent and freely rotating segments in its simplest case. The elastic behaviour of polymers is described based on three adjustable parameters namely: the elasticity of the segments (K_s), the contour length of the molecule (L_c) and the Kuhn length (l_k). The segment elasticity refers to the polymer's resistance to extension, the contour length to the full, but not elongated, length of the polymer and the Kuhn length to the size of the independent segments.

Applying these models, studies by previous researchers confirmed that the elasticity of many polysaccharides can be manipulated by force-induced conformational transitions.

In their study, Marszalek et al. combined the AFM technique with computational chemistry and also showed that the elasticity of some polysaccharides is governed by force-induced conformational transitions of the pyranose ring and that the resulting force–extension spectrum produced by these transitions is characteristic of the ground-energy conformation of the pyranose ring and the type of glycosidic linkages. The “shoulder” feature in the force-extension curve of amylose represents the lengthening of the distance between consecutive glycosidic oxygen atoms upon the force-induced conformational transition of the R-D-glycopyranose rings from their 4C_1 chair conformation to a boat-like conformation. The boat conformation limits the possible boat conformers to only that that gives the largest O1-O4 distance. Therefore, the elasticity changes are due to the reduced conformational space of the stretched boat compared with the relaxed chair forms. Of the five different polysaccharides studied (amylose, dextran, pullulan, pectin and cellulose), the force spectrum obtained from stretching amylose and dextran showed a single transition that occurred at 280 and 850 pN. This resulted in the molecule being overstretched by 17 – 10%.

This transition can be described as a molecular rearrangement or a change in enthalpy resulting in the modification of the elastic properties of the polysaccharide. In terms of the FJC model, at forces below 280 pN the optimal Kuhn length to fit the data is close to the length of a single glucopyranose ring. At forces above 280 pN, i.e. after the transition, the Kuhn length is longer, and the extensibility is decreased. This suggests that the transition in the elasticity of the amylose molecule is caused by a change in conformation of the polysaccharide ring due to an increase in the distance between the consecutive glycosidic oxygen molecules. The elongation of the molecule is therefore due to the force-induced flipping of the pyranose rings from their ground-energy chair (4C_1) conformation to the boat-like conformation.

The force spectrum obtained from stretching cellulose was found to follow the freely jointed chain (FJC) model of polymer elasticity. This will be the case for all polysaccharides whose glycosidic linkages are attached equatorially to the pyranose ring.

Stretching pullulan (a polysaccharide polymer consisting of maltotriose units) resulted in a spectrum which was a linear combination of the spectra of amylose and dextran whereas pectin showed two transitions at 300 and 900 pN. They explained this to the force-induced two-step chair inversion transition in the α -D-galactopyranuronic acid ring i.e. a transition of the galactose rings from the chair conformation to the boat conformation and a subsequent flip of the boat to the inverted chair conformation. Therefore, each molecule’s transitions produce unique atomic fingerprints in the force–extension spectrum which

they successfully used, although at only 10% efficiency, to identify single polysaccharides molecules in solution.

In similar experiments, Marszalek et al. [31, 41, 50, 53] captured the conformational changes in single polysaccharide molecules by making use of force-ramp atomic force microscopy. In the force-ramp model polysaccharide molecules are stretched with a linearly increasing force. Force-ramp AFM allowed them to capture the ring transitions under conditions where the entropic elasticity of the molecule is separated from its conformational transitions. Quantitative analysis of the resulting data provided them with the physico-chemical characteristics of the ring transitions i.e. the width of the energy barrier, the relative energy of the conformers and their enthalpic elasticity. They demonstrated that one can increase the transition probability by controlling the applied force and that a simple two-state model can describe the changes in length resulting from the chair-to-boat transitions of the monomers.

The force-extension graphs (plots of the end-to-end length versus force for the polysaccharide molecules) of amylose and dextran obtained under the force-ramp and the extension-ramp protocols could be divided into four regions. At forces below 50 pN and up to 200 pN the entropic extensibility of the polymer is visible. This force range of above the entropic region and below the conformational transition is dominated by the enthalpic elasticity of the polysaccharide chain. Marszalek et al. suggested that this stage of the extensibility of the chain could be due to forced changes in the mutual orientation of the monomers. The flexibility of the chair conformation of the pyranose ring can also be attributed to the presence of several distorted chair conformations that are of equal conformational energy but have very different torsional and bond angles i.e. changes in the length of the O1-O4 distance can occur without changing the conformational energy.

At above 200 pN there is a sudden increase in the elongation of the chain resulting from the chair-boat transition of the pyranose rings. The boat conformation limits the possible boat conformers to only that that gives the largest O1-O4 distance, therefore, the change in elasticity is due to the reduced length of the stretched boat compared with the relaxed chair forms.

At approximately 350 pN, the transition is complete and it is proposed that the chain is then composed of the rings in the boat-like conformation. At forces above 350 pN small additional extensions come only from deforming the rings and bending the glycosidic linkages (intrinsic enthalpic elasticity of the segments).

They concluded that polysaccharides with axial linkages, such as dextran, amylose and pectin, were found to undergo abrupt force-induced length transitions which were caused by the shift of individual

pyranose rings from the chair conformation to the boat or the inverted chair conformations which provide an increased distance between glycosidic bonds.

In another study, Marszalek et al. [46, 49] investigated atomic levers of single polysaccharide molecules that control the pyranose ring conformation. They made use of AFM experiments to examine the pyranose ring conformation from a chair to a boat by stretching single amylose molecules.

Should a force of 200 pN be applied, a conformational change in the pyranose ring and a sudden elongation of the molecule can be observed, which changes the elasticity of the molecule. They proposed that the change in elasticity results from an increase in the distance between glycosidic oxygen atoms caused by a force-induced transition between the chair and boat conformations of the pyranose ring. In the case of amylose, the glycosidic bonds are disposed in the C4 - O4 (equatorial) and the C1 - O1 (axial) configuration.

This configuration reveals a stretching force applied to the axial glycosidic oxygen O1 has a larger lever arm relative to the C2-O5 axis. This produces torque about this axis, causing a rotation around C-C bonds which promotes the transition to the boat conformation. Therefore, it is proposed that the glycosidic bonds act as mechanical levers, driving the conformational transitions of the pyranose ring.

However, if the force is applied to the equatorial oxygen atom O4 the C4-O4 bond does not produce any significant torque about this axis, causing no conformational change. This was also observed in cellulose, a polysaccharides with equatorial linkages. Cellulose did not undergo force-induced conformational transitions upon stretching because these linkages generate minimal torque on the pyranose ring and also provide a maximal separation of the glycosidic oxygen atoms in the ground energy conformation.

Therefore axial linkages generate torque and equatorial linkages do not. From this they concluded that the torque generated by these levers determines the conformers and the number of transitions that can be reached during the elongation of the molecule when applying a force.

Marszalek et al. [10] also used single molecule force spectroscopy to examine the mechanical properties of heparin molecules. Heparin is a polysaccharide that is comprised of glucose monomers that form $\alpha(1\rightarrow4)$ glucose glycosidic linkages, similar to amylose and pectin.

The force-extension curve produced from the AFM experiments showed a pronounced plateau at forces above 200 pN, marking an enthalpic transition. They interpreted the plateau as an increased extensibility of the molecules. They also noted that the force at which heparin molecules display their enthalpic elasticity coincides with the force at which α -D-glucopyranose residues of amylose flip from their chair to

a boat-like conformation. This plateau, at a force of 200 pN, is indicative of (1→4) linkages between the pyranose monomers, since other linkages, such as (1→6) linkages, produces plateaus at higher forces. For example, AFM experiments performed on dextran, whose backbone is primarily formed by (1→6) linkages, showed a transition at a force of 800 pN.

They concluded that characteristic to other α -linked glucans, the enthalpic elasticity of heparin originates in sugar rings which undergo force-induced conformational transitions within α -D-GlcN and α -L-IdoA units flipping to more energetic and more extended conformations. Therefore, these residues provide axial linkages in their ground energy conformations that lengthen the molecule when placed under a stretching force.

To summarise, Marszalek et al. showed through AFM experiments that polysaccharides with axial linkages, such as dextran, amylose and pectin, were found to undergo abrupt force-induced length transitions which were caused by the shift of individual pyranose rings from the chair conformation to the boat or the inverted chair conformations which provide an increased distance between glycosidic bonds. They observed that a variety of polysaccharides derived from glucopyranose, like amylose, undergo a similar transition, but at different forces. In their AFM experiments with amylose they recorded similar forces for the different stages of the force-induced length transitions caused by the chair-to-boat transition.

2.4. Molecular Dynamics Simulations

MD simulations compute atomic trajectories by solving equations of motion numerically using empirical force fields, such as the CHARMM [6] force field, that approximate the actual atomic force in biopolymer systems. Molecular dynamics alters the intra-molecular degrees of freedom in a step-wise fashion, analogous to energy minimisation. The steps in molecular dynamics represent the changes in atomic position over time (i.e. velocity). The molecular dynamics simulation method is based on Newton's second law or the equation of motion (Force = mass x acceleration):

$$F_i = m_i a_i$$

where F_i is the force exerted on the particle, m_i is its mass and a_i is its acceleration. The force can also be expressed as the gradient of the potential energy,

$$F_i = -\nabla_i V$$

Combining these two equations yields

$$-\frac{dV}{dr_i} = m_i \frac{d^2 r_i}{dt^2}$$

where V is the potential energy of the system. Newton's equation of motion can then relate the derivative of the potential energy to the changes in position as a function of time [7].

The rate and direction of motion (velocity) are governed by the forces that the atoms of the system exert on each. Molecular dynamics calculate the force on each atom and the position of each atom throughout a specified period of time. The force on an atom can be calculated from the change in energy between its current position and its position a small distance away. Knowing the atomic forces and masses, it is possible to determine the acceleration of each atom in the system and the positions of each atom along a series of small time steps. The resulting series of structural changes over time is called a trajectory i.e. the trajectory describes the positions, velocities and accelerations of the particles as they vary with time. Once the positions and velocities of each atom are known, the state of the system can be predicted at any time in the future or the past.

In the design of a molecular dynamics simulation one should take into account the available computational power. Simulation size, time-step and total time duration must be selected so that the calculation can finish within a reasonable amount of time. Complex molecules will take considerably longer to calculate. The most CPU intensive task during a MD simulation is the evaluation of the potential (force field) as a function of the particle's internal coordinates. Force fields are empirical and consist of a summation of bonded forces associated with chemical bonds, bond angles, and bond dihedrals, and non-bonded forces associated with van der Waals forces and electrostatic charge.

Another factor that impacts total CPU time required is the size of the integration time-step. This is the time length between evaluations of the potential. Typical time-steps for MD simulations are in the order of 1 femto-second.

2.5. Steered Molecular Dynamics

Steered molecular dynamics (SMD) is a computational method that permits qualitative as well as quantitative analysis of molecular properties. For instance, the unbinding of ligands and conformational changes in bio-molecules can be studied using this technique [1].

The basic idea behind SMD simulations is to apply a time-dependent external force to one or more atoms, referred to as SMD atoms, and then to analyse the response of the molecule. The SMD method, therefore, examines the behaviour of molecules when they are driven out of their equilibrium conformations by external forces.

SMD simulations in this study will be performed with NAMD code. NAMD is a parallel molecular dynamics program designed for high-performance simulations in structural biology and is capable of performing several different kinds of SMD, including rotation or translation of one or more atoms. NAMD was designed to run efficiently on parallel machines for simulation of large molecules which require enormous computing power. Within NAMD [5], there are two typical SMD protocols namely: SMD with constant pulling velocity and constant force. This study will focus on constant force stretching simulations.

To perform constant force stretching simulations, one would keep one group of atoms fixed and pull on another, thereby stretching and unfolding the molecule. By doing this one can study the behaviour of the molecule under various conditions. Important structural information about the molecule can then be obtained from the analysis of the interactions, as well as the recording (as a function of time) of the applied forces and ligand position.

This approach has the advantage that it corresponds closely to micromanipulation through optical tweezers and AFM experiments (discussed in the next section), where the molecule is being pulled by the tip of the cantilever.

2.5.1. Steered Molecular Dynamics Simulations

Molecular dynamics simulation is particularly suitable for modelling single molecule experiments. Various researchers have made use of SMD simulations to explain the force-extension curves obtained from AFM experiments. Rief et al. [29, 30] studied dextran linked to a gold surface using MD simulations for 5 ring model systems and CHARMM force field. Li et al. [30] measured the difference in $\alpha(1\rightarrow4)$ (amylose) and $\beta(1\rightarrow4)$ (cellulose) linked polysaccharides and, as mentioned in the previous section, Marszalek et al. [2, 31, 41, 9] demonstrated that polysaccharide elasticity is governed by chair-boat transitions of the glucopyranose rings. These chair-boat transitions were observed in force-ramp AFM experiments. In force ramp experiments the pulling force is linearly increased and the geometrical changes of the pulled molecule are then captured. Results from these experiments showed that the barrier for the chair-to-boat transition in α D-glucose ranges from 14 to 15 kcal/mol.

In a study Lu et al. [45] performed steered molecular dynamics simulations combined with similar AFM experiments for single amylose chains composed of 10 glucopyranose rings in solution. The SMD

simulations matched the experimentally measured force-extension curve and the results showed that the force-induced chair-to-boat transitions of glucopyranose rings are responsible for the characteristic plateau in the force-extension curve of amylose.

They characterised the chair-to-boat transition using the O1-C1-C2-O2 angle. Looking at the force-extension curve they observed an abrupt change of the O1-C1-C2-O2 dihedral angles that flipped from about $+60^\circ$ to -60° which indicated that the sugar ring (the reducing end) switched from an envelope to a boat conformation at pulling forces in a range of 400-800 pN.

The chair-to-boat transition for each individual sugar ring allowed the O4-O1 distance to be elongated. They also observed that with the increased tension in the amylose chain, all the neighbouring glucose rings rotated about the C4-O4 bonds to orient themselves in a parallel fashion at the end of the simulations, even though they were initially arranged in an anti-parallel orientation.

Therefore, by combining their experimental (AFM) and SMD simulation results, they concluded that the non-entropic elastic behaviour of amylose is governed by the mechanics of pyranose rings themselves and their force-induced conformational transitions.

Nowak et al. [44] investigated recent advances and trends in applications of computer simulations, such as steered or biased molecular dynamics, to help with the interpretation of experimental data obtained from single biopolymer molecules during atomic force microscope experiments.

They found that when stretching single dextran molecules in the AFM instrument that the elasticity of dextran differs from both cellulose and pustulan (also a 1 \rightarrow 6 linked polysaccharide). The results suggest that dextran's $\alpha(1\rightarrow6)$ linkages induce the rotation about the C6-C5 bond and also trigger various ring instabilities. They then applied SMD simulations, using NAMD2 code, to investigate the deformations of the pyranose ring produced by forces attached to the ring at carbon atom C1 and through a rotatable C6-C5 bond.

The SMD simulation results showed that deforming the pyranose ring by $\alpha(1\rightarrow6)$ linkages, using the O6 - C6 cranks and axial C1-O1 levers reorients the O6-C6 and produced ring instabilities, which flipped the pyranose structure to a boat-like conformation.

Neelov et al. [43] investigated the extension of dextran under constant forces of different magnitudes in vacuum, using molecular dynamics with three different force fields (AMBER94, AMBER-GLYCAM04 and CHARMM).

Previous single molecule AFM experiments of the extension of (1→6) polysaccharides showed that in the case of dextran there was a plateau in the force-extension curve at forces of 700-900pN for native dextran and at 250-350pN for carboxymethylated dextran. Some researchers speculated that this plateau was attributed to a rotation around the C5-C6 bond (i.e. to conformational transition of the O5-C5-C6-O6 dihedral angle) in each monomer. Other theories suggested that the plateau occurs due to a chair-boat transition of the glucopyranose rings during the extension of dextran chain.

Neelov et al. observed a third state of the glucopyranose ring; inverted chair as apposed to chair and boat, at forces between 700 and 1000 pN. They explained the force-extension profile by the transition of the glucopyranose ring from chair (4C_1) to inverted chair (1C_4). They also noted that at smaller forces there was rotation around the C5-C6 bond and at higher forces chair-to-boat transitions.

The results observed by applying the different force fields suggest different molecular mechanisms for the plateau region in the force-extension curve. At room temperature, AMBER94 and AMBER-GLYCAM04 associate the plateau to the chair-inverted chair transition while CHARMM assigns the plateau region to chair-boat transitions. They concluded that the two chair states (chair and inverted chair) are well-separated along the predominant axis of extension, but the boat state, which acts as a transition state between them is almost orthogonal to the extensional axis, contributing much less to the extension of the monomer.

Kuttel et al. [51, 52] performed stretching simulations on an 18-unit amylose fragment making use of CHARMM. By combining stretching simulations with free energy calculations they revealed that the primary mechanism for relieving tensile strain in α -linked polysaccharides, like amylose, involves complex rotations of the glycosidic linkages and that the chair-to-boat transitions of the pyranose rings play a smaller role.

The force-extension curves produced were similar to the distinctive transitions seen in AFM stretching experiments by other researchers. They identified four distinct stages of conformational transitions.

During stage I they observed that the oligomer strand relieves tensile strain by rotating the glycosidic linkage torsion angles resulting in a more extended helix compared to that of the initial helical conformation. They calculated the β -maltose Ramachandran free energy surface as a function of the ϕ , ψ dihedrals to establish the entire range of motion for the glycosidic linkages. The ϕ and ψ dihedral angles for the $\alpha(1\rightarrow4)$ -linkage are defined $\phi = H1-C1-O1-C4'$, $\psi = C1-O1-C4'-H4'$.

During stage II the amylose strand switches from a helical conformation to a flatter "ribbon" conformation and as the glycosidic linkages are subjected to further strain a slight lengthening of the stiff ribbon

conformation can be observed. They explained that this conformation was due to a forced rotation of most of the glycosidic ψ dihedral angles from *syn* to *anti* conformations which disrupted the helical character of the strand.

Stage III shows a rapid increase in length and 2 of the 18 pyranose rings converting from a chair to a boat conformation. The chair to a boat conformations however is not responsible for the extension of the molecule, but rather the ψ dihedrals reverting from *anti* to *syn*, thereby producing a maximally extended helical conformation. By the end of stage III the extension of the molecule approaches its contour length which means that any further rotations of the ϕ , ψ glycosidic dihedral angles can no longer lengthen the chain.

During stage IV the majority of the chair-to-boat transitions of the pyranose rings occur. They suggest however that the chair-to-boat transitions play a minor role in the lengthening of the molecule and that the stretching mechanism is dominated by the rotational freedom of the glycosidic linkages.

To summarise, Lu et al. [45], showed through SMD simulations that the force-induced chair-to-boat transitions of glucopyranose rings are responsible for the characteristic plateau in the force-extension curve of amylose and, therefore, that the non-entropic elastic behaviour of amylose is governed by the mechanics of pyranose rings themselves and their force-induced conformational transitions. Neelov et al. [43] explained the force-extension profile by the transition of the glucopyranose ring from chair to inverted chair, whereas, Kuttel et al. [51, 52] revealed that the primary mechanism for relieving tensile strain in α -linked polysaccharides, like amylose, involves complex rotations of the glycosidic linkages and that the chair-to-boat transitions of the pyranose rings play a smaller role.

Chapter 3

3. Simulation Methods

3.1. Stretching Simulations

As noted in Chapter 2, computational methods, such as SMD simulations, have significantly contributed to the investigation of conformations of amylose and glucose rings and have proved invaluable to the interpretation of AFM measurements.

In this study, NAMD SMD simulations are used to simulate AFM stretching experiments. There are two main SMD simulation methods used in NAMD namely: constant velocity and constant force pulling. In this study the elastic properties of amylose were investigated by stretching amylose fragments in vacuum by applying a constant force. Water plays an important role in polysaccharide conformation. In fact, particularly in solution, many polysaccharides are highly flexible molecules. The interactions with the aqueous solvent may determine the preferred conformation by disrupting intra-molecular hydrogen bonding. Simulations were therefore performed in vacuum, since it is computationally expensive to model the interactions with a solvent.

The simulations were performed to determine the effect that different oligosaccharide lengths and ramping rates have on the stretching behaviour of amylose. During each stretching simulation, the force was ramped (by increasing the force for each consecutive simulation) at regular intervals, which produced a series of distributions corresponding to the extension of the molecule at specific forces. These distributions were then used to plot force-extension profiles. Each force-extension profile consists of the force applied at each step against the average molecular extension determined from the corresponding distribution. These force-extension graphs for amylose fragments of different lengths were then compared to those produced by AFM experiments.

3.1.1. Simulation Conditions

SMD simulations were performed using the NAMD (version 2.6) program [1]. The CSFF parameter set for the CHARMM force field was used to model the amylose molecules [6]. All simulations were performed in vacuum under the Canonical ensemble (constant n, V, T) and using stochastic Langevin dynamics with a damping coefficient of 62.5 to maintain a constant temperature of 300K [1]. Initial velocities for the atoms were selected at random from a Boltzmann distribution at 300 K. The equations of motion were integrated

using a Leap-Frog Verlet integrator [55] with a step size of 1 fs. The non-bonded interactions were truncated using a switching function applied on a neutral group basis between 10.0 and 12.0 Å.

3.1.2. Materials and Computational Methods

The elastic properties of amylose were investigated by stretching amylose fragments of different lengths (4, 6, 8, 10 and 16 units) in vacuum by applying a constant force. PSF (molecule structural information) files for each of the oligosaccharide lengths were generated with CHARMM [6].

SMD simulations were performed with NAMD2 code on an Apple XServe comprising 8 dual core XServes. In each simulation atom O4 on the non-reducing end was fixed, while atom O1 on the reducing end (Figure 4) was subjected to a time-dependent spring force in the direction defined by the vector between both atoms. As the molecule change shape during the extension, the vector change direction as well. This was compensated for by making use of the SMD procedure implemented in VMD, where the vector is updated at each step [54].

To perform a constant force NAMD SMD simulation the following files are needed:

- A Protein Data Bank (pdb) molecule structure file (Appendix E). This contains information such as the name of the compound, stoichiometry, secondary structure locations, crystal lattice and stores atomic coordinates and/or velocities for the system.
- A CHARMM force field parameter file (Appendix D). This contains all of the numerical constants needed to evaluate forces and energies. Force fields are used to calculate molecular energies and configurations. In other words it provides a mapping between bonded and non-bonded interactions and specific spring constants and similar parameters for all of the bond, angle, dihedral, improper and van der Waals terms in the CHARMM potential function.
- A structure (psf) file (Appendix F). This contains all of the molecule-specific information (structural information such as various types of bonding interactions) needed to apply a particular force field to a molecular system. The PSF file is generated from the force field topology file.

To instruct NAMD as to how the simulation is to be run, a NAMD configuration file was created for each simulation. This file specifies all the options that NAMD should adopt in running a simulation (Appendix A). Refer to Appendix C for the step by step process followed to set up the constant force pulling simulations.

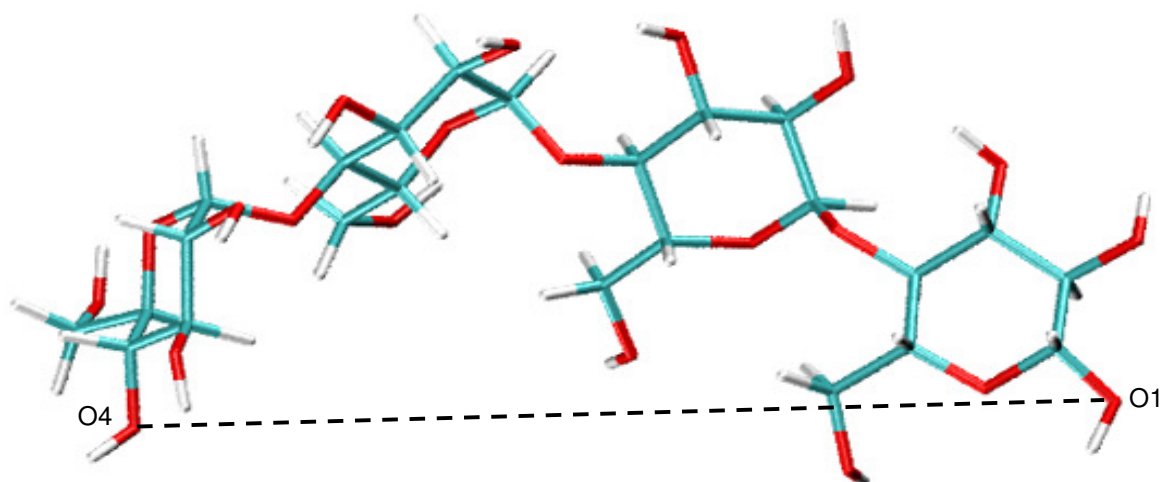


Figure 4: Three-dimensional structure of a 4-unit amylose oligosaccharide, showing the O1-O4 end-to-end distance (r). The glycosidic linkages are numbered from the non-reducing and to the reducing and of the chain.

NAMD uses a column of a PDB file to determine which atoms will be fixed and which atoms will be pulled. In addition, another three columns are used to specify the direction of the constant force that will be applied to the SMD atom. This information is stored in a reference (ref) file (Appendix G). Refer to Appendix C for the step by step process followed to generate the reference file.

For the initial simulations, the force was ramped by 27.79 pN ($0.4 \text{ kcal.mol}^{-1}.\text{\AA}^{-1}$) at intervals of 20 ns, up to a maximum force of 2779 pN. The longer polysaccharides had longer intervals for stretching (Table 2). All simulations were started with a force of 27.79 pN to prevent the molecule from folding in on itself in the vacuum. Each simulation step consisted of 1ns of equilibration, followed by 19 ns of data collection. A total of 100 ramping steps were applied over the course of each simulation.

Previous studies showed that the faster the pulling rate an amylose fragment was subjected to, the larger the forces required to reach a particular molecular extension. Also, if the force was ramped too quickly, the force-extension curve for amylose did not show the same distinctive features of the experimental force-extension curve [4, 31]. To determine the effect of different ramping rates on the stretching response, additional simulations were performed on the 8-, 10- and 16-unit amylose oligomer (Table 3). For these simulations the force was incremented by 6.948 pN ($0.1 \text{ kcal.mol}^{-1}.\text{\AA}^{-1}$) for each consecutive simulation at intervals of 2 ns. These ramping rates were found to be adequate for reproduction of the experimental curve.

Amylose fragment	Interval (ns)	Ramping force (kcal.mol ⁻¹ .Å ⁻¹)
4-unit	20	0.4
6-unit	20	0.4
8-unit	20	0.4
10-unit	20	0.4
16-unit	40	0.4

Table 2: Interval lengths (ns) and ramping force per increment (pN) used per simulation for each amylose fragment.

Amylose fragment	Interval (ns)	Ramping force (kcal.mol ⁻¹ .Å ⁻¹)
8-unit	2	0.1
10-unit	2	0.1
16-unit	2	0.1

Table 3: Interval lengths (ns) and ramping force per increment (pN) used to determine the effect of different ramping rates for each amylose fragment.

A Linux bash script was implemented to ramp the force at regular intervals (Appendix B). Because of the enormous computing power required, the simulations took between 3 (for the smaller chains like 4-unit amylose) and 6 (for the larger chains like 16-unit amylose) months to complete. The ramping rate simulations took between 3 and 4 weeks to complete, since we were using a much lower interval length of 2 ns vs. 20 ns. Each simulation was performed on a quad-core Xeon machine.

Each stretching simulation produced a series of distributions corresponding to the extension of the molecule at specific forces. The data was stored in trajectory (dcd) files. A separate trajectory file is generated for each force ramping step applied.

Molecules were displayed and analysed using the Visual Molecular Dynamics (VMD) [54] program and the Twister and Paperchain visualisations algorithms. Refer to Appendix C for the step-by-step process followed to do the analysis using VMD.

A .Net C# program (Appendix B) was written to process the analysis data i.e. to convert the output data from VMD into meaningful force and distance data. A force/extension relationship was then obtained by plotting the average extension during each production step against the applied force. All curves were normalised by dividing by the maximum extension of the oligomer achieved by the end of the simulation.

Chapter 4

4. Results and Discussion

The force-extension profiles obtained from simulated stretching of 4-, 6-, 8-, 10- and 16-unit amylose fragments are shown in Figure 5. From these curves it is evident that the stretching profile can be divided into four stages, which we label I - IV. The curve displays the same distinctive transitions seen in force-ramp AFM stretching experiments (Figures 6 and 7) [31, 53, 41, 45, 50]. Generally AFM stretching experiments recorded the transitions at lower forces than those recorded in this study. Various SMD stretching simulations [4, 45, 51] produced similar curves, but in this case the forces recorded were much closer to that observed in this study. We will now consider the molecular mechanisms responsible for each stage of the stretching curve.

4.1. Stage I

The initial stage (< 55 pN) of the stretching curve of the tetramer is characterised by a steep slope indicating rapid extension of the strand from a compact to a more extended conformation, with a low elasticity of 35 pN/nm. The 6- and 8-unit amylose strands show the same steep slope during this stage, although at slightly higher forces of 83 and 166 pN respectively. These higher forces might be because the molecules are folded in on each other. The initial stages (< 250 pN) of the stretching of the 10- and 16-unit chains also show low elasticities between 35 to 44 pN/nm. During this stage, all strands extend without any ψ rotations or chair-to-boat transitions.

Similar stretching simulations were performed by Kuttel et al. [4, 51] on an 18-unit amylose [6]. During this stage they also observed a more extended helix compared to that of the initial helical conformation. They attributed the mechanism of this stage to the oligomer strand relieving tensile strain by rotating the glycosidic linkage torsion angles resulting in a more extended helix compared to that of the initial helical conformation.

4.2. Stage II

In all the oligomers, Stage II is associated with transitions of ψ dihedral angles from *syn* to *anti* conformations, in agreement with Kuttel et al. [4]. The 4-, 6- and 8-unit strands showed no chair-to-boat transitions at this stage. For example, in the tetramer the ψ_2 dihedral angle twice makes a transition from

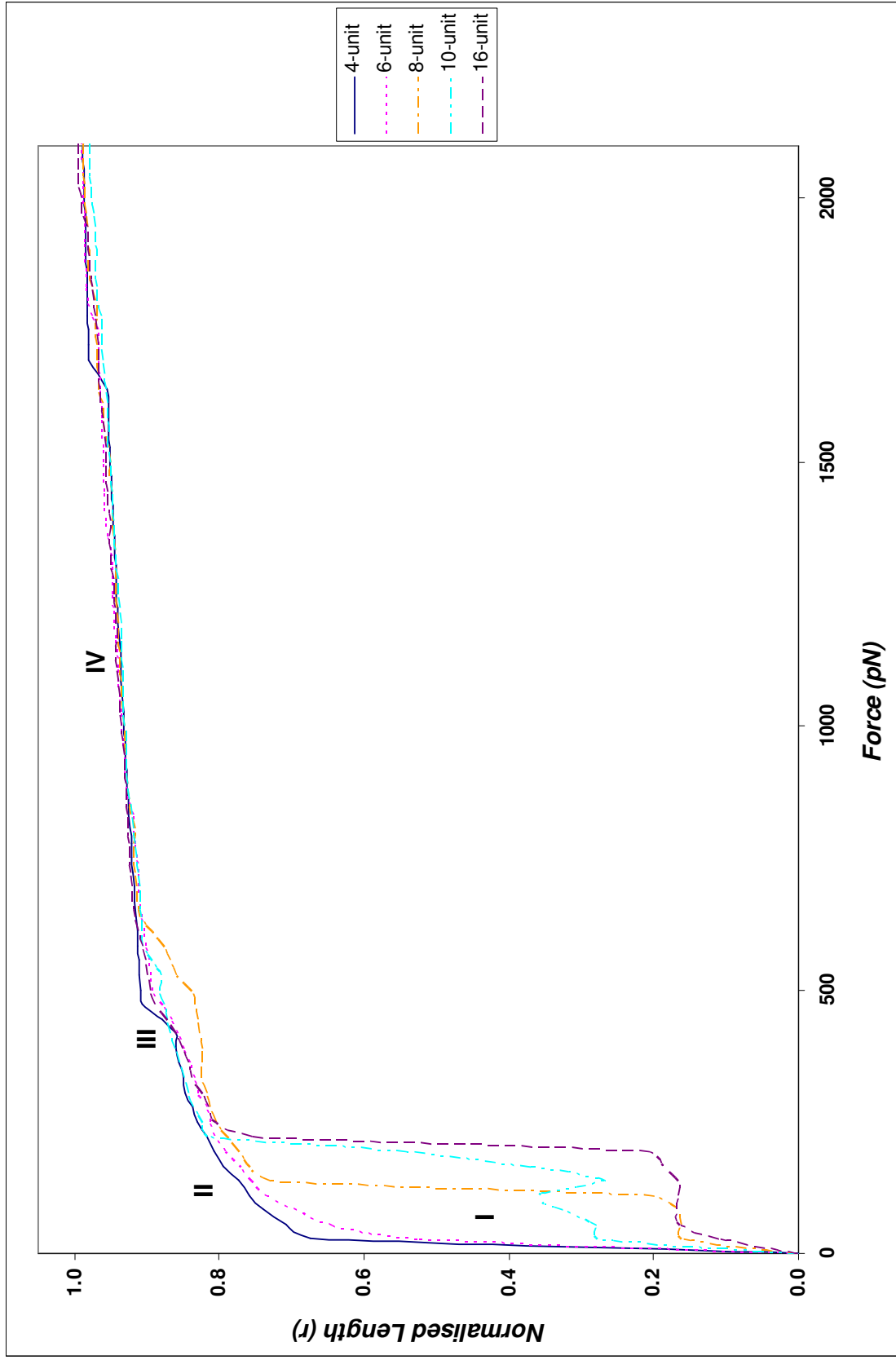


Figure 5: The force-extension curves produced by stretching simulations of 4, 6, 8, 10 and 16-unit amylose fragments.

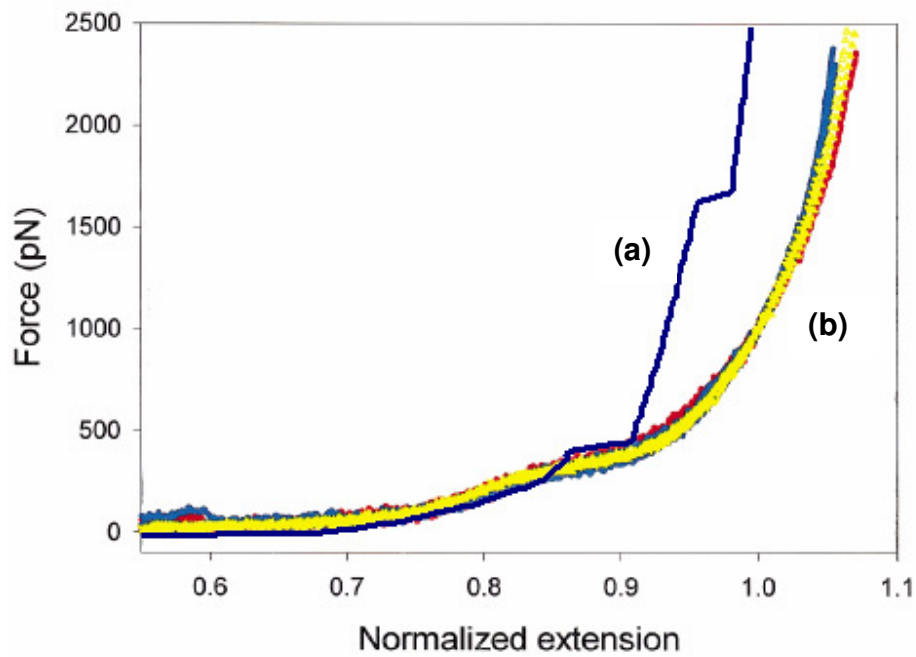


Figure 6: Comparison between the SMD (a) and AFM (b) [2] force-extension curves for a 4-unit amylose fragment.

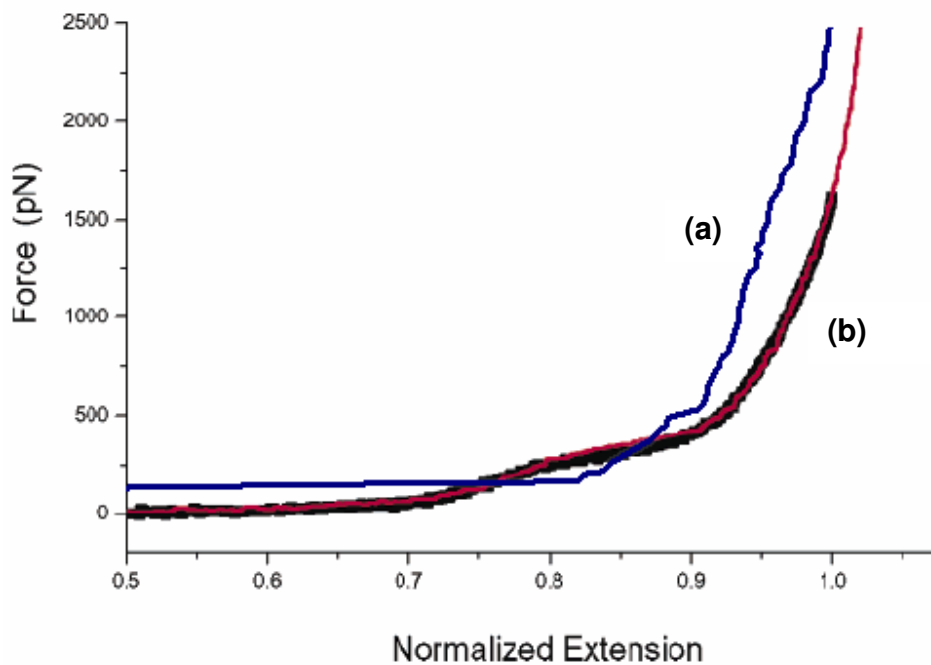


Figure 7: Comparison between the SMD (a) and AFM (b) [45] force-extension curves for a 10-unit amylose fragment.

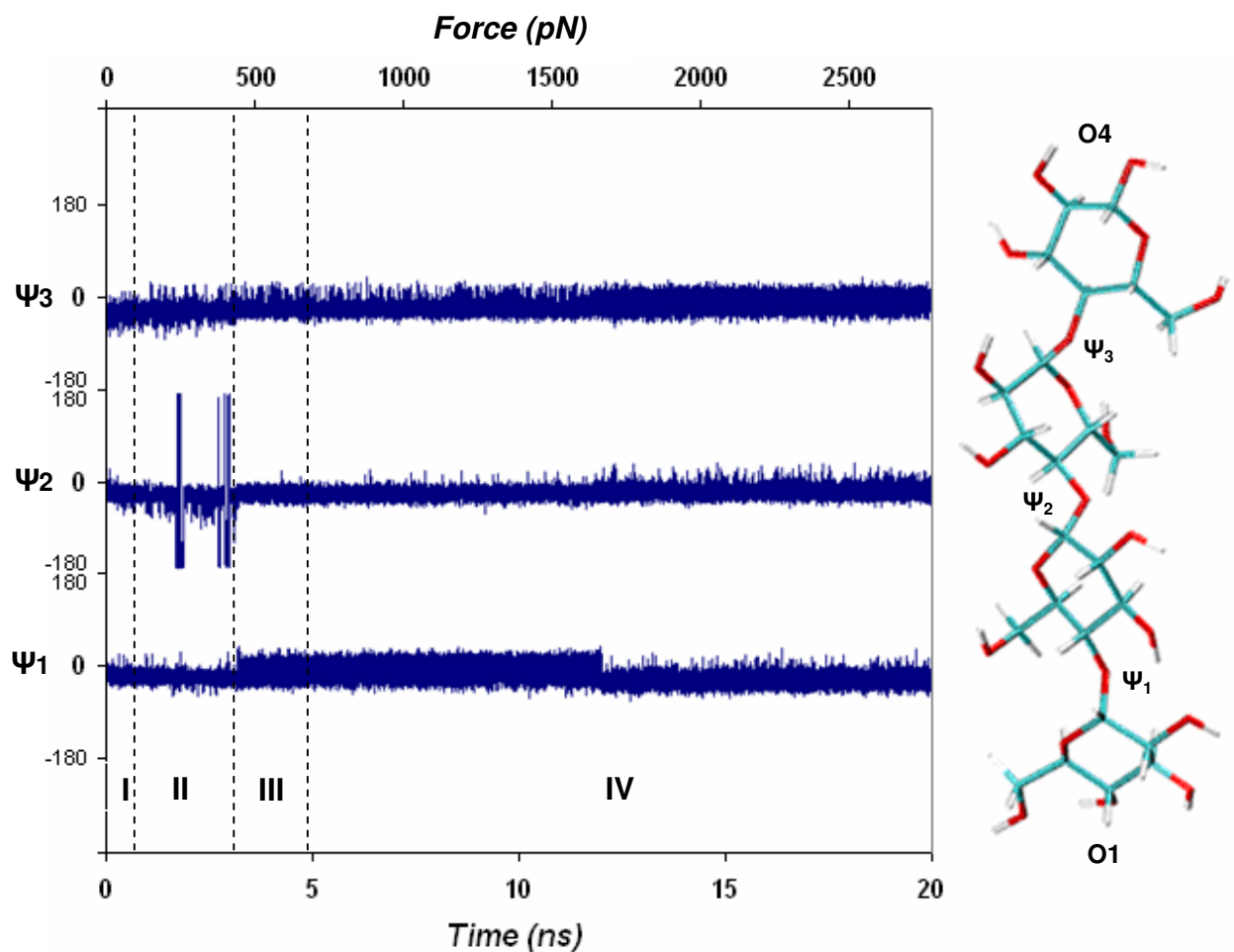


Figure 8: A section of the dihedral angle time series from the stretching simulation of the tetramer, showing transitions to anti conformations that occur during stage II in the force-extension curve.

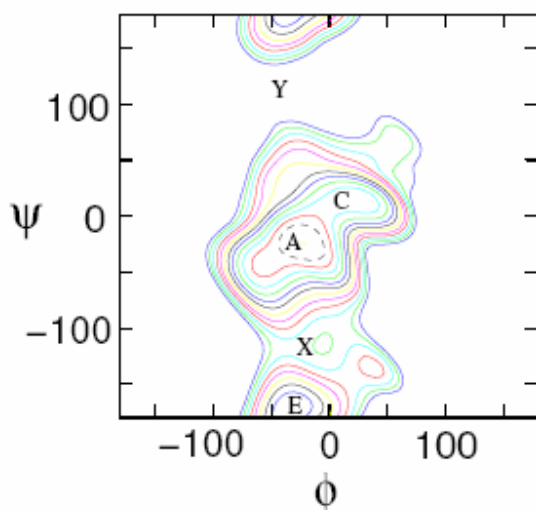


Figure 9: Contoured ϕ, ψ energy surfaces (PMF) for maltose in vacuum as calculated by Kuttel et al [4]. Contours are at 1 kcal/mol intervals above the global energy minimum, to a maximum of 12 kcal/mol. The first contour at 1 kcal/mol is dashed.

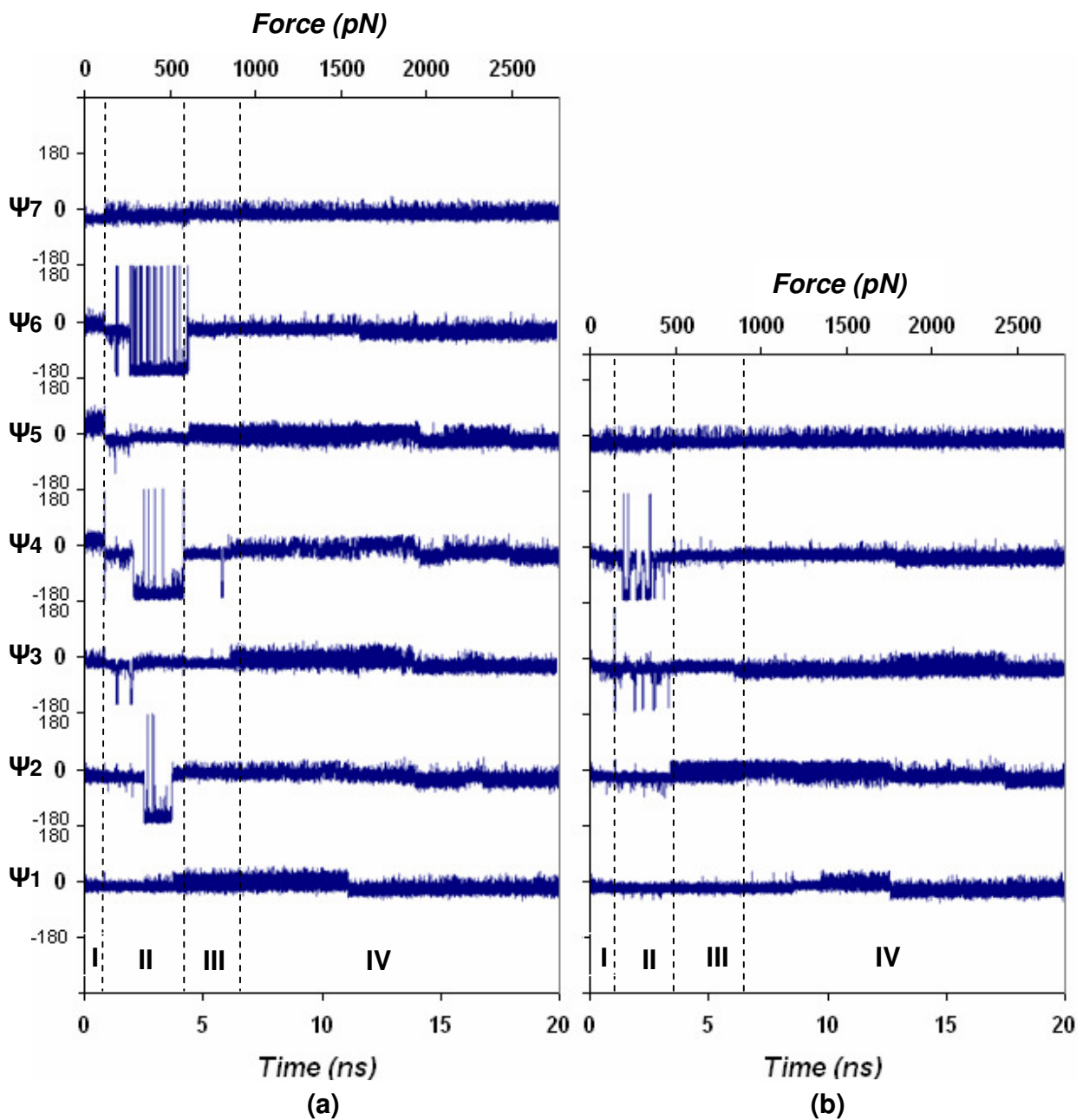


Figure 10: A section of the dihedral angle time series from the stretching simulation of the 8-unit (a) and 6-unit (b) amylose fragment, showing transitions to anti conformations that occur during stage II in the force-extension curve.

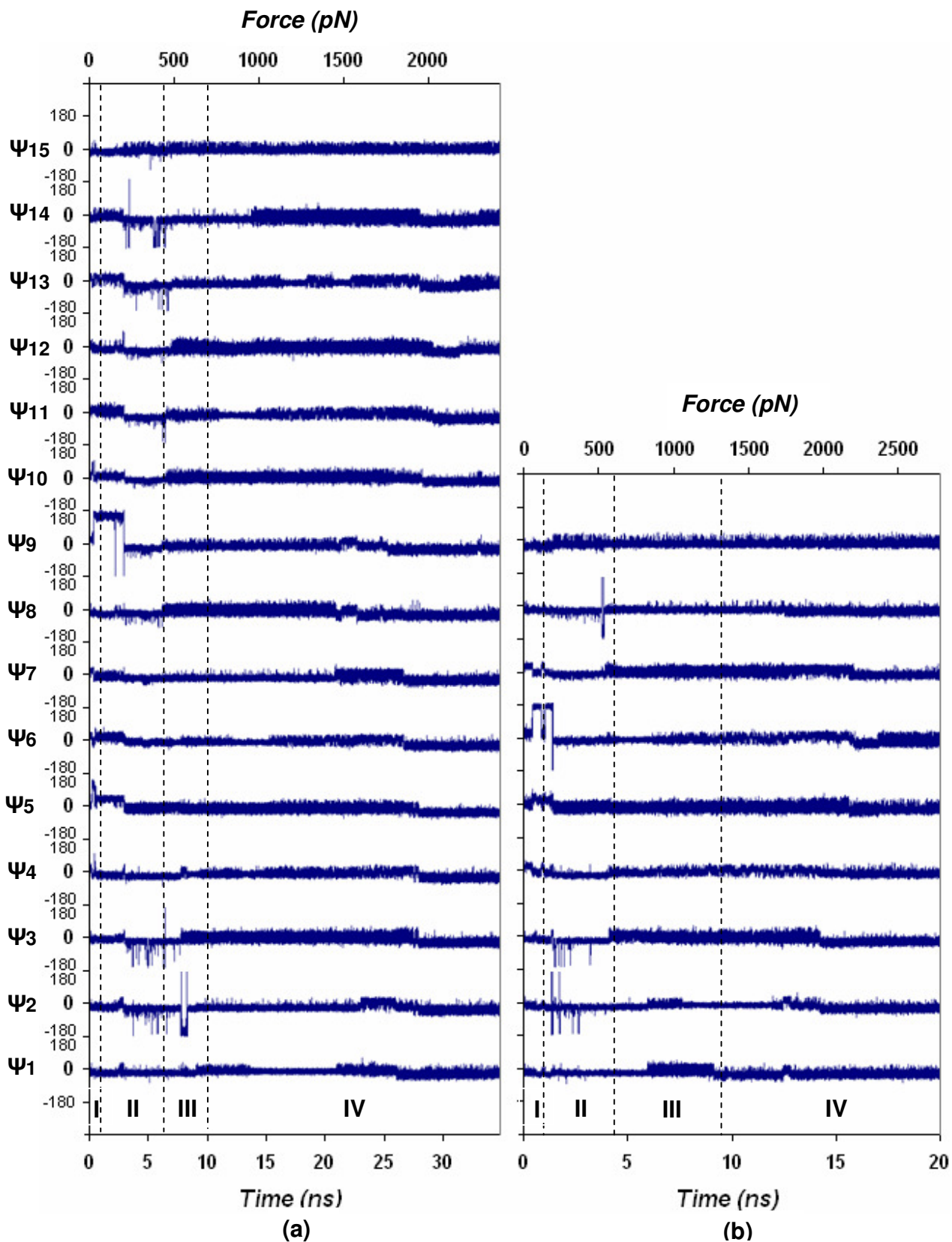


Figure 11: A section of the dihedral angles time series from the stretching simulation of the 16-unit (a) and 10-unit (b) amylose fragment, showing transitions to anti conformations that occur during stage II and III in the force-extension curve.

a *syn* to and *anti* conformation during this period, resulting in a flatter “semi-ribbon”. This can be seen in the time series plot in Figure 8: the ψ_2 angles moves from a range between 0 and -25 degrees (a *syn* conformation) to around 180 degrees (an *anti* conformation).

Figure 9 shows the contoured ϕ , ψ free energy plots calculated by Kuttel et al. [4], showing two possible low energy conformations for the ψ angle. Stretching provides enough energy to enable this dihedral angle to make the transition from the global energy minimum (marked A) to the next highest minimum (marked E). This stage corresponds to the same region previously identified by Kuttel et al. [51]. They observed that the amylose strand switches from a helical conformation to a flatter “ribbon” conformation and as the glycosidic linkages are subjected to further strain a slight lengthening of the stiff ribbon conformation can be observed. They explained that this conformation was due to a forced rotation of most of the glycosidic ψ dihedral angles from *syn* to *anti* conformations which disrupted the helical character of the strand. They also recorded an elasticity of 800 pN/nm. Marszalek et al. [31, 53], however, proposed that at this stage (forces below 50 pN and up to 200 pN) the flexibility of the chair conformation of the pyranose ring can be attributed to the presence of several distorted chair conformations that are of equal conformational energy but have very different torsional and bond angles.

Note that, for the tetramer, only ψ_2 makes the transition to the *anti*-conformation (twice, at 230 and 380 pN) - the other angles do not rotate. Similarly, the second stage of the 6-unit strand (< 472 pN) shows rotation of the ψ_3 and the ψ_4 dihedral to the *anti*-conformation, as depicted in Figure 10. In the 8-unit strand, four of the seven ψ angles (ψ_2 , ψ_3 , ψ_4 and ψ_6) made the transition to the *anti*-conformation.

Marszalek et al. [50] observed this stage at lower forces. They found that at approximately 250 pN the transition was complete and the chain was then composed of the rings in the boat-like conformation. At forces above 350 pN they found that small additional extensions come only from deforming the rings and bending the glycosidic linkages (intrinsic enthalpic elasticity of the segments).

The 10-unit fragment shows the rotation of the ψ_2 , ψ_3 , ψ_6 and the ψ_8 dihedral to the *anti*-conformation, whereas, in the case of the 16-unit fragment, most of the ψ dihedral angles transform to the *anti*-conformation (Figure 11). The second stage is, therefore, characterised by the transition of the dihedral angles to the *anti*-conformation.

Although the shorter chains had no chair-to-boat transitions at Stage II, the longer strands (10-, and 16-units) showed some chair-to-boat transitions. Residue 6 made the chair-to-boat transition for the 10-unit fragment and residues 6 and 9 flipped in the 16-unit fragment. It seems, therefore, that the longer the chain, the lower the force required before the first chair-to-boat transitions occur. This phenomenon could be due to not enough equilibration or kinks in the strand.

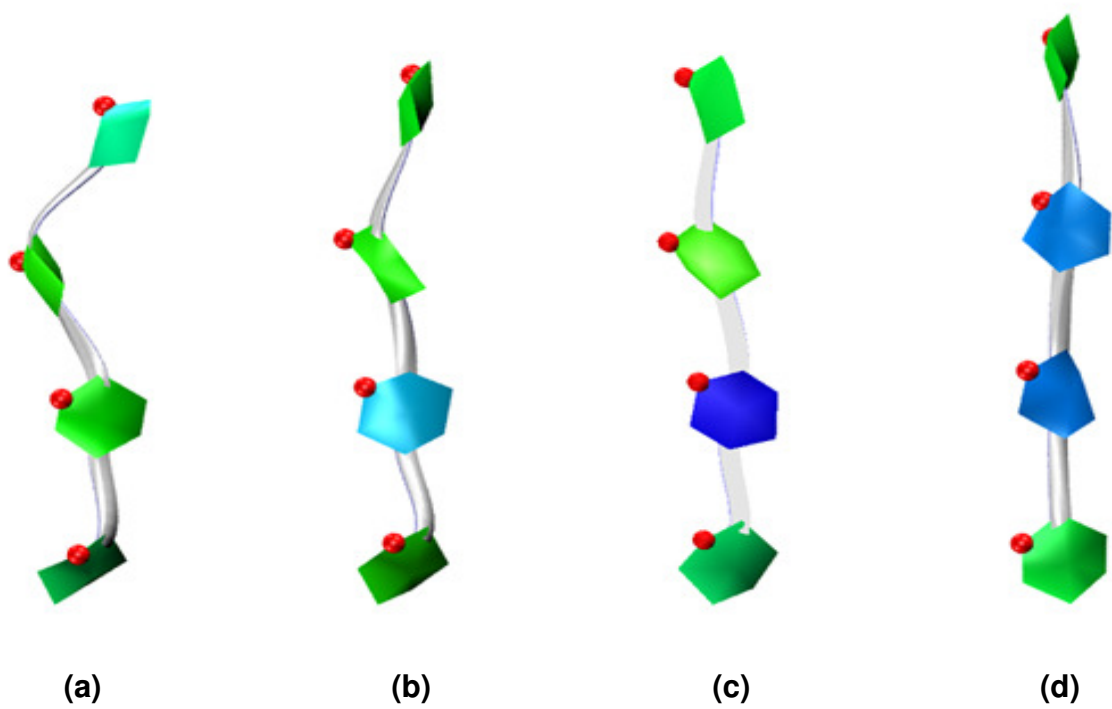


Figure 12: Snapshots from the stretching simulation of the tetramer depicted with the PaperChain, Twister and CPK (showing O5) VMD visualisation algorithms. (a) a helical conformation from Stage I and II (138 pN) of the force-extension curve, (b) snapshot from Stage III (444 pN), showing the second residue in a boat conformation (c) the twist-boat conformations from Stage IV (639 pN) and (d) snapshot showing the second and third residues in boat conformations.

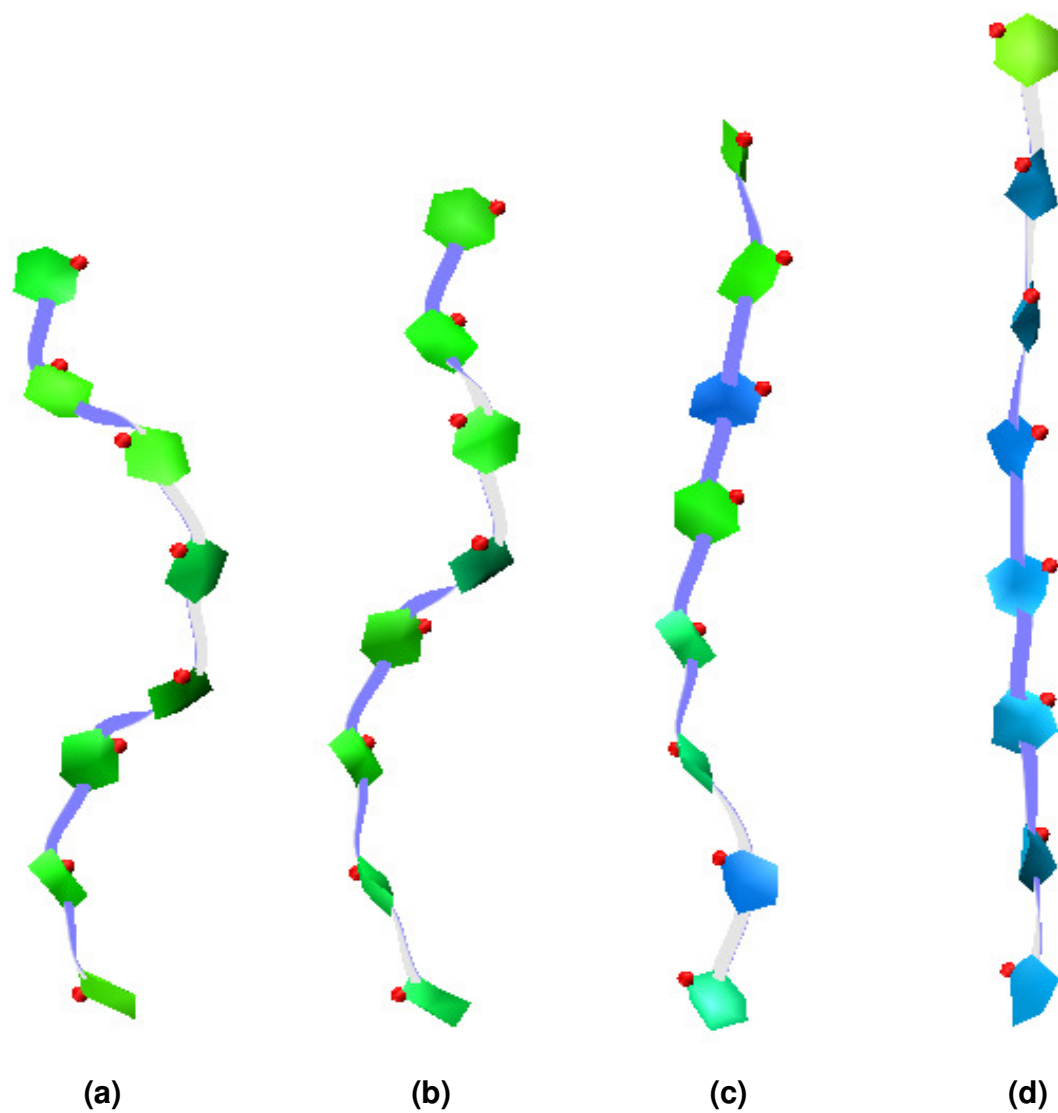


Figure 13: The stretching of the 8-unit fragment depicted with the PaperChain, Twister and CPK (showing O5) VMD visualisation algorithms, showing (a and b) a helical conformation from Stage I (138 pN) and II (333 pN) of the force-extension curve, (c) the chair-to-boat transitions from Stage III (528 pN) and (d) the chair-to-boat transitions of residue 1 to 7 from Stage IV (1973 pN).

4.3. Stage III

The third stage in the stretching of the oligomers involves a rapid increase in length, associated with transition of many of the residues in all strands from chair-to-boat transitions. Tables 4 – 8 show the respective chair-to-boat transitions for the different amylose strands.

Fisher et al. [8] observed the same characteristics at this stage when stretching a 5-unit amylose strand, at just above 200 pN, which is about 244 pN lower than we found in this study. During this stage, they saw a sudden increase in the elongation of the chain resulting from the chair-boat transitions of the constituent pyranose rings. Kuttel et al. [51], however, found that chair-to-boat transitional changes are not responsible for the extension of the molecule during this stage, but rather the ψ dihedrals reverting from *anti* to *syn*, thereby producing a maximally extended helical conformation.

For the tetramer, Stage III runs from 444 to 472 pN and has an elasticity of 443 pN/nm. During this period, the second residue converted from a chair to a boat conformation at 444 pN, as illustrated in Figure 12. This chair-to-boat transition can also be observed in the dihedral angle plot (Figure 8). The graph shows a distinct change around 444 pN: the ψ_3 angle transitions to the *anti*-conformation at the same time as the residue flips into boat conformation.

The third stage in the stretching of the 6-unit strand occurs at a slightly higher force of between 472 and 528 pN, with a single transition of the third residue from a chair to a boat conformation at 472 pN. The increase in length is not as rapid as that of the tetramer, resulting in a lower elasticity of 586 pN/nm.

During Stage III, the 8-unit strand shows two ring flips at 528 pN (second residue) and 583 pN (sixth residue), with an elasticity of 584 pN/nm. This is shown in Figure 12. The ψ_2 , ψ_4 and ψ_6 angles explore a wider range at the same time as the second and sixth residue flips into boat conformation (Figure 10).

During this stage the 10- and 16-unit strand shows two and three ring flips respectively at forces between 458 and 636 pN and elasticities of between 322 – 568 pN/nm.

4.4. Stage IV

Stage IV of the stretching for all oligomers is associated with a high elastic constant (4400 pN/nm for the tetramer, 4129 pN/nm for the hexamer and 3833 pN/nm for the octamer). Chair-boat conformational flips occur during this stage. This is in agreement with Kuttel et al. [4, 51], who found that most of the chair-to-boat transitions for an 18-unit strand occurred during this stage at forces between 800 pN and 2500 pN. Lu et al. [45], however, observed an abrupt change of the O1-C1-C2-O2 dihedral angles that flipped from

about $+60^\circ$ to -60° , which indicated that the sugar ring (the reducing end) switched from an envelope to a boat conformation at pulling forces in a range of 400 - 800 pN.

At 472 pN of the tetramer stretching simulation, the second pyranose ring switches between chair-boat and twist-boat conformation (Figure 12), with a small increase in molecular length. At forces above 1639 pN the tetramer shows another rapid increase in length as a second pyranose ring, the third residue, converted from a chair to a boat conformation. For this stage, the observed elasticity is 1029 pN/nm. Once again, this conformation can be observed by the sudden change in dihedral angle (Figure 8) for residues 1 to 2 and 3 to 4 at this force. At around 2779 pN, three of the four pyranose rings (residues 1, 2 and 3) have been converted from chair to boat. The fourth residue never reaches this conformation.

During Stage IV (> 528 pN) of the stretching of the 6-unit strand, the majority of the chair-to-boat transitions of the pyranose rings occur. At the end of the stage (1750 pN), four of the six pyranose rings (residue 1 to 4) have been converted from chair-to-boat. The same was observed for the 8-unit strand for this stage (> 639 pN). At 1834 pN, six of the 8 pyranose rings have been converted from chair to boat. The conformations can also be observed by the sudden change in dihedral angle (Figure 10) for residues 3, 4 and 6. The 6- and 8-unit strands also showed an additional chair-to-boat transition, with the fifth and seventh residues converting at 1779 and 1806 pN respectively.

Stage IV for the 10- and 16-unit occurs at forces of 833 and 625 pN, respectively. Once again, most of the chair-to-boat transitions take place at this stage. The conformations can be observed by the sudden change in dihedral angles (Figure 11). By the end of the stage (< 2779 pN), all but one (the last residue) of the pyranose rings have been converted from chair to boat. The last residue never reaches this conformation. In fact, this is true for all of the strands. The final residue (which is in β conformation) never flips.

Most of the chair-to-boat transitions, therefore, occur at higher forces and are responsible for most of the lengthening of the chain. Tables 4 – 8 shows the respective chair-to-boat transitions for the different amylose strands.

During stage II, the stretching mechanism is dominated by the rotational freedom of the glycosidic linkages. These stages were also where the lowest elasticities were measured. The rotations of the glycosidic torsion angles, therefore, also affect the elastic behaviour of amylose at lower forces. The shorter chains, however, had less dihedral rotations. The chair-to-boat transitions in the shorter chains produced a much bigger "shoulder" in the stretching curve than that of the longer chains. This anomaly occurs because, for the short chains, the conversion of one ring increases the end-to-end distance more than for a longer chain length.

Stage	Force (pN)	No. of Chair-to-Boat Transitions	Residue
III	444	1	2
IV	1639	2	2, 3
IV	1661	3	2, 3, 1

Table 4: The chair-to-boat transitional changes for the stretching of the tetramer at an interval length of 20 ns.

Stage	Force (pN)	No. of Chair-to-Boat Transitions	Residue
III	472	1	3
IV	834	2	3, 4
IV	1195	3	3, 4, 1
IV	1751	4	3, 4, 1, 2
IV	1779	5	3, 4, 1, 2, 5

Table 5: The chair-to-boat transitional changes for the stretching of the hexamer at an interval length of 20 ns.

Stage	Force (pN)	No. of Chair-to-Boat Transitions	Residue
III	528	1	2
III	611	2	2, 6
IV	861	3	2, 4, 6
IV	1556	4	1, 2, 4, 6
IV	1611	5	1, 2, 4, 6, 7
IV	1834	6	1, 2, 4, 6, 7, 3
IV	1973	7	1, 2, 4, 6, 7, 3, 5

Table 6: The chair-to-boat transitional changes for the stretching of the 8-unit fragment at an interval length of 20 ns.

Stage	Force (pN)	No. of Chair-to-Boat Transitions	Residue
I	138	1	6
II	555	2	6, 8
III	583	3	6, 8, 4
III	833	4	6, 8, 4, 2
IV	1278	5	6, 8, 4, 2, 1
IV	1750	6	6, 8, 4, 2, 1, 9
IV	1973	7	6, 8, 4, 2, 1, 9, 3
IV	2195	8	6, 8, 4, 2, 1, 9, 3, 5
IV	2223	9	6, 8, 4, 2, 1, 9, 3, 5, 7

Table 7: The chair-to-boat transitional changes for the stretching of the 10-unit fragment at an interval length of 20 ns.

Stage	Force (pN)	No. of Chair-to-Boat Transitions	Residue
I	55	1	6
II	416	2	6, 9
III	458	3	6, 9, 11
III	486	4	6, 9, 11, 13
III	528	5	6, 9, 11, 13, 4
IV	625	6	6, 9, 11, 13, 4, 1
IV	953	7	6, 9, 11, 13, 4, 1, 15
IV	1452	8	6, 9, 11, 13, 4, 1, 15, 8
IV	1757	9	6, 9, 11, 13, 4, 1, 15, 8, 10
IV	1807	10	6, 9, 11, 13, 4, 1, 15, 8, 10, 2
IV	1854	11	6, 9, 11, 13, 4, 1, 15, 8, 10, 2, 7
IV	1940	12	6, 9, 11, 13, 4, 1, 15, 8, 10, 2, 7, 3
IV	1950	13	6, 9, 11, 13, 4, 1, 15, 8, 10, 2, 7, 3, 14
IV	1995	14	6, 9, 11, 13, 4, 1, 15, 8, 10, 2, 7, 3, 14, 12

Table 8: The chair-to-boat transitional changes for the stretching of the 16-unit fragment at an interval length of 40 ns.

Our SMD simulations overestimate the forces necessary to stretch the amylose fragment as compared to AFM measurements. The elasticities calculated from the curves of each stretching stage are lower than those of the AFM experiments. In most of the AFM experiments, at around 200 pN, chair-boat transitions of the pyranose rings were observed. In our simulations, however, the first chair-boat transitions were observed around 450 pN.

This is probably because the ramping rate used in the simulations was much faster than the experimental ramping rate. Faster ramping rates were found to increase the force required to reach a particular extension of an amylose fragment [57] i.e. a faster ramping rate will result in a higher force measured for a particular transition. One would therefore expect the forces measured in the simulations to be higher compared to that of the AFM experiments (refer to section 4.5).

Moreover, the SMD simulations were performed in vacuum, whereas the AFM experiment was performed using a molecule lifted from solution. In vacuum, a higher force is required to stretch the strand, because of the strong intra-molecular interactions between successive residues as well as neighbouring helical turns. These interactions are considerably reduced in solution due to the general electrostatic masking effect of the solvent and the hydrogen bonding capabilities of the water molecules.

Kuttel et al. also observed this in their simulations performed in vacuum. They attributed this to the fact that the AFM estimations were based on a two-state freely jointed chain (FJC) model which required a prediction of the number of monomers in the strand being stretched and neglected to take into account possible helical conformations of the chain. It is therefore likely that the two-state model underestimated the actual contour length of the chain which could result in an underestimate of the number of monomers present in the molecule, and thus the lower forces measured during each stretching stage.

4.5. The Effect of the Ramping Rate on the Stretching Curve.

To establish the effect of the stretching speed on the force-extension curve, stretching simulations were performed on the 8-, 10- and 16-unit fragments with a slower ramping rate (Figure 14). For these simulations the force was incremented by 6.948 pN ($0.1 \text{ kcal.mol}^{-1}.\text{\AA}^{-1}$) for each consecutive simulation.

The slower ramping rate results in a lower observed force for the features in the stretching curve. This is because the strength of intermolecular interactions is dependent on the applied force [57]. A faster ramping rate will therefore require higher forces to achieve the same extension.

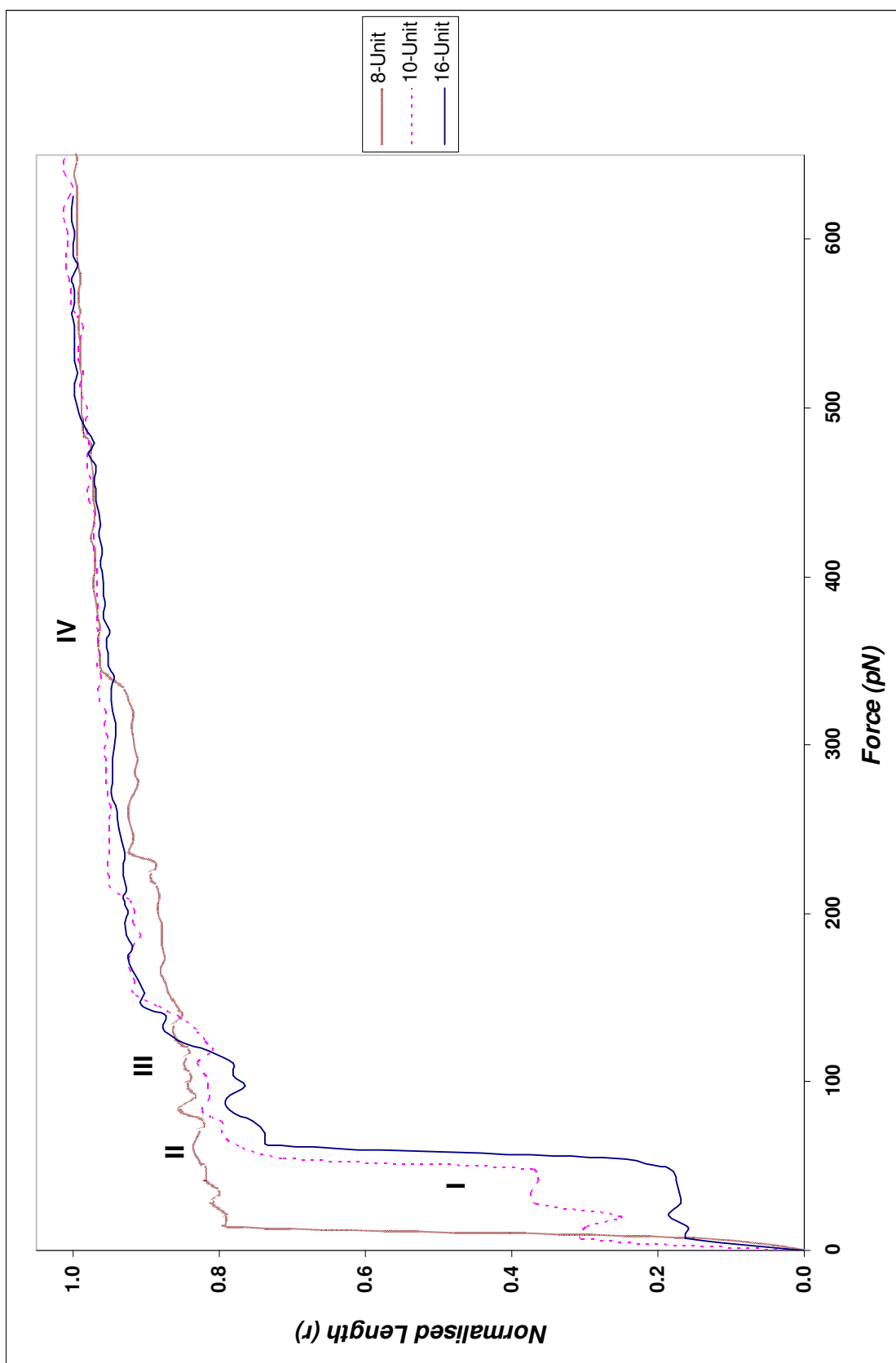


Figure 14: The force-extension curves produced by stretching simulations of an 8-, 10- and 16-unit amylose fragment at a ramping force of $0.1 \text{ kcal.mol}^{-1} \text{ \AA}^{-1}$.

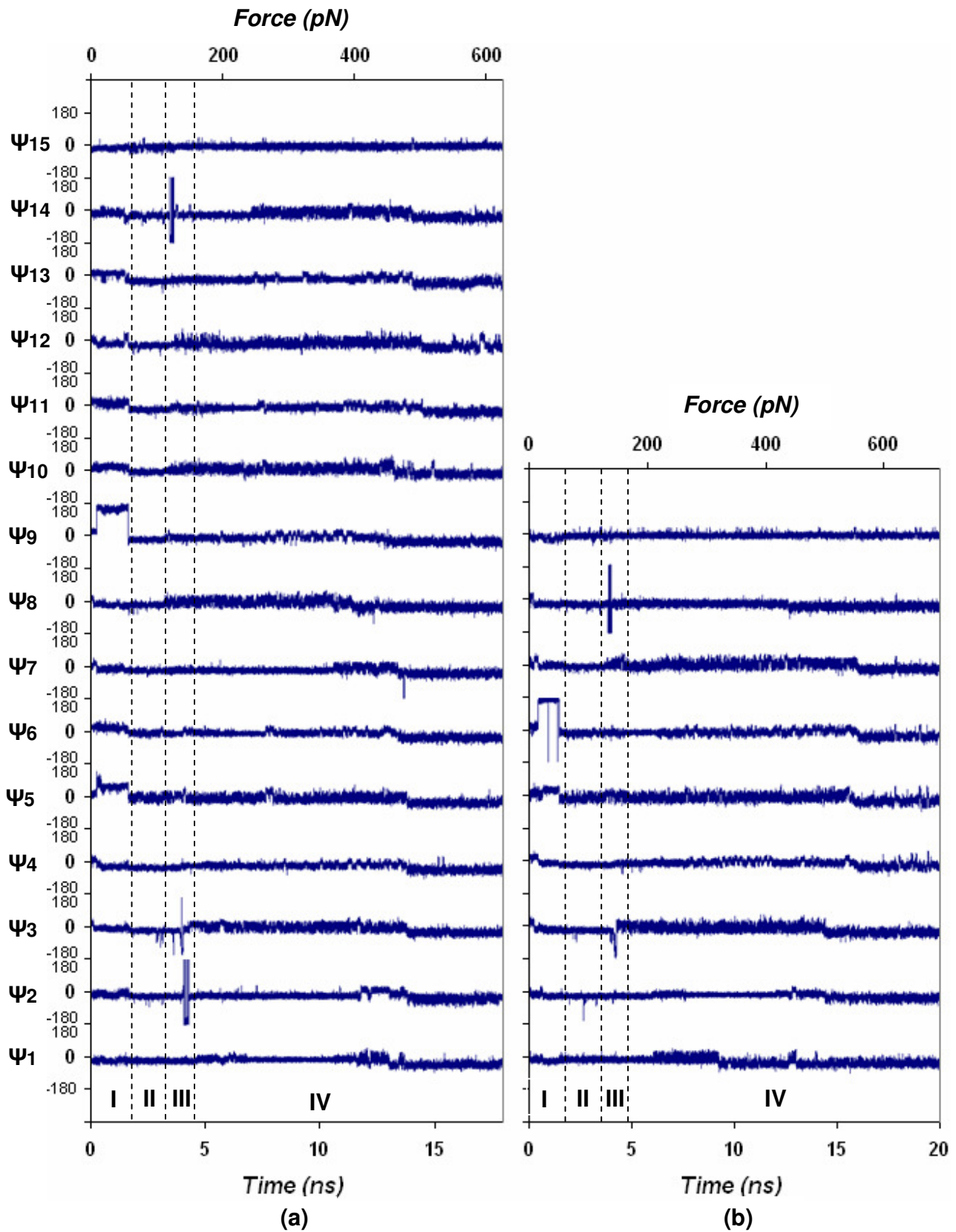


Figure 15: A section of the dihedral angles time series from the stretching simulation of the 16-unit (a) and 10-unit (b) amylose fragment, showing transitions to anti conformations that occur during stage II and III in the force-extension curve.

Stage	Force (pN)	No. of Chair-to-Boat Transitions	Residue
IV	233	1	2
IV	333	2	2, 4
IV	341	3	2, 4, 6
IV	450	4	2, 4, 6, 1

Table 9: The chair-to-boat transitions of the 8-unit fragment at a ramping force of $0.1 \text{ kcal.mol}^{-1}.\text{\AA}^{-1}$.

Stage	Force (pN)	No. of Chair-to-Boat Transitions	Residue
I	6	1	6
III	139	2	6, 8
III	146	3	6, 8, 4
IV	208	4	6, 8, 4, 2
IV	230	5	6, 8, 4, 2, 1
IV	438	6	6, 8, 4, 2, 1, 9
IV	501	7	6, 8, 4, 2, 1, 9, 3
IV	549	8	6, 8, 4, 2, 1, 9, 3, 5
IV	556	9	6, 8, 4, 2, 1, 9, 3, 5, 7

Table 10: The chair-to-boat transitions of the 10-unit fragment at a ramping force of $0.1 \text{ kcal.mol}^{-1}.\text{\AA}^{-1}$.

Stage	Force (pN)	No. of Chair-to-Boat Transitions	Residue
I	14	1	6
II	111	2	6, 9
III	118	3	6, 9, 11
III	125	4	6, 9, 11, 13
III	139	5	6, 9, 11, 13, 4
IV	160	6	6, 9, 11, 13, 4, 1
IV	244	7	6, 9, 11, 13, 4, 1, 15
IV	368	8	6, 9, 11, 13, 4, 1, 15, 8
IV	445	9	6, 9, 11, 13, 4, 1, 15, 8, 10
IV	466	11	6, 9, 11, 13, 4, 1, 15, 8, 10, 2, 7
IV	479	13	6, 9, 11, 13, 4, 1, 15, 8, 10, 2, 7, 3, 5
IV	486	14	6, 9, 11, 13, 4, 1, 15, 8, 10, 2, 7, 3, 5, 14
IV	500	15	6, 9, 11, 13, 4, 1, 15, 8, 10, 2, 7, 3, 5, 14, 12

Table 11: The chair-to-boat transitions of the 16-unit fragment at a ramping force of $0.1 \text{ kcal.mol}^{-1}.\text{\AA}^{-1}$.

Once again, the curves display the same distinctive transitions seen in force-ramp AFM stretching experiments [31, 53, 41, 45, 50], but in this case the forces recorded were much closer to the experimental values (Tables 9 - 11). During the first stage (< 69 pN) all strands extend without any psi (ψ) dihedral angle rotations (except for residue 6 on the 10-unit fragment) or chair-to-boat transitions, with a low elasticity in the region of 9 pN/nm.

Stage II of the faster ramping rate simulations was once again associated with transitions of ψ -dihedral angles from *syn* to *anti* conformations. In this case, however, the molecular mechanism is not determined by the *syn* to *anti* conformations of the dihedral angles. No psi (ψ) rotations were observed, with only the 16-unit fragment showing chair-to-boat transitions of residues 6 and 9 (Figure 15). This stage recorded a higher elasticity of 349 and 124 pN/nm for the 10- and 16-unit molecules respectively.

Stage III (< 152 pN) shows the first abrupt transition in the force-extension curve at a force of 132 pN. This rapid increase in length is associated with not only chair-to-boat transitions, but also some brief rotations of the dihedral angles from *syn* to *anti* conformations. The 10-unit fragment shows the rotation of the ψ_8 dihedral to the *anti*-conformation, whereas, in the case of the 16-unit fragment, the ψ_2 , ψ_3 and ψ_{14} dihedral angles transform to the *anti*-conformation (Figure 15). These dihedral angle rotations were previously observed during stage II in the simulations performed with the faster ramping rates. The 10- and 16-unit strands show three and five ring flips respectively for this region, with a low elasticity of between 33 and 47 pN/nm. What is interesting to note here is that the order of the chair-to-boat transitions are identical to that of the faster ramping rate simulations (every alternating ring) but at much lower forces (Table 9, 10, 11).

The force range of this stage (between 132 and 152 pN) is also much closer to that observed by Marszalek et al. [31, 53, 41, 8] for the same region during their AFM experiments. They found that at forces up to 200 pN the flexibility of the chair conformation of the pyranose ring can be attributed to the presence of several distorted chair conformations that are of equal conformational energy but have very different torsional and bond angles.

Stage IV (> 152 pN) is associated with chair-boat conformational flips with a high elastic constant (1255 pN/nm for the 10-unit and 618 pN/nm for the 16-unit fragment). Most of the chair-to-boat transitions occurred during this stage with each transition resulting in a small “shoulder” in the stretching curve. No psi (ψ) rotations were observed. At the end of the stage (695 pN), nine of the 10 pyranose rings (residue 1 to 9) converted from chair to boat conformations for the 10-unit strand. The same was observed for the 16-unit strand, with fifteen of the sixteen pyranose rings converting from chair to boat. In both cases the last residue never reaches this conformation, because it is in the β conformation. As can be seen from tables 9 – 11, the chair-to-boat transitions continued until 556 pN during this stage.

Throughout the simulations, the faster ramping rate produced a shorter molecule length at the same force, compared to that of the slower ramping rate. The transitions are similar in shape (though less smooth), but occur at lower forces, proving that decreasing the ramping rate lowers the expected force. The mechanism is essentially the same, with very little change from the first batch of simulations. This confirms the fact that faster ramping rates requires higher forces to reach a particular extension of an amylose fragment and therefore does affect the molecular mechanism. The slower ramping rates were found to be adequate for reproduction of the experimental curve, although the curves are more jagged. Similar jagged profiles were seen in previous studies performed by Lu et al. [45]. This is attributable to the shorter simulation intervals used (2 vs. 20 ns), which resulted in less equilibration for the strand.

Kuttel et al. [4, 51] suggested that the primary mechanism for relieving tensile strain in α -linked polysaccharides, like amylose, involves complex rotations of the glycosidic linkages and that the chair-to-boat transitions of the pyranose rings play a smaller role. Marszalek et al. [31, 41, 50, 53] and Lu et al. [45], however, concluded that polysaccharides with axial linkages, such as amylose, undergo abrupt force-induced length transitions, which were caused by the shift of individual pyranose rings from the chair conformation to the boat or the inverted chair conformations which provide an increased distance between glycosidic bonds. Our slower ramping rate stretching simulations suggest that the molecular mechanism can be explained by a combination of psi (ψ) rotations and chair-to-boat transitional changes. The chair-to-boat transitions dominate this mechanism since these produced distinct “shoulders” in the stretching curves even at high forces. Almost half the chair-to-boat transitional changes occur in quick succession in the first part of the curves and then the rest follow later, with a much greater interval between them whereas, only a few psi (ψ) rotations occurred during stage III.

4.6. The Effect of Oligosaccharide Length on the Stretching Curve.

Different chain lengths were used in this study to investigate the effect of oligosaccharide length on the stretching curve. The ratio of *anti*-conformations observed in the longer chains is higher than that of the shorter chains. Chair-to-boat transitional changes of the pyranose rings of the shorter chains only occurred anti-cooperatively at high stretching forces whereas much lower forces were recorded for the longer chains. Furthermore, for the shorter chains most of these conversions produced the characteristic “shoulder” in the amylose stretching curve. These conversions occurred at lower forces in the longer chains and produced a less pronounced “shoulder” in the stretching curve. This is because the short chain length makes the conversion of one ring much greater than it would appear for a longer chain length. These distinctive transitions are not that clear in the stretching profile of the 8-unit fragment and is therefore not considered a good ‘model’ to determine the molecular mechanism.

5. Conclusions and Future Work

Measurement of force-induced elongation with steered molecular dynamics simulations can determine the structural and mechanical properties of single-molecule polysaccharides and therefore offer a new perspective in the identification and characterisation of mechanical functions of polysaccharides in their helical states.

In this work, we confirmed that the elastic behaviour of amylose is governed by the mechanics of the pyranose rings and their force-induced conformational transitions. The molecular mechanism can be explained by a combination of *syn* and *anti*-parallel conformational changes of the dihedral angles (ψ rotations) and chair-to-boat transitional changes. The chair-to-boat transitions dominate this mechanism since these produced distinct “shoulders” in the stretching curves even at high forces. Almost half the chair-to-boat transitional changes of the pyranose rings occur in quick succession in the first part of the curves (cooperatively) and then the rest follow later (anti-cooperatively) at higher forces, with a much greater interval between them. At low forces, the amylose stretching profile is characterised by the transition of the dihedral angles to the *anti*-conformation with low elasticities measured for all the chain lengths. The *anti*-conformation affects the elasticity of the molecule at lower forces, whereas, the chair-to-boat transitions accounted for most of the elastic behaviour of amylose at higher forces. Chair-to-boat transitional changes of the pyranose rings of the shorter chains only occurred anti-cooperatively at high stretching forces whereas much lower forces were recorded for the longer chains.

The elasticities calculated from the curves of each stretching stage were considerably lower than those of the AFM experiments. This was attributed to the fact that the ramping rate used in the SMD simulations was much faster than the experimental ramping rate. Simulations performed to determine the effect of ramping rates on the molecule’s stretching behaviour showed that faster ramping rates produced a shorter molecule length at the same force, compared to that of the slower ramping rates. The transitions are similar in shape, but occur at lower forces, proving that decreasing the ramping rate lowers the expected force. The mechanism is essentially the same, with very little change from the first batch of simulations. We therefore confirmed that faster ramping rates requires higher forces to reach a particular extension of an amylose fragment and therefore does affect the molecular mechanism. The simulations performed with the slower ramping rates were found to be adequate for reproduction of the experimental curve.

Future work could include further SMD stretching simulations on other oligosaccharides such as the $\alpha(1\rightarrow4)$ -linked pectin and the $\alpha(1\rightarrow6)$ -linked dextran molecules. The amylose molecule could also be explored more thoroughly by performing simulations on longer chain lengths (32 units and up) and by changing simulation parameters such as force increments and ramping rates. Also, since the simulations in this study were all performed in vacuum, the effect of solution on oligosaccharides could be investigated with solution simulations.

6. References

1. S. Izrailev, S. Stepaniants, B. Israilewitz, D. Kosztin, H. Lu, F. Molnar, W. Wriggers, and K. Schulten. Beckman Institute. University of Illinois at Urbana-Champaign. Tutorial, Steered Molecular Dynamics.
2. P. E. Marszalek, H. Li, and J.M. Fernandez. Fingerprinting polysaccharides with single molecule atomic force microscopy. *Nat. Biotechnol*, 19, 2001.
3. R. Hoover. Composition, molecular structure, and physicochemical properties of tuber and root starches. *Carbohydrate Polymer*, 45:253-267, 2001.
4. M. M. Kuttel. Carbohydrate Conformational Dynamics and Thermodynamics. Ph.D. University of Cape Town, 2003.
5. L. Kale, R. Skeel, M. Bhandarkar, R. Brunner, A. Gursoy, N. Krawetz, J. Phillips, A. Shinozaki, K. Varadarajan, and K. Schulten. NAMD2: Greater scalability for parallel molecular dynamics. *J. Comp. Phys.*, 151:283-312, 1999.
6. B. R. Brooks, R. E. Bruccoleri, B. D. Olafson, D. J. States, S. Swaminathan, and M. Karplus. CHARMM: A program for macromolecular energy, minimization and dynamics calculations. *J. Comput. Chem.*, 4(2):187-217, 1983.
7. D. Larry, P.E. Hanke. Handbook of Analytical Methods. Materials Evaluation and Engineering. Atomic Force Microscope, 1:7-11, 2006.
8. T. E. Fisher, P. E. Marszalek, A. F. Oberhauser, M. Carrion-Vazquez, and J. M. Fernandez. The micro-mechanics of single molecules studied with atomic force microscopy. *The Journal of Physiology*, 520.1: 5-14, 1999.
9. Q. Zhang, Z. Lu, H. Hu, W. Yang, and P. E. Marszalek. Direct Detection of the Formation of V-Amylose Helix by Single Molecule Force Spectroscopy. *J. Am. Chem. Soc.*, 128:9387-9393, 2005.

10. P. E. Marszalek, A. F. Oberhauser, H. Li, and J. M. Fernandez. The Force-Driven Conformations of Heparin Studied with Single Molecule Force Microscopy. *Biophysical Journal*, 85:2696-2704, 2003.
11. P. Buléon, V. Colonna, and S. Ball. Starch granules: structure and biosynthesis. *J. Biol. Macromol.*, 23:85-112, 1998.
12. B. J. Hardy, A. Gutierrez, K. Lesiak, E. Seidl, and G. Widmalm. Structural analysis of the solution conformation of methyl 4-O- β -D-glucopyranosyl- α -D-glucopyranoside by Molecular Mechanics and *ab initio* calculation, stochastic dynamics simulation and NMR spectroscopy. *J. Phys. Chem.*, 100:9187-9192, 1996.
13. A. Vishnyakov, G. Widmalm, J. Kowalewski, and A. Laaksonen. Molecular dynamics simulation of the α -D-Man ρ -(1 - 3)- β -D-Glc ρ -OMe disaccharide in water and water/DMSO solution. *J. Am. Chem. Soc.*, 121:5403-5412, 1999.
14. J. W. Brady. Molecular dynamics simulations of α -D-glucose in aqueous solution. *J. Am. Chem. Soc.*, 111:5155-5165, 1989.
15. D. A. Brant. Shapes and motions of polysaccharide chains. *Pure & Appl. Chem.*, 69(9):1885-1892, 1997.
16. R. Parker and S. G. Ring. Aspects of the physical chemistry of starch. *J. Cereal Sci.*, 34:1-17, 2001.
17. E. K. Wilson. Calculating carbohydrates. *Chemical & Engineering News*, 17:36-39, 2004.
18. H. Montès, and J. Y. Cavaille. Secondary relaxations in dried amorphous cellulose and dextran. *Polymer*, 40:2649-2657, 1999.
19. K. Gessler, T. Takaha, N. Krauss, S. M. Smith, S. Okada, G. M. Sheldrick, and W. Saenger. V-amylose at atomic resolution: X-ray structure of a cycloamylose with 26 glucose residues (cyclomaltohexacosaoase). *Proc. Natl. Acad. Sci. USA*, 96:4246-4251, 1999.
20. P. Zugenmaier. Conformation and packing of various crystalline cellulose fibers. *Prog. Polym. Sci.*, 26:1341-1417, 2001.

21. D. A. Brant, H. S. Liu, and Z. S. Zhu. The dependence of glucan conformational dynamics on linkage position and stereochemistry. *Carbohydr. Res.*, 278:11-26, 1995.
22. D. A. Brant. Shapes and motions of polysaccharide chains. *Pure & Appl. Chem.*, 69:1885-1892, 1997.
23. H. Sugiyama, K. Hisamichi, T. Usui, K. Sakai, and J. I. Ishiyama. A study of the conformation of β -1, 4-linked glucose oligomers, cellobiose to cellohexaose, in solution. *J. Mol. Struct.*, 556:173-177, 2000.
24. D. A. Rees, and D. Thorn. Polysaccharide conformation. Solvent and temperature effects on the optical rotation and conformation of model carbohydrates. *J. C. S. Perkin II*, 10:191-201, 1977.
25. E. S. Stevens, and B. K. Sathyanarayana. Potential energy surfaces of cellobiose and maltose in aqueous solution: a new treatment of disaccharide optical rotation. *J. Am. Chem. Soc.*, 12:4149-4154, 1989.
26. R. Stenutz, and G. Widmalm. Conformational exibility of carbohydrates: A folded conformer at the ϕ dihedral angle of a glycosidic linkage. *J. Am. Chem. Soc.*, 119:8695-8698, 1997.
27. G. M. Lipkind, V. E. Verovsky, and N. K. Kochetkov. Conformational states of maltose and cellobiose in solution: a comparison of calculated and experimental data. *Carbohydr. Res.*, 133:1-13, 1984.
28. D. A. Brant. Novel approaches to the analysis of polysaccharide structures. *Curr. Opin. Struc. Biol.*, 9:556-562, 1999.
29. M. Rief, F. Oesterhelt, B. Heymann, and H. E. Gaub. Single molecule force spectroscopy on polysaccharides by atomic force microscopy. *Science*, 275:1295-1297, 1997.
30. H. Li, M. Rief, F. Oesterhelt, H. E. Gaub, X. Zhang, and J. Shen. Single-molecule force spectroscopy on polysaccharides by AFM. *Chem. Phys. Lett.*, 305:197-201, 1999.
31. P. E. Marszalek, H. Li, A. F. Oberhauser, and J. M. Fernandez. Chair-boat transitions in single polysaccharide molecules observed with force-ramp AFM. *Proc. Natl. Acad. Sci. USA*, 7:4278-4283, 2002.

32. M. Kadkhodaei, H. Wu, and D. A. Brant. Comparison of the conformational dynamics of the (1 - 4) and (1 - 6)-linked α -D-glucans using ^{13}C -NMR relaxation. *Biopolymers*, 31:1581-1592, 1991.
33. P. O'Donoghue, and Z. A. Luthey-Schulten. Barriers to forced transitions in polysaccharides. *J. Phys. Chem. B.*, 104:10398-10405, 2000.
34. J. Sugiyama, R. Vuong, and H. Chanzy. Electron diffraction study on the two crystalline phases occurring in native cellulose from an algal cell wall. *Macromolecules*, 24:4168-4175, 1991.
35. W. Hindrichs, M. Steifa, C. Betzel, V. Zabel, B. Pfannemüller, and W. Saenger. An amylose antiparallel double helix at atomic resolution. *Science*, 238:205-208, 1987.
36. W. Banks, and C. T. Greenwood. The hydrodynamic behaviour of amylose in good solvents. *Carbohydr. Res.*, 7:414-420, 1968.
37. A. Perico, M. Mormino, R. Urbani, A. Cesàro, E. Tylianakis, P. Dais, and D. A. Brant. Local dynamics of carbohydrates. Dynamics of simple glycans with different chain linkages. *J. Phys. Chem. B*, 103:8162-8171, 1999.
38. D. A. Brant, and W. L. Dimp. A theoretical interpretation of the aqueous solution properties of amylose and its derivatives. *Macromolecules*, 3:655-665, 1970.
39. M. Rief, F. Oesterhelt, B. Heymann, and H. E. Gaub. Single molecule force spectroscopy on polysaccharides by atomic force microscopy. *Science*, 275:1295-1297, 1997.
40. S. Cross and M. M. Kuttel. *Visualisation of Cyclic and Multi-Branched Molecules with VMD*. University of Cape Town, 2009.
41. T. E. Fisher, P. E. Marszalek, and J. M. Fernandez. Stretching single molecules into novel conformations using the atomic force microscope. *Nature Structural Biology*, 7:719-723, 2000.
42. S. J. Angyal. The composition and conformation of sugars in solution. *Chem. Int. Ed. Engl.*, 8:157-226, 1969.

43. M. Neelov, D. B. Adolf, T. C. B. McLeish, and E. Paci. Molecular dynamics simulation of dextran extension by constant force in single molecule AFM. *Biophys.*, 1-9, 2006.
44. W. Nowak, and P. E. Marszalek. Molecular dynamics simulations of single molecule atomic force microscope experiments. *Computational Chemistry*, 9:47-72, 2003.
45. Z. Lu, W. Nowak, G. Lee, P. E. Marszalek, and W. Yang. Elastic Properties of Single Amylose Chains in Water: A Quantum Mechanical and AFM Study. *J. Am. Chem. Soc.*, 126: 9033-9041, 2004.
46. P. E. Marszalek, et al. Atomic levers control pyranose ring conformations. *Proc. Natl. Acad. Sci. USA*, 96:7894-7898, 1999.
47. F. Franks. Physical chemistry of small carbohydrates - equilibrium solution properties. *Pure & Appl. Chem.*, 59:1189-1202, 1987.
48. W. Banks and C. T. Greenwood. Amylose: a non-helical polymer in aqueous solution. *Polymer*, 12:141-145, 1971.
49. Q. Zhang, and P. E. Marszalek. Identification of Sugar Isomers by Single-Molecule Force Spectroscopy. *J. Am. Chem. Soc.*, 128:5596-5597, 2005.
50. Q. Zhang, and P. E. Marszalek. Solvent effects on the elasticity of polysaccharide molecules in disordered and ordered states by single-molecule force spectroscopy. *Polymer*, 47:2526-2532, 2006.
51. M. Kuttel, and K. J. Naidoo. Glycosidic Linkage Rotations Determine Amylose Stretching Mechanism. *J. Am. Chem. Soc.*, 127:12-13, 2005.
52. M. Kuttel, and K. J. Naidoo. Ramachandran free-energy surfaces for disaccharides: trehalose, a case study. *Science Direct. Carbohydrate Research*, 340:875-879, 2005.
53. G. Lee, W. Nowak, J. Jaroniec, Q. Zhang, and P. E. Marszalek. Molecular Dynamics Simulations of Forced Conformational Transitions in 1,6-Linked Polysaccharides. *Biophysical Journal*, 87:1456-1465, 2004.

54. W. Humphrey, A. Dalke, and K Schulten. VMD: Visual Molecular Dynamics. *J. Molec. Graphics*, 14:33-38, 1996.
55. R. W. Hockney. The potential calculation and some applications. *Methods in Computational Physics*, 9:136-211, 1970.
56. J. P. Ryckaert, G. Ciccotti, and H. J. C. Berendsen. Numerical integration of the Cartesian equations of motion of a system with numerical constraints: molecular dynamics of n-alkanes. *J. Comput. Phys.*, 23:327-341, 1977.
57. E. Evans and K. Richie. Dynamic strength of molecular adhesion bonds. *Biophys. J.*, 72:1541-1555, 1997.

7. Appendix A

NAMD Configuration (CONF) File

The NAMD configuration file is where the user specifies all the options that NAMD should adopt in running a simulation i.e. the configuration file tells NAMD how the simulation is to be run.

The following file is the configuration file used for simulations performed on an 8 unit amylose molecule.

```
#####
## JOB DESCRIPTION                                     ##
#####

# glc_14_glc_8 dynamics SMD simulation with Constant Force Pulling
# Rudolf van den Berg
# Feb 2008

#####
## ADJUSTABLE PARAMETERS                             ##
#####

# Set external variables
set n $env(R)
set t $env(FIRST_TIMESTEP)
set p $env(PREVIOUS)
set r $env(RUN)

set temperature      300

# Input files
structure            glc_14_glc_8.psf
coordinates          glc_14_glc_8.pdb
binaryoutput yes

# Continuing a job from the restart files
if {$p} {
print "continuation"
set inputname        glu8_NAMD_SMD_equil_$p
bincoordinates       $inputname.coor
binvelocities        $inputname.vel ;# remove the "temperature" entry if you
use this!
extendedSystem       $inputname.xsc
} else {
# protocol
# NOTE: Do not set the initial velocity temperature if you
# have also specified a .vel restart file!
temperature          $temperature
}

#Output files
outputname glu8_NAMD_SMD_equil_$n
```

```

restartname glu8_NAMD_SMD_equil_$.n

DCDfile glu8_NAMD_SMD_equil_$.n.dcd
velDCDfile glu8_NAMD_SMD_equil_vel_$.n.dcd

#####
## SIMULATION PARAMETERS ##
#####

# Input
paraTypeCharmm      on
parameters          CSFF_parm.inp

# Force-Field Parameters
# In CHARMM, by default directly bonded atoms and the 1-3 atoms of an angle
# are excluded
# from the nonbond calculation.
exclude             scaled1-4
1-4scaling          1.0
cutoff              12
switching           on
switchdist          10.0
pairlistdist        14 #equal to cutnb
margin              0
#dielectric 1
#approximations

# Integrator Parameters
timestep            1.0 # 2fs/step
stepspercycle       25
rigidBonds          all # needed for 2fs steps - shake
#nonbondedFreq      1
#fullElectFrequency 2

# Constant Temperature Control
langevin            on      # do langevin dynamics
langevinDamping     62.5    # damping coefficient (gamma) of 5/ps
langevinTemp        $temperature
langevinHydrogen    no      # don't couple langevin bath to hydrogens

restartfreq         500     # 500steps = every 1ps
dcdfreq             500
xstFreq             500
outputEnergies      100
#outputPressure     100

tCouple             off
tCoupleTemp         $temperature

# Fixed Atoms Constraint (set PDB beta-column to 1)
# SMD simulation - initially just trying constant velocity
if {1} {
fixedAtoms          on
fixedAtomsFile      gluSMD$.n
fixedAtomsCol       B
}

```

```
#####  
## EXTRA PARAMETERS ##  
#####  
  
constantforce yes  
consforcefile gluSMD$n  
  
#####  
## EXECUTION SCRIPT ##  
#####  
  
run $r; # timesteps, 20 ns
```


8. Appendix B

Programs

1. NAMD Bash Script

The following Linux bash script was implemented to increment the force during simulations. The variables in this script are being used to set the parameters in the NAMD configuration file.

```
R=1
PREVIOUS=$((R-1))
FIRST_TIMESTEP=$((PREVIOUS*20000000+1))
RUN=20000000
FRC=0.40
MULT=1
export R FIRST_TIMESTEP RUN PREVIOUS

while [ $R -lt 200 ];
do

awk -f ~/AWK_Scripts/alterForce.awk FORCE=$FRC MULT=$MULT glc_14_glc_8.ref >
gluSMD$R
/usr/local/src/NAMD_2.6_Linux-i686/charmrun ++local +p4 /usr/local/bin/namd2
glc_14_glc_8.conf > glc_14_glc_8$R.tmp

PREVIOUS=$((R))
R=$((R+1))
FIRST_TIMESTEP=$((FIRST_TIMESTEP+R))
MULT=$((MULT+1))
echo $R $PREVIOUS $FIRST_TIMESTEP
export R FIRST_TIMESTEP RUN PREVIOUS

done
```

2. Microsoft .Net 3.5 C# Program

The following c# program was written to process the analysis data i.e. to convert the output data from VMD into meaningful force and distance data. The program has two methods that can be used to process the data. The first method uses a normal stream reader and writer to read the data from the .dat file and write it to a .csv file. The second method uses LINQ to read and write directly to Excel.

```

using System;
using System.Configuration;
using System.Data;
using System.Data.Common;
using System.IO;
using System.Text.RegularExpressions;

namespace FixForceData
{
    class Program
    {
        private static readonly string inputFileName =
            ConfigurationSettings.AppSettings["InputFileName"];
        private static readonly string outputFileName =
            ConfigurationSettings.AppSettings["OutputFileName"];
        private static readonly int Increment =
            Int32.Parse(ConfigurationSettings.AppSettings["Increment"]);

        // 27.79 pN = 0.4 kcal.mol-1.Å-1
        private const double ForceConversionFactor = 27.79;

        static void Main(string[] args)
        {
            ProcessData();
            // LINQProcessData();
        }

        /// <summary>
        /// Process the data by reading the .dat file directly and writing the
        output to a .csv file.
        /// </summary>
        private static void ProcessData()
        {
            // Create data structure for storing data
            DataTable dt = new DataTable();
            dt.Columns.Add("Frame");
            dt.Columns.Add("Distance");

            String line;
            StreamReader objInput = new StreamReader(inputFileName,
                System.Text.Encoding.Default);

            // Read and display lines from the file until the end of the file.
            while ((line = objInput.ReadLine()) != null)
            {
                string[] split = Regex.Split(line, "\\t+", RegexOptions.None);
                DataRow row = dt.NewRow();

                row["Frame"] = split[0];
                row["Distance"] = split[1];

                dt.Rows.Add(row);
            }

            int incr = Increment;
            double totalDistance = 0;
            int counter = 0;

```

```

        StreamWriter writer = new StreamWriter(outputFileName);

        for (int i = 0; i < dt.Rows.Count; i++)
        {
            double frame = double.Parse(dt.Rows[i].ItemArray[0].ToString());
            double distance =
double.Parse(dt.Rows[i].ItemArray[1].ToString());
            totalDistance += distance;

            if (i == incr - 1)
            {
                counter++;
                double avgDistance = totalDistance / Increment;
                double force = counter * ForceConversionFactor;

                // Write to the .csv output file
                writer.WriteLine(string.Format("{0},{1},{2},{3}", frame,
distance, force, avgDistance));

                incr += Increment;
                totalDistance = 0;
            }
        }

        writer.Flush();
        writer.Close();
    }

    /// <summary>
    /// Process the data by making use of LINQ to read data directly from
the .xls file and
    /// write it back the the same file in a different sheet.
    /// </summary>
    private static void LINQProcessData()
    {
        string DataSheetName =
ConfigurationSettings.AppSettings["DataSheetName"];
        string ProcessedSheetName =
ConfigurationSettings.AppSettings["ProcessedSheetName"];

        // This says the spreadsheet is located in the current directory and
called [inputFileName],
        // and the first row is a header row containing the names of the
columns.
        string connectionString =
            string.Format(
                @"Provider=Microsoft.Jet.OLEDB.4.0;Data Source={0};Extended
Properties=""Excel 8.0;HDR=YES;""", inputFileName);

        DbProviderFactory factory =
DbProviderFactories.GetFactory("System.Data.OleDb");

        DbDataAdapter adapter = factory.CreateDataAdapter();

        DbCommand command = factory.CreateCommand();

```

```

        command.CommandText = string.Format("SELECT Frame, Distance FROM
[{{0}}$]", DataSheetName);

        DbConnection connection = factory.CreateConnection();
        connection.ConnectionString = connectionString;

        command.Connection = connection;

        adapter.SelectCommand = command;

        DataSet ds = new DataSet();

        adapter.Fill(ds);

        DataTable dt = ds.Tables[0];

        int incr = Increment;
        double totalDistance = 0;
        int counter = 0;

        for (int i = 0; i < dt.Rows.Count; i++)
        {
            double frame = double.Parse(dt.Rows[i].ItemArray[0].ToString());
            double distance =
double.Parse(dt.Rows[i].ItemArray[1].ToString());
            totalDistance += distance;

            if (i == incr - 1)
            {
                counter++;
                double avgDistance = totalDistance / Increment;
                double force = counter * ForceConversionFactor;

                command.CommandText =
                    string.Format(
                        "INSERT INTO [{{0}}$] (PFrame, PDistance, Force,
AvgDistance) VALUES ({{1}}, {{2}}, {{3}}, {{4}})",
                        ProcessedSheetName, frame, distance, force,
avgDistance);

                connection.Open();
                command.ExecuteNonQuery();
                connection.Close();

                incr += Increment;
                totalDistance = 0;
            }
        }
    }
}
}
}

```

9. Appendix C

NAMD Configuration and Analysis Process

The following outlines the step by step process followed to set up a constant force pulling simulation in NAMD:

1. The SMD Atom

NAMD uses a column of a data bank (pdb) file to determine which atoms will be fixed and which atoms will be pulled. The pdb file contains information such as the name of the compound, stoichiometry, secondary structure locations, crystal lattice and stores atomic coordinates and/or velocities for the system (see Appendix C).

In addition, another three columns are used to specify the direction of the constant force that will be applied to the SMD atom. This information is stored in a reference (ref) file. The first step therefore is to build the ref file (see Appendix E):

- Open a VMD session. Choose the File – New Molecule menu item and using the Browse and Load buttons, load the structure (psf) file. The psf file, contains all of the moleculespecific information (structural information such as various types of bonding interactions) needed to apply a particular force field to a molecular system (see Appendix D). Close the Molecule File Browser window.
- Using the mouse select the molecule in the VMD Main window and then choose the Load Data into Molecule menu item. Again, using the Browse and Load buttons, load the pdb file. Close the Molecule File Browser.
- The next step is to define the fixed atom. In the VMD TkCon window, type the following commands:

```
set allatoms [atomselect top all]
```

This creates a selection called allatoms which contains all atoms.

```
$allatoms set beta 0
```

In this way you set the B column of all atoms equal to 0.

```
set fixedatom [atomselect top "resid 1 and name O4"]
```

This creates a selection that contains the fixed atom, namely the O_α atom of the first residue.

```
$fixedatom set beta 1
```

This sets the value of the B column for the fixed atom to 1 and, therefore, NAMD will keep this atom now fixed.

- The next step is to define the SMD atom. NAMD uses another column of a pdb file to set which atom is to be pulled i.e. the SMD atom. For this purpose it uses the occupancy column of the pdb file. In the VMD TkCon window, type the following commands:

```
$allatoms set occupancy 0
```

This sets the occupancy column of every atom to 0.

```
set smdatom [atomselect top "resid 8 and name O4"]
```

The smd atom selection contains the O atom of the last residue, in this case the O atom of an 8 unit molecule.

```
$smdatom set occupancy 0.4
```

Now, the occupancy column of the smd atom selection is 0.4, and NAMD will pull this atom.

- Now that the fixed and SMD atom is defined, we need to specify the direction in which the pulling will be performed. This is determined by the direction of the vector that links the fixed and the SMD atoms. Type the following commands in the VMD TkCon window:

```
set smdpos [lindex [$smdatom get {x y z}] 0]  
set fixedpos [lindex [$fixedatom get {x y z}] 0]  
vecnorm [vecsub $smdpos $fixedpos]
```

This outputs three numbers, namely, the x, y, and z components of the normalized direction between the fixed and the SMD atom.

- The direction of the force will be specified in the coordinates of the SMD atom. To write the normal vector type:

```
$smdatom set x nx  
$smdatom set y ny  
$smdatom set z nz
```

where n_x , n_y , and n_z have to be replaced by the appropriate values calculated above.

- Finally, save the coordinates into a file by typing:

```
$allatoms writepdb glc_14_glc_8.ref
```

This will write a file (ref) in pdb format that contains all the atoms with the updated B and occupancy columns. The created ref file can be checked by finding the line or row that corresponds to the O4 atom for residue number 1. In that line one should be able to see how the B column was switched to 1, while the B column for all the other atoms is 0. The ref file also contains the appropriate information required by NAMD to identify the SMD atom. Again, check this by finding the row or line that corresponds to the O1 atom for residue number 8. This atom, that should have occupancy 0.4 and the coordinates, will be pulled in the simulation (see Appendix E).

- Delete the current molecule by choosing the Molecule - Delete Molecule menu item and keep VMD opened.

2. Configuration File

The next step is to create the NAMD configuration file. To do this we modified the provided NAMD template with the following (see Appendix A):

- Set the external variables (from the bash script in Appendix F):

```
set n $env(R)  
set t $env(FIRST_TIMESTEP)
```

```
set p $env(PREVIOUS)
set r $env(RUN)
```

- In the Adjustable Parameters section set:

```
structure glc_14_glc_8.psf
coordinates glc_14_glc_8.pdb

outputName glu8_NAMD_SMD_equil_$n
restartname glu8_NAMD_SMD_equil_$n

DCDfile glu8_NAMD_SMD_equil_$n.dcd
velDCDfile glu8_NAMD_SMD_equil_vel_$n.dcd
```

- In the Input section set:

```
parameters CSFF_parm.inp
```

- The temperature control should be disabled in order to disturb the movement of the atoms as little as possible. Switch off the Constant Temperature Control by changing:

```
langevin on - langevin off
```

- Enable the Fixed Atoms Constraint by changing the following lines:

```
if {1} {
fixedAtoms      on
fixedAtomsFile  gluSMD$n
fixedAtomsCol   B}
```

NAMD will keep fixed the atoms which have a B value of 1 in the file glc_14_glc_8.ref.

- In the Extra Parameters section add the following lines:

```
Constantforce   yes
Consforcefile   gluSMD$n
```


NAMD will apply a constant force to the atoms that have occupancy different from 0. The force is calculated from the file as $(x, y, z) \times O$, where O is the value of the occupancy column.

- Finally, in the Execution Script section of the configuration file disable the minimization and change the number of time steps the simulation will run by replacing:

```
run $r;
```

3. Running the SMD Simulation

Check that all the files are in the respective directories. Run your simulation by executing the script in Appendix F by typing the following in a Terminal Window:

```
./autoGlu8 &
```

4. Analysis of Results

- Copy the ReadManyDCD script, .dcd, .pdb and .psf files into the VMD root install directory
- In VMD choose the File - New Molecule. Using the Browse... and the Load buttons load the .psf file
- Next we load the multiple .dcd files. Open Extensions/Tk console and type:

```
source ReadManyDCD.tcl
ReadManyDCD 1 100 "glu8_NAMD_SMD_equil_%d.dcd" 100
```

- In the OpenGL Display window you will see the trajectory of the constant force pulling simulation.
- Once the complete trajectory is loaded, use the slider in the VMD Main window to go back to the first frame.
- Choose the Graphics - Representations... menu item. In the Graphical Representations window press the Create Rep button in order to create a new representation. In the Selected Atoms text entry delete the word all and type:

```
resid 1 and name O4
```

This will identify O4 in the first residue.

- Press the Create Rep button in order to create a new representation. In the Selected Atoms text entry delete the word all and type:

```
resid 8 and name O1
```

This will identify O1 in the last residue (e.g. 8).

- For the above representations choose the VDW drawing method. You should be able to see the two O_x atoms at the end of your molecule as spheres.
- Click in the OpenGL Display window and press the key 2 (Shortcut to bond labels). Your cursor should look like a cross. Pick the two spheres displayed. A line linking both atoms should appear with the distance between them displayed.
- Choose the Graphics - Labels... menu item. In the Labels window, choose the label type Bonds. Select the bond displayed, click on the Graph tab and then click on the Graph button. This will create a plot of the distance between these two atoms over time. You also have the option to write the data and to a file, which can then be read by Excel.

10. Appendix D

CHARMM Force Field Parameter (INP) File

A CHARMM force field parameter file contains all of the numerical constants needed to evaluate forces and energies. Force fields are used to calculate molecular energies and configurations. In other words it provides a mapping between bonded and non-bonded interactions and specific spring constants and similar parameters for all of the bond, angle, dihedral, improper and van der Waals terms in the CHARMM potential function.

A force field is a mathematical expression of the potential which atoms in the system experience. CHARMM, X-PLOR, AMBER, and GROMACS are four types of force fields.

```
*****
* Carbohydrate parameter file CSFF_parm.inp
*   for pyranose simulations
* Michelle Kuttel, J. W. Brady and Kevin J. Naidoo
* Aug/Sep 2001
* Modified from the PHLB (Palma-Himmel-Liang-Brady) force field parameters:
*   added CPS atom type and altered primary alcohol
*   dihedral force constants from CTS values
*   to lower energy the barriers to primary alcohol rotation
* Comments to Kevin J. Naidoo email:naidoo,science.uct.ac.za
*****
*
!
!references
!
! M. Kuttel and J. W. Brady and K. J. Naidoo. "Carbohydrate Solution
! Simulations: Producing a Force Field with Experimentally Consistent
! Primary Alcohol Rotational Frequencies and Populations",
! J. Comput. Chem., 2002,23:1236-1243
!
!PHLB force field precursor
!
!R. Palma and M. E. Himmel and G. Liang and J. W. Brady. "Molecular
!Mechanics Studies of Cellulases" in "Glycosyl Hydrolases in Biomass
!Conversion: ACS Symposium Series", published by ACS, 2001, editor
!M. E. Himmel
!
!HFBF force field precursor
!
!S. N. Ha and A. Giammona and M. Field and J. W. Brady, "A revised
!potential-energy surface for molecular studies of carbohydrates",
!Carbohydr. Res., 1988,180,207-221
! NOTE: messages about multiple dihedral terms on reading this file are
```

! normal and signify that the multiple dihedral terms have in fact
! correctly been read (see CHARMM docs - parmfile.doc)

BONDS

HOS	OHS	460.5000	0.9595	
HAS	CTS	335.6034	1.1000	
HAS	CPS	335.6034	1.1000	
HAS	CBS	335.6034	1.1052	
CTS	OHS	384.0792	1.4066	
CPS	OHS	384.0792	1.4066	
CBS	OHS	384.0792	1.3932	
CTS	CTS	325.5297	1.5066	
CTS	CPS	325.5297	1.5066	
CBS	CTS	325.5297	1.5074	
CTS	OES	385.3133	1.4165	
CPS	OES	385.3133	1.4165	
CBS	OES	385.3133	1.4202	
HSPC	OSPC	450.0	1.0	! SPC Geometry
HSPC	HSPC	0.0	1.6329931	! SPC Geometry (for SHAKE)
HT	OT	450.0	0.9572	! TIP3P geometry
HT	HT	0.0	1.5139	! TIP3P geometry (for SHAKE)

THETAS

HAS	CTS	CTS	42.9062	109.7502	
HAS	CBS	CTS	42.9062	109.7502	
HAS	CTS	CBS	42.9062	109.7502	
HAS	CTS	CPS	42.9062	109.7502	
HAS	CPS	CTS	42.9062	109.7502	
OHS	CTS	CTS	112.2085	107.6019	
OHS	CBS	CTS	112.2085	107.6019	
OHS	CTS	CBS	112.2085	107.6019	
OHS	CPS	CTS	112.2085	107.6019	
OHS	CTS	CPS	112.2085	107.6019	
HOS	OHS	CTS	57.5478	109.1722	
HOS	OHS	CBS	57.5478	109.1722	
HOS	OHS	CPS	57.5478	109.1722	
HAS	CTS	HAS	36.8220	106.1784	
HAS	CPS	HAS	36.8220	106.1784	
HAS	CTS	OHS	52.5070	109.3850	
HAS	CBS	OHS	52.5070	109.3850	
HAS	CPS	OHS	52.5070	109.3850	
HT	OT	HT	55.0	104.52	! FROM TIPS3P GEOMETRY
HSPC	OSPC	HSPC	55.0	109.47122	! FROM SPC GEOMETRY
HAS	CTS	OES	62.2500	106.4025	
HAS	CBS	OES	62.2500	106.4025	
HAS	CPS	OES	62.2500	106.4025	
CTS	CTS	CTS	167.3535	110.6156	
CBS	CTS	CTS	167.3535	110.6156	
CPS	CTS	CTS	167.3535	110.6156	
CTS	CTS	OES	169.0276	108.3759	
CBS	CTS	OES	169.0276	108.3759	
CPS	CTS	OES	169.0276	108.3759	
CTS	CPS	OES	169.0276	108.3759	
CTS	CBS	OES	169.0276	108.3759	
CTS	OES	CTS	92.5892	111.5092	
CTS	OES	CPS	92.5892	111.5092	
CBS	OES	CTS	92.5892	111.5092	
OES	CTS	OHS	74.2586	115.7322	
OES	CBS	OHS	74.2586	110.3385	

OES	CTS	OES		37.4370		112.1882	
OES	CBS	OES		37.4370		106.9160	
DIHEDRALS							
CTS	CTS	CTS	CTS	-1.0683	1	0.0	
CTS	CTS	CTS	CTS	-0.5605	2	0.0	
CTS	CTS	CTS	CTS	0.1955	3	0.0	
CBS	CTS	CTS	CTS	-1.0683	1	0.0	
CBS	CTS	CTS	CTS	-0.5605	2	0.0	
CBS	CTS	CTS	CTS	0.1955	3	0.0	
CPS	CTS	CTS	CTS	-1.0683	1	0.0	!MK - CTS value unchanged
CPS	CTS	CTS	CTS	-0.5605	2	0.0	!MK - CTS value unchanged
CPS	CTS	CTS	CTS	0.1955	3	0.0	!MK - CTS value unchanged
CTS	CTS	CTS	OES	-1.2007	1	0.0	
CTS	CTS	CTS	OES	-0.3145	2	0.0	
CTS	CTS	CTS	OES	-0.0618	3	0.0	
CBS	CTS	CTS	OES	-1.2007	1	0.0	
CBS	CTS	CTS	OES	-0.3145	2	0.0	
CBS	CTS	CTS	OES	-0.0618	3	0.0	
CPS	CTS	CTS	OES	-1.2007	1	0.0	!MK - CTS value unchanged
CPS	CTS	CTS	OES	-0.3145	2	0.0	!MK - CTS value unchanged
CPS	CTS	CTS	OES	-0.0618	3	0.0	!MK - CTS value unchanged
CTS	CTS	CBS	OES	-1.2007	1	0.0	
CTS	CTS	CBS	OES	-0.3145	2	0.0	
CTS	CTS	CBS	OES	-0.0618	3	0.0	
CTS	CTS	CPS	OES	-1.2007	1	0.0	!MK - CTS value unchanged
CTS	CTS	CPS	OES	-0.3145	2	0.0	!MK - CTS value unchanged
CTS	CTS	CPS	OES	-0.0618	3	0.0	!MK - CTS value unchanged
CTS	CTS	CTS	OHS	-1.9139	1	0.0	
CTS	CTS	CTS	OHS	0.2739	2	0.0	
CTS	CTS	CTS	OHS	-0.0340	3	0.0	
CTS	CTS	CBS	OHS	-1.9139	1	0.0	
CTS	CTS	CBS	OHS	-0.3739	2	0.0	
CTS	CTS	CBS	OHS	-0.0340	3	0.0	
CTS	CTS	CPS	OHS	-1.7139	1	0.0	!MK - changed from -1.9139
CTS	CTS	CPS	OHS	-1.0239	2	0.0	!MK - changed from -0.3739
CTS	CTS	CPS	OHS	-0.0340	3	0.0	!MK - CTS value unchanged
CBS	CTS	CTS	OHS	-1.9139	1	0.0	
CBS	CTS	CTS	OHS	-0.3739	2	0.0	
CBS	CTS	CTS	OHS	-0.0340	3	0.0	
CPS	CTS	CTS	OHS	-1.9139	1	0.0	!MK - CTS value unchanged
CPS	CTS	CTS	OHS	-0.3739	2	0.0	!MK - CTS value unchanged
CPS	CTS	CTS	OHS	-0.0340	3	0.0	!MK - CTS value unchanged
CTS	OES	CTS	CTS	-0.8477	1	0.0	
CTS	OES	CTS	CTS	-0.3018	2	0.0	
CTS	OES	CTS	CTS	0.3763	3	0.0	
CTS	OES	CTS	CPS	-0.8477	1	0.0	!MK - CTS value unchanged
CTS	OES	CTS	CPS	-0.3018	2	0.0	!MK - CTS value unchanged
CTS	OES	CTS	CPS	0.3763	3	0.0	!MK - CTS value unchanged
CBS	OES	CTS	CTS	-0.8477	1	0.0	
CBS	OES	CTS	CTS	-0.3018	2	0.0	
CBS	OES	CTS	CTS	0.3763	3	0.0	
CBS	OES	CTS	CPS	-0.8477	1	0.0	!MK - CTS value unchanged
CBS	OES	CTS	CPS	-0.3018	2	0.0	!MK - CTS value unchanged
CBS	OES	CTS	CPS	0.3763	3	0.0	!MK - CTS value unchanged
CBS	OES	CPS	CTS	-0.8477	1	0.0	!MK - CTS value unchanged
CBS	OES	CPS	CTS	-0.3018	2	0.0	!MK - CTS value unchanged
CBS	OES	CPS	CTS	0.3763	3	0.0	!MK - CTS value unchanged

CPS	OES	CTS	CTS	-0.8477	1	0.0	!MK - CTS value unchanged
CPS	OES	CTS	CTS	-0.3018	2	0.0	!MK - CTS value unchanged
CPS	OES	CTS	CTS	0.3763	3	0.0	!MK - CTS value unchanged
CTS	OES	CBS	CTS	-0.8477	1	0.0	
CTS	OES	CBS	CTS	-0.3018	2	0.0	
CTS	OES	CBS	CTS	0.3763	3	0.0	
CTS	OES	CPS	CTS	-0.8477	1	0.0	!MK - CTS value unchanged
CTS	OES	CPS	CTS	-0.3018	2	0.0	!MK - CTS value unchanged
CTS	OES	CPS	CTS	0.3763	3	0.0	!MK - CTS value unchanged
CPS	OES	CBS	CTS	-0.8477	1	0.0	!MK - CTS value unchanged
CPS	OES	CBS	CTS	-0.3018	2	0.0	!MK - CTS value unchanged
CPS	OES	CBS	CTS	0.3763	3	0.0	!MK - CTS value unchanged
HAS	CTS	CTS	CTS	0.0000	1	0.0	
HAS	CTS	CTS	CTS	0.0000	2	0.0	
HAS	CTS	CTS	CTS	0.1441	3	0.0	
HAS	CBS	CTS	CTS	0.0000	1	0.0	
HAS	CBS	CTS	CTS	0.0000	2	0.0	
HAS	CBS	CTS	CTS	0.1441	3	0.0	
HAS	CPS	CTS	CTS	0.0000	1	0.0	!MK - CTS value unchanged
HAS	CPS	CTS	CTS	0.0000	2	0.0	!MK - CTS value unchanged
HAS	CPS	CTS	CTS	0.1441	3	0.0	!MK - CTS value unchanged
HAS	CTS	CTS	CBS	0.0000	1	0.0	
HAS	CTS	CTS	CBS	0.0000	2	0.0	
HAS	CTS	CTS	CBS	0.1441	3	0.0	
HAS	CTS	CTS	CPS	0.0000	1	0.0	!MK - CTS value unchanged
HAS	CTS	CTS	CPS	0.0000	2	0.0	!MK - CTS value unchanged
HAS	CTS	CTS	CPS	0.1441	3	0.0	!MK - CTS value unchanged
HAS	CTS	CTS	HAS	0.0000	1	0.0	
HAS	CTS	CTS	HAS	0.0000	2	0.0	
HAS	CTS	CTS	HAS	0.1595	3	0.0	
HAS	CBS	CTS	HAS	0.0000	1	0.0	
HAS	CBS	CTS	HAS	0.0000	2	0.0	
HAS	CBS	CTS	HAS	0.1595	3	0.0	
HAS	CPS	CTS	HAS	0.0000	1	0.0	!MK - CTS value unchanged
HAS	CPS	CTS	HAS	0.0000	2	0.0	!MK - CTS value unchanged
HAS	CPS	CTS	HAS	0.1595	3	0.0	!MK - CTS value unchanged
HAS	CTS	OES	CTS	0.0000	1	0.0	
HAS	CTS	OES	CTS	0.0000	2	0.0	
HAS	CTS	OES	CTS	0.2840	3	0.0	
HAS	CBS	OES	CTS	0.0000	1	0.0	
HAS	CBS	OES	CTS	0.0000	2	0.0	
HAS	CBS	OES	CTS	0.2840	3	0.0	
HAS	CBS	OES	CPS	0.0000	1	0.0	!MK - CTS value unchanged
HAS	CBS	OES	CPS	0.0000	2	0.0	!MK - CTS value unchanged
HAS	CBS	OES	CPS	0.2840	3	0.0	!MK - CTS value unchanged
HAS	CPS	OES	CTS	0.0000	1	0.0	!MK - CTS value unchanged
HAS	CPS	OES	CTS	0.0000	2	0.0	!MK - CTS value unchanged
HAS	CPS	OES	CTS	0.2840	3	0.0	!MK - CTS value unchanged
HAS	CTS	OES	CBS	0.0000	1	0.0	
HAS	CTS	OES	CBS	0.0000	2	0.0	
HAS	CTS	OES	CBS	0.2840	3	0.0	
HAS	CTS	OES	CPS	0.0000	1	0.0	!MK - CTS value unchanged
HAS	CTS	OES	CPS	0.0000	2	0.0	!MK - CTS value unchanged
HAS	CTS	OES	CPS	0.2840	3	0.0	!MK - CTS value unchanged
HAS	CPS	OES	CBS	0.0000	1	0.0	!MK - CTS value unchanged
HAS	CPS	OES	CBS	0.0000	2	0.0	!MK - CTS value unchanged
HAS	CPS	OES	CBS	0.2840	3	0.0	!MK - CTS value unchanged

HOS	OHS	CTS	CTS	1.0504	1	0.0	
HOS	OHS	CTS	CTS	0.1336	2	0.0	
HOS	OHS	CTS	CTS	0.3274	3	0.0	
HOS	OHS	CBS	CTS	1.0504	1	0.0	
HOS	OHS	CBS	CTS	0.1336	2	0.0	
HOS	OHS	CBS	CTS	0.3274	3	0.0	
HOS	OHS	CPS	CTS	1.0504	1	0.0	!MK - CTS value unchanged
HOS	OHS	CPS	CTS	0.1336	2	0.0	!MK - CTS value unchanged
HOS	OHS	CPS	CTS	0.3274	3	0.0	!MK - CTS value unchanged
HOS	OHS	CTS	CBS	1.0504	1	0.0	
HOS	OHS	CTS	CBS	0.1336	2	0.0	
HOS	OHS	CTS	CBS	0.3274	3	0.0	
HOS	OHS	CTS	HAS	0.0000	1	0.0	!MK - CTS * 40% (hyd rot)
HOS	OHS	CTS	HAS	0.0000	2	0.0	!MK - CTS * 40% (hyd rot)
HOS	OHS	CTS	HAS	0.0677	3	0.0	!MK - CTS * 40% (hyd rot)
HOS	OHS	CBS	HAS	0.0000	1	0.0	!MK - CTS * 40% (hyd rot)
HOS	OHS	CBS	HAS	0.0000	2	0.0	!MK - CTS * 40% (hyd rot)
HOS	OHS	CBS	HAS	0.0677	3	0.0	!MK - CTS * 40% (hyd rot)
HOS	OHS	CPS	HAS	0.0000	1	0.0	!MK - CTS * 40% (hyd rot)
HOS	OHS	CPS	HAS	0.0000	2	0.0	!MK - CTS * 40% (hyd rot)
HOS	OHS	CPS	HAS	0.0677	3	0.0	!MK - CTS * 40% (hyd rot)
OES	CTS	CTS	HAS	0.0000	1	0.0	
OES	CTS	CTS	HAS	0.0000	2	0.0	
OES	CTS	CTS	HAS	0.1686	3	0.0	
OES	CBS	CTS	HAS	0.0000	1	0.0	
OES	CBS	CTS	HAS	0.0000	2	0.0	
OES	CBS	CTS	HAS	0.1686	3	0.0	
OES	CPS	CTS	HAS	0.0000	1	0.0	!MK - CTS value unchanged
OES	CPS	CTS	HAS	0.0000	2	0.0	!MK - CTS value unchanged
OES	CPS	CTS	HAS	0.1686	3	0.0	!MK - CTS value unchanged
OES	CTS	CBS	HAS	0.0000	1	0.0	
OES	CTS	CBS	HAS	0.0000	2	0.0	
OES	CTS	CBS	HAS	0.1686	3	0.0	
OES	CTS	CPS	HAS	0.0000	1	0.0	!MK - CTS value unchanged
OES	CTS	CPS	HAS	0.0000	2	0.0	!MK - CTS value unchanged
OES	CTS	CPS	HAS	0.2086	3	0.0	!MK - changed from 0.1686
OES	CTS	CTS	OES	-2.6785	1	0.0	
OES	CTS	CTS	OES	0.7851	2	0.0	
OES	CTS	CTS	OES	0.2552	3	0.0	
OES	CBS	CTS	OES	-2.6785	1	0.0	
OES	CBS	CTS	OES	0.7851	2	0.0	
OES	CBS	CTS	OES	0.2552	3	0.0	
OES	CPS	CTS	OES	-2.6785	1	0.0	!MK - CTS value unchanged
OES	CPS	CTS	OES	0.7851	2	0.0	!MK - CTS value unchanged
OES	CPS	CTS	OES	0.2552	3	0.0	!MK - CTS value unchanged
OES	CTS	CTS	OHS	-3.7993	1	0.0	
OES	CTS	CTS	OHS	0.5688	2	0.0	
OES	CTS	CTS	OHS	0.4204	3	0.0	
OES	CBS	CTS	OHS	-3.7993	1	0.0	
OES	CBS	CTS	OHS	0.5688	2	0.0	
OES	CBS	CTS	OHS	0.4204	3	0.0	
OES	CTS	CBS	OHS	-3.7993	1	0.0	
OES	CTS	CBS	OHS	0.5688	2	0.0	
OES	CTS	CBS	OHS	0.4204	3	0.0	
OES	CTS	CPS	OHS	-4.0193	1	0.0	!MK changed from -3.7993
OES	CTS	CPS	OHS	-1.2688	2	0.0	!MK changed from +0.5686
OES	CTS	CPS	OHS	-0.9704	3	0.0	!MK CHANGED from +0.4202

OES	CTS	OES	CTS	0.1948	1	0.0	
OES	CTS	OES	CTS	0.9778	2	0.0	
OES	CTS	OES	CTS	0.9115	3	0.0	
OES	CTS	OES	CPS	0.1948	1	0.0	!MK - CTS value unchanged
OES	CTS	OES	CPS	0.9778	2	0.0	!MK - CTS value unchanged
OES	CTS	OES	CPS	0.9115	3	0.0	!MK - CTS value unchanged
OES	CBS	OES	CTS	0.1948	1	0.0	
OES	CBS	OES	CTS	0.9778	2	0.0	
OES	CBS	OES	CTS	0.9115	3	0.0	
OES	CBS	OES	CPS	0.1948	1	0.0	!MK - CTS value unchanged
OES	CBS	OES	CPS	0.9778	2	0.0	!MK - CTS value unchanged
OES	CBS	OES	CPS	0.9115	3	0.0	!MK - CTS value unchanged
OHS	CTS	OES	CTS	1.9193	1	0.0	
OHS	CTS	OES	CTS	1.0102	2	0.0	
OHS	CTS	OES	CTS	0.7294	3	0.0	
OHS	CBS	OES	CTS	1.9193	1	0.0	
OHS	CBS	OES	CTS	1.0102	2	0.0	
OHS	CBS	OES	CTS	0.7294	3	0.0	
OES	CTS	OHS	HOS	1.2936	1	0.0	
OES	CTS	OHS	HOS	1.3295	2	0.0	
OES	CTS	OHS	HOS	0.4323	3	0.0	
OES	CBS	OHS	HOS	1.2936	1	0.0	
OES	CBS	OHS	HOS	1.3295	2	0.0	
OES	CBS	OHS	HOS	0.4323	3	0.0	
OHS	CTS	CTS	HAS	0.0000	1	0.0	
OHS	CTS	CTS	HAS	0.0000	2	0.0	
OHS	CTS	CTS	HAS	0.1472	3	0.0	
OHS	CBS	CTS	HAS	0.0000	1	0.0	
OHS	CBS	CTS	HAS	0.0000	2	0.0	
OHS	CBS	CTS	HAS	0.1472	3	0.0	
OHS	CPS	CTS	HAS	0.0000	1	0.0	!MK - CTS value unchanged
OHS	CPS	CTS	HAS	0.0000	2	0.0	!MK - CTS value unchanged
OHS	CPS	CTS	HAS	0.1472	3	0.0	!MK - CTS value unchanged
OHS	CTS	CBS	HAS	0.0000	1	0.0	
OHS	CTS	CBS	HAS	0.0000	2	0.0	
OHS	CTS	CBS	HAS	0.1472	3	0.0	
OHS	CTS	CTS	OHS	-4.9362	1	0.0	
OHS	CTS	CTS	OHS	0.2907	2	0.0	
OHS	CTS	CTS	OHS	0.4638	3	0.0	
OHS	CBS	CTS	OHS	-4.9362	1	0.0	
OHS	CBS	CTS	OHS	0.2907	2	0.0	
OHS	CBS	CTS	OHS	0.4638	3	0.0	

IMPROPER

```

NONBONDED  NBXMOD 5  atom CDIEL shift vatom VDISTANCE VSWITCH -
             CUTNB 13.0 CTOFNB 12.0 CTONNB 10.0 EPS 1.0 E14FAC 1.0 WMIN 1.5
!
!           Emin           Rmin
!           (kcal/mol)    (A)
HSPC           0.0000    -0.0000    1.3750    ! SPC water hydrogen
HT             0.00     -0.046     0.2245    ! TIP3P
OSPC           0.0000    -0.1554    1.7766    ! SPC
OT             0.00     -0.1521    1.7682    ! TIP3P
HOS            0.00     -0.0460    0.2245    !
HAS            0.00     -0.0220    1.3200    !
CTS            0.00     -0.0200    2.2750    0.0000    -0.01000    1.90000 !

```



```

CBS      0.00      -0.0200      2.2750      0.000      -0.01000      1.90000 !
CPS      0.00      -0.0200      2.2750      0.000      -0.01000      1.90000 !
OHS      0.00      -0.1521      1.7700      ! from para_na, on5
OES      0.00      -0.1521      1.7700      ! from para_na, on6

!
NBFIX
!
!      NBFIX the TIP3P water-water interactions
OT  OT      -0.152073  3.5365  ! TIPS3P VDW INTERACTION
HT  HT      -0.04598  0.4490
HT  OT      -0.08363  1.9927
!
!      the following will fix the SPC-sugar interaction terms
!
OSPC OSPC      -0.15539  3.5532  ! SPC VDW INTERACTION
HSPC HSPC      -0.00000  0.4490
HSPC OSPC      -0.00000  1.9927
OSPC OHS      -0.15888  3.4657
OSPC OES      -0.15888  3.4657
OSPC CTS      -0.13067  3.4733
OSPC CBS      -0.13067  3.4733
OSPC CPS      -0.13067  3.4733
OSPC HAS      -0.11015  2.7973
OSPC HOS      -0.00000  1.8
!
!
! this force field treats hbonds implicitly using charges; therefore the
! following section wildcards all the energies to 0. Note that you should
! also set the IHBFRQ to zero in all calcs, to avoid wasting time updating
! the hydrogen bond list!
!
HBOND AEXP 4 REXP 6 HAEX 4 AAEX 0 NOACCEPTORS HBNOEXCLUSIONS ALL-
      CUTHB 0.5 CTOFHB 5.0 CTONHB 4.0 CUTHA 5.0 CTOFHA 90.0 CTONHA 90.0
!
H*  O*      -0.00      2.0
END

```

11. Appendix E

NAMD Data Bank (PDB) File

The data bank (PDB) file contains information such as the name of the compound, stoichiometry, secondary structure locations, crystal lattice and stores atomic coordinates and/or velocities for the system.

The following file is the PDB file used for simulations performed on an 8 unit amylase molecule. The columns in the file in order from left to right are the record type, atom ID, atom name, residue name, residue ID, x, y, and z coordinates, occupancy, temperature factor, segment name, and line number.

```
REMARK COORDINATES FOR GLUCAN4
REMARK IN VACUUM.
REMARK DATE: 8/26/ 8 15:24:43 CREATED BY USER: mkuttel
ATOM 1 C1 AGLC 1 -0.901 0.420 -0.683 1.00 0.00 MAIN
ATOM 2 H1 AGLC 1 -1.474 -0.430 -1.083 1.00 0.00 MAIN
ATOM 3 O1 AGLC 1 -1.281 0.650 0.677 1.00 0.00 MAIN
ATOM 4 C5 AGLC 1 -0.663 2.788 -1.059 1.00 0.00 MAIN
ATOM 5 H5 AGLC 1 -0.876 2.962 0.009 1.00 0.00 MAIN
ATOM 6 O5 AGLC 1 -1.298 1.560 -1.445 1.00 0.00 MAIN
ATOM 7 C2 AGLC 1 0.614 0.213 -0.805 1.00 0.00 MAIN
ATOM 8 H2 AGLC 1 0.828 -0.041 -1.855 1.00 0.00 MAIN
ATOM 9 O2 AGLC 1 1.072 -0.849 0.036 1.00 0.00 MAIN
ATOM 10 HO2 AGLC 1 2.037 -0.887 -0.063 1.00 0.00 MAIN
ATOM 11 C3 AGLC 1 1.371 1.486 -0.464 1.00 0.00 MAIN
ATOM 12 H3 AGLC 1 1.227 1.702 0.608 1.00 0.00 MAIN
ATOM 13 O3 AGLC 1 2.759 1.307 -0.735 1.00 0.00 MAIN
ATOM 14 HO3 AGLC 1 3.197 2.148 -0.537 1.00 0.00 MAIN
ATOM 15 C4 AGLC 1 0.834 2.661 -1.268 1.00 0.00 MAIN
ATOM 16 H4 AGLC 1 1.036 2.478 -2.336 1.00 0.00 MAIN
ATOM 17 O4 AGLC 1 1.488 3.856 -0.846 1.00 0.00 MAIN
ATOM 18 HO4 AGLC 1 1.275 4.590 -1.433 1.00 0.00 MAIN
ATOM 19 C6 AGLC 1 -1.261 3.942 -1.852 1.00 0.00 MAIN
ATOM 20 H61 AGLC 1 -0.740 4.884 -1.622 1.00 0.00 MAIN
ATOM 21 H62 AGLC 1 -1.145 3.775 -2.935 1.00 0.00 MAIN
ATOM 22 O6 AGLC 1 -2.630 4.087 -1.516 1.00 0.00 MAIN
ATOM 23 HO6 AGLC 1 -3.120 3.263 -1.688 1.00 0.00 MAIN
ATOM 24 C1 AGLC 2 -3.673 -0.908 3.637 1.00 0.00 MAIN
ATOM 25 H1 AGLC 2 -4.370 -1.547 4.201 1.00 0.00 MAIN
ATOM 26 O1 AGLC 2 -3.742 0.433 4.142 1.00 0.00 MAIN
ATOM 27 C5 AGLC 2 -3.468 -0.097 1.382 1.00 0.00 MAIN
ATOM 28 H5 AGLC 2 -3.621 0.935 1.737 1.00 0.00 MAIN
ATOM 29 O5 AGLC 2 -4.153 -0.956 2.304 1.00 0.00 MAIN
ATOM 30 C2 AGLC 2 -2.240 -1.414 3.648 1.00 0.00 MAIN
ATOM 31 H2 AGLC 2 -2.244 -2.445 3.257 1.00 0.00 MAIN
ATOM 32 O2 AGLC 2 -1.689 -1.413 4.967 1.00 0.00 MAIN
```

ATOM	33	HO2	AGLC	2	-0.759	-1.678	4.874	1.00	0.00	MAIN
ATOM	34	C3	AGLC	2	-1.369	-0.561	2.742	1.00	0.00	MAIN
ATOM	35	H3	AGLC	2	-1.277	0.441	3.194	1.00	0.00	MAIN
ATOM	36	O3	AGLC	2	-0.083	-1.167	2.639	1.00	0.00	MAIN
ATOM	37	HO3	AGLC	2	0.352	-0.861	1.818	1.00	0.00	MAIN
ATOM	38	C4	AGLC	2	-1.970	-0.418	1.346	1.00	0.00	MAIN
ATOM	39	H4	AGLC	2	-1.793	-1.358	0.801	1.00	0.00	MAIN
ATOM	40	C6	AGLC	2	-4.097	-0.201	-0.009	1.00	0.00	MAIN
ATOM	41	H61	AGLC	2	-3.671	0.572	-0.663	1.00	0.00	MAIN
ATOM	42	H62	AGLC	2	-3.839	-1.171	-0.462	1.00	0.00	MAIN
ATOM	43	O6	AGLC	2	-5.510	-0.062	0.032	1.00	0.00	MAIN
ATOM	44	HO6	AGLC	2	-5.840	0.031	-0.884	1.00	0.00	MAIN
ATOM	45	C1	AGLC	3	-5.613	2.478	7.254	1.00	0.00	MAIN
ATOM	46	H1	AGLC	3	-6.260	2.620	8.132	1.00	0.00	MAIN
ATOM	47	O1	AGLC	3	-5.461	3.733	6.574	1.00	0.00	MAIN
ATOM	48	C5	AGLC	3	-5.750	1.255	5.187	1.00	0.00	MAIN
ATOM	49	H5	AGLC	3	-5.619	2.208	4.650	1.00	0.00	MAIN
ATOM	50	O5	AGLC	3	-6.353	1.568	6.449	1.00	0.00	MAIN
ATOM	51	C2	AGLC	3	-4.253	1.864	7.577	1.00	0.00	MAIN
ATOM	52	H2	AGLC	3	-4.436	0.950	8.164	1.00	0.00	MAIN
ATOM	53	O2	AGLC	3	-3.435	2.753	8.342	1.00	0.00	MAIN
ATOM	54	HO2	AGLC	3	-2.567	2.322	8.417	1.00	0.00	MAIN
ATOM	55	C3	AGLC	3	-3.514	1.467	6.307	1.00	0.00	MAIN
ATOM	56	H3	AGLC	3	-3.233	2.382	5.759	1.00	0.00	MAIN
ATOM	57	O3	AGLC	3	-2.344	0.740	6.678	1.00	0.00	MAIN
ATOM	58	HO3	AGLC	3	-2.071	0.159	5.938	1.00	0.00	MAIN
ATOM	59	C4	AGLC	3	-4.392	0.602	5.411	1.00	0.00	MAIN
ATOM	60	H4	AGLC	3	-4.475	-0.378	5.906	1.00	0.00	MAIN
ATOM	61	C6	AGLC	3	-6.681	0.385	4.338	1.00	0.00	MAIN
ATOM	62	H61	AGLC	3	-6.289	0.314	3.309	1.00	0.00	MAIN
ATOM	63	H62	AGLC	3	-6.694	-0.640	4.739	1.00	0.00	MAIN
ATOM	64	O6	AGLC	3	-8.004	0.908	4.323	1.00	0.00	MAIN
ATOM	65	HO6	AGLC	3	-8.502	0.526	3.592	1.00	0.00	MAIN
ATOM	66	C1	AGLC	4	-6.648	7.692	7.203	1.00	0.00	MAIN
ATOM	67	H1	AGLC	4	-7.171	8.515	7.714	1.00	0.00	MAIN
ATOM	68	O1	AGLC	4	-6.460	8.040	5.823	1.00	0.00	MAIN
ATOM	69	C5	AGLC	4	-7.191	5.407	6.679	1.00	0.00	MAIN
ATOM	70	H5	AGLC	4	-7.024	5.643	5.616	1.00	0.00	MAIN
ATOM	71	O5	AGLC	4	-7.581	6.626	7.320	1.00	0.00	MAIN
ATOM	72	C2	AGLC	4	-5.325	7.274	7.844	1.00	0.00	MAIN
ATOM	73	H2	AGLC	4	-5.518	7.110	8.916	1.00	0.00	MAIN
ATOM	74	O2	AGLC	4	-4.319	8.279	7.700	1.00	0.00	MAIN
ATOM	75	HO2	AGLC	4	-3.498	7.887	8.041	1.00	0.00	MAIN
ATOM	76	C3	AGLC	4	-4.817	5.963	7.254	1.00	0.00	MAIN
ATOM	77	H3	AGLC	4	-4.523	6.133	6.204	1.00	0.00	MAIN
ATOM	78	O3	AGLC	4	-3.689	5.538	8.017	1.00	0.00	MAIN
ATOM	79	HO3	AGLC	4	-3.562	4.573	7.907	1.00	0.00	MAIN
ATOM	80	C4	AGLC	4	-5.900	4.893	7.300	1.00	0.00	MAIN
ATOM	81	H4	AGLC	4	-6.020	4.629	8.363	1.00	0.00	MAIN
ATOM	82	C6	AGLC	4	-8.319	4.373	6.740	1.00	0.00	MAIN
ATOM	83	H61	AGLC	4	-8.084	3.525	6.076	1.00	0.00	MAIN
ATOM	84	H62	AGLC	4	-8.387	3.962	7.759	1.00	0.00	MAIN
ATOM	85	O6	AGLC	4	-9.569	4.948	6.374	1.00	0.00	MAIN
ATOM	86	HO6	AGLC	4	-10.206	4.252	6.180	1.00	0.00	MAIN
ATOM	87	C1	AGLC	5	-7.216	11.340	3.373	1.00	0.00	MAIN
ATOM	88	H1	AGLC	5	-7.649	12.316	3.108	1.00	0.00	MAIN
ATOM	89	O1	AGLC	5	-7.048	10.558	2.183	1.00	0.00	MAIN

ATOM	90	C5	AGLC	5	-8.010	9.451	4.640	1.00	0.00	MAIN
ATOM	91	H5	AGLC	5	-7.881	8.825	3.743	1.00	0.00	MAIN
ATOM	92	O5	AGLC	5	-8.245	10.787	4.184	1.00	0.00	MAIN
ATOM	93	C2	AGLC	5	-5.917	11.381	4.176	1.00	0.00	MAIN
ATOM	94	H2	AGLC	5	-6.080	12.053	5.034	1.00	0.00	MAIN
ATOM	95	O2	AGLC	5	-4.824	11.876	3.399	1.00	0.00	MAIN
ATOM	96	HO2	AGLC	5	-4.031	11.759	3.949	1.00	0.00	MAIN
ATOM	97	C3	AGLC	5	-5.566	9.999	4.717	1.00	0.00	MAIN
ATOM	98	H3	AGLC	5	-5.314	9.336	3.872	1.00	0.00	MAIN
ATOM	99	O3	AGLC	5	-4.446	10.132	5.590	1.00	0.00	MAIN
ATOM	100	HO3	AGLC	5	-4.380	9.341	6.166	1.00	0.00	MAIN
ATOM	101	C4	AGLC	5	-6.743	9.407	5.482	1.00	0.00	MAIN
ATOM	102	H4	AGLC	5	-6.815	10.005	6.404	1.00	0.00	MAIN
ATOM	103	C6	AGLC	5	-9.229	8.912	5.395	1.00	0.00	MAIN
ATOM	104	H61	AGLC	5	-9.109	7.831	5.575	1.00	0.00	MAIN
ATOM	105	H62	AGLC	5	-9.287	9.388	6.386	1.00	0.00	MAIN
ATOM	106	O6	AGLC	5	-10.432	9.154	4.675	1.00	0.00	MAIN
ATOM	107	HO6	AGLC	5	-11.158	8.666	5.077	1.00	0.00	MAIN
ATOM	108	C1	AGLC	6	-7.551	10.933	-1.925	1.00	0.00	MAIN
ATOM	109	H1	AGLC	6	-7.927	11.331	-2.880	1.00	0.00	MAIN
ATOM	110	O1	AGLC	6	-7.327	9.524	-2.051	1.00	0.00	MAIN
ATOM	111	C5	AGLC	6	-8.506	10.676	0.277	1.00	0.00	MAIN
ATOM	112	H5	AGLC	6	-8.403	9.582	0.185	1.00	0.00	MAIN
ATOM	113	O5	AGLC	6	-8.648	11.185	-1.056	1.00	0.00	MAIN
ATOM	114	C2	AGLC	6	-6.312	11.608	-1.349	1.00	0.00	MAIN
ATOM	115	H2	AGLC	6	-6.518	12.689	-1.282	1.00	0.00	MAIN
ATOM	116	O2	AGLC	6	-5.161	11.403	-2.172	1.00	0.00	MAIN
ATOM	117	HO2	AGLC	6	-4.409	11.757	-1.668	1.00	0.00	MAIN
ATOM	118	C3	AGLC	6	-6.031	11.084	0.053	1.00	0.00	MAIN
ATOM	119	H3	AGLC	6	-5.769	10.014	-0.008	1.00	0.00	MAIN
ATOM	120	O3	AGLC	6	-4.941	11.822	0.602	1.00	0.00	MAIN
ATOM	121	HO3	AGLC	6	-4.883	11.659	1.568	1.00	0.00	MAIN
ATOM	122	C4	AGLC	6	-7.259	11.249	0.941	1.00	0.00	MAIN
ATOM	123	H4	AGLC	6	-7.308	12.334	1.127	1.00	0.00	MAIN
ATOM	124	C6	AGLC	6	-9.769	10.943	1.100	1.00	0.00	MAIN
ATOM	125	H61	AGLC	6	-9.723	10.381	2.048	1.00	0.00	MAIN
ATOM	126	H62	AGLC	6	-9.808	12.009	1.375	1.00	0.00	MAIN
ATOM	127	O6	AGLC	6	-10.944	10.590	0.379	1.00	0.00	MAIN
ATOM	128	HO6	AGLC	6	-11.709	10.625	0.963	1.00	0.00	MAIN
ATOM	129	C1	AGLC	7	-7.396	6.452	-4.807	1.00	0.00	MAIN
ATOM	130	H1	AGLC	7	-7.634	5.851	-5.698	1.00	0.00	MAIN
ATOM	131	O1	AGLC	7	-7.143	5.582	-3.696	1.00	0.00	MAIN
ATOM	132	C5	AGLC	7	-8.599	8.000	-3.398	1.00	0.00	MAIN
ATOM	133	H5	AGLC	7	-8.512	7.300	-2.552	1.00	0.00	MAIN
ATOM	134	O5	AGLC	7	-8.587	7.197	-4.590	1.00	0.00	MAIN
ATOM	135	C2	AGLC	7	-6.246	7.434	-4.967	1.00	0.00	MAIN
ATOM	136	H2	AGLC	7	-6.485	8.104	-5.809	1.00	0.00	MAIN
ATOM	137	O2	AGLC	7	-5.010	6.771	-5.237	1.00	0.00	MAIN
ATOM	138	HO2	AGLC	7	-4.326	7.460	-5.193	1.00	0.00	MAIN
ATOM	139	C3	AGLC	7	-6.103	8.273	-3.708	1.00	0.00	MAIN
ATOM	140	H3	AGLC	7	-5.814	7.617	-2.869	1.00	0.00	MAIN
ATOM	141	O3	AGLC	7	-5.086	9.250	-3.929	1.00	0.00	MAIN
ATOM	142	HO3	AGLC	7	-5.094	9.907	-3.199	1.00	0.00	MAIN
ATOM	143	C4	AGLC	7	-7.418	8.971	-3.372	1.00	0.00	MAIN
ATOM	144	H4	AGLC	7	-7.470	9.784	-4.112	1.00	0.00	MAIN
ATOM	145	C6	AGLC	7	-9.935	8.728	-3.243	1.00	0.00	MAIN
ATOM	146	H61	AGLC	7	-9.988	9.205	-2.250	1.00	0.00	MAIN

ATOM	147	H62	AGLC	7	-9.997	9.542	-3.982	1.00	0.00	MAIN
ATOM	148	O6	AGLC	7	-11.029	7.835	-3.417	1.00	0.00	MAIN
ATOM	149	HO6	AGLC	7	-11.844	8.253	-3.120	1.00	0.00	MAIN
ATOM	150	C1	AGLC	8	-6.736	1.658	-2.610	1.00	0.00	MAIN
ATOM	151	H1	AGLC	8	-6.821	2.066	-1.582	1.00	0.00	MAIN
ATOM	152	O1	AGLC	8	-6.711	0.269	-2.596	1.00	0.00	MAIN
ATOM	153	HO1	AGLC	8	-7.622	-0.004	-2.438	1.00	0.00	MAIN
ATOM	154	C5	AGLC	8	-8.143	3.425	-3.337	1.00	0.00	MAIN
ATOM	155	H5	AGLC	8	-8.234	3.715	-2.279	1.00	0.00	MAIN
ATOM	156	O5	AGLC	8	-7.893	2.015	-3.340	1.00	0.00	MAIN
ATOM	157	C2	AGLC	8	-5.521	2.227	-3.332	1.00	0.00	MAIN
ATOM	158	H2	AGLC	8	-5.516	1.805	-4.351	1.00	0.00	MAIN
ATOM	159	O2	AGLC	8	-4.296	1.887	-2.680	1.00	0.00	MAIN
ATOM	160	HO2	AGLC	8	-3.591	2.099	-3.306	1.00	0.00	MAIN
ATOM	161	C3	AGLC	8	-5.624	3.739	-3.431	1.00	0.00	MAIN
ATOM	162	H3	AGLC	8	-5.483	4.159	-2.420	1.00	0.00	MAIN
ATOM	163	O3	AGLC	8	-4.591	4.202	-4.299	1.00	0.00	MAIN
ATOM	164	HO3	AGLC	8	-4.708	5.161	-4.468	1.00	0.00	MAIN
ATOM	165	C4	AGLC	8	-6.980	4.183	-3.978	1.00	0.00	MAIN
ATOM	166	H4	AGLC	8	-6.886	4.033	-5.065	1.00	0.00	MAIN
ATOM	167	C6	AGLC	8	-9.472	3.745	-4.028	1.00	0.00	MAIN
ATOM	168	H61	AGLC	8	-9.712	4.813	-3.894	1.00	0.00	MAIN
ATOM	169	H62	AGLC	8	-9.365	3.583	-5.112	1.00	0.00	MAIN
ATOM	170	O6	AGLC	8	-10.533	2.939	-3.524	1.00	0.00	MAIN
ATOM	171	HO6	AGLC	8	-11.376	3.211	-3.900	1.00	0.00	MAIN
END										

12. Appendix F

NAMD Structure (PSF) File

The structure (PSF) file, contains all of the moleculespecific information (structural information such as various types of bonding interactions) needed to apply a particular force field to a molecular system. The PSF file is generated from the force field topology file. The PSF file contains five main sections of interest: atoms, bonds, angles, dihedrals, and impropers. The following file is the PSF file used for simulations performed on an 8 unit amylase molecule.

* PSF GLU4

* DATE: 8/26/ 8

```
171 !NATOM
  1 MAIN 1    AGLC C1    CTS    0.300000    12.0110    0
  2 MAIN 1    AGLC H1    HAS    0.100000    1.00800   0
  3 MAIN 1    AGLC O1    OES   -0.400000    15.9994   0
  4 MAIN 1    AGLC C5    CTS    0.100000    12.0110   0
  5 MAIN 1    AGLC H5    HAS    0.100000    1.00800   0
  6 MAIN 1    AGLC O5    OES   -0.400000    15.9994   0
  7 MAIN 1    AGLC C2    CTS    0.140000    12.0110   0
  8 MAIN 1    AGLC H2    HAS    0.900000E-01  1.00800   0
  9 MAIN 1    AGLC O2    OHS   -0.660000    15.9994   0
 10 MAIN 1    AGLC HO2   HOS    0.430000    1.00800   0
 11 MAIN 1    AGLC C3    CTS    0.140000    12.0110   0
 12 MAIN 1    AGLC H3    HAS    0.900000E-01  1.00800   0
 13 MAIN 1    AGLC O3    OHS   -0.660000    15.9994   0
 14 MAIN 1    AGLC HO3   HOS    0.430000    1.00800   0
 15 MAIN 1    AGLC C4    CTS    0.140000    12.0110   0
 16 MAIN 1    AGLC H4    HAS    0.900000E-01  1.00800   0
 17 MAIN 1    AGLC O4    OHS   -0.660000    15.9994   0
 18 MAIN 1    AGLC HO4   HOS    0.430000    1.00800   0
 19 MAIN 1    AGLC C6    CPS    0.500000E-01  12.0110   0
 20 MAIN 1    AGLC H61   HAS    0.900000E-01  1.00800   0
 21 MAIN 1    AGLC H62   HAS    0.900000E-01  1.00800   0
 22 MAIN 1    AGLC O6    OHS   -0.660000    15.9994   0
 23 MAIN 1    AGLC HO6   HOS    0.430000    1.00800   0
 24 MAIN 2    AGLC C1    CTS    0.300000    12.0110   0
 25 MAIN 2    AGLC H1    HAS    0.100000    1.00800   0
 26 MAIN 2    AGLC O1    OES   -0.400000    15.9994   0
 27 MAIN 2    AGLC C5    CTS    0.100000    12.0110   0
 28 MAIN 2    AGLC H5    HAS    0.100000    1.00800   0
 29 MAIN 2    AGLC O5    OES   -0.400000    15.9994   0
 30 MAIN 2    AGLC C2    CTS    0.140000    12.0110   0
 31 MAIN 2    AGLC H2    HAS    0.900000E-01  1.00800   0
 32 MAIN 2    AGLC O2    OHS   -0.660000    15.9994   0
 33 MAIN 2    AGLC HO2   HOS    0.430000    1.00800   0
 34 MAIN 2    AGLC C3    CTS    0.140000    12.0110   0
 35 MAIN 2    AGLC H3    HAS    0.900000E-01  1.00800   0
 36 MAIN 2    AGLC O3    OHS   -0.660000    15.9994   0
```

37	MAIN	2	AGLC	HO3	HOS	0.430000	1.00800	0
38	MAIN	2	AGLC	C4	CTS	0.100000	12.0110	0
39	MAIN	2	AGLC	H4	HAS	0.100000	1.00800	0
40	MAIN	2	AGLC	C6	CPS	0.500000E-01	12.0110	0
41	MAIN	2	AGLC	H61	HAS	0.900000E-01	1.00800	0
42	MAIN	2	AGLC	H62	HAS	0.900000E-01	1.00800	0
43	MAIN	2	AGLC	O6	OHS	-0.660000	15.9994	0
44	MAIN	2	AGLC	HO6	HOS	0.430000	1.00800	0
45	MAIN	3	AGLC	C1	CTS	0.300000	12.0110	0
46	MAIN	3	AGLC	H1	HAS	0.100000	1.00800	0
47	MAIN	3	AGLC	O1	OES	-0.400000	15.9994	0
48	MAIN	3	AGLC	C5	CTS	0.100000	12.0110	0
49	MAIN	3	AGLC	H5	HAS	0.100000	1.00800	0
50	MAIN	3	AGLC	O5	OES	-0.400000	15.9994	0
51	MAIN	3	AGLC	C2	CTS	0.140000	12.0110	0
52	MAIN	3	AGLC	H2	HAS	0.900000E-01	1.00800	0
53	MAIN	3	AGLC	O2	OHS	-0.660000	15.9994	0
54	MAIN	3	AGLC	HO2	HOS	0.430000	1.00800	0
55	MAIN	3	AGLC	C3	CTS	0.140000	12.0110	0
56	MAIN	3	AGLC	H3	HAS	0.900000E-01	1.00800	0
57	MAIN	3	AGLC	O3	OHS	-0.660000	15.9994	0
58	MAIN	3	AGLC	HO3	HOS	0.430000	1.00800	0
59	MAIN	3	AGLC	C4	CTS	0.100000	12.0110	0
60	MAIN	3	AGLC	H4	HAS	0.100000	1.00800	0
61	MAIN	3	AGLC	C6	CPS	0.500000E-01	12.0110	0
62	MAIN	3	AGLC	H61	HAS	0.900000E-01	1.00800	0
63	MAIN	3	AGLC	H62	HAS	0.900000E-01	1.00800	0
64	MAIN	3	AGLC	O6	OHS	-0.660000	15.9994	0
65	MAIN	3	AGLC	HO6	HOS	0.430000	1.00800	0
66	MAIN	4	AGLC	C1	CTS	0.300000	12.0110	0
67	MAIN	4	AGLC	H1	HAS	0.100000	1.00800	0
68	MAIN	4	AGLC	O1	OES	-0.400000	15.9994	0
69	MAIN	4	AGLC	C5	CTS	0.100000	12.0110	0
70	MAIN	4	AGLC	H5	HAS	0.100000	1.00800	0
71	MAIN	4	AGLC	O5	OES	-0.400000	15.9994	0
72	MAIN	4	AGLC	C2	CTS	0.140000	12.0110	0
73	MAIN	4	AGLC	H2	HAS	0.900000E-01	1.00800	0
74	MAIN	4	AGLC	O2	OHS	-0.660000	15.9994	0
75	MAIN	4	AGLC	HO2	HOS	0.430000	1.00800	0
76	MAIN	4	AGLC	C3	CTS	0.140000	12.0110	0
77	MAIN	4	AGLC	H3	HAS	0.900000E-01	1.00800	0
78	MAIN	4	AGLC	O3	OHS	-0.660000	15.9994	0
79	MAIN	4	AGLC	HO3	HOS	0.430000	1.00800	0
80	MAIN	4	AGLC	C4	CTS	0.100000	12.0110	0
81	MAIN	4	AGLC	H4	HAS	0.100000	1.00800	0
82	MAIN	4	AGLC	C6	CPS	0.500000E-01	12.0110	0
83	MAIN	4	AGLC	H61	HAS	0.900000E-01	1.00800	0
84	MAIN	4	AGLC	H62	HAS	0.900000E-01	1.00800	0
85	MAIN	4	AGLC	O6	OHS	-0.660000	15.9994	0
86	MAIN	4	AGLC	HO6	HOS	0.430000	1.00800	0
87	MAIN	5	AGLC	C1	CTS	0.300000	12.0110	0
88	MAIN	5	AGLC	H1	HAS	0.100000	1.00800	0
89	MAIN	5	AGLC	O1	OES	-0.400000	15.9994	0
90	MAIN	5	AGLC	C5	CTS	0.100000	12.0110	0
91	MAIN	5	AGLC	H5	HAS	0.100000	1.00800	0
92	MAIN	5	AGLC	O5	OES	-0.400000	15.9994	0
93	MAIN	5	AGLC	C2	CTS	0.140000	12.0110	0

94	MAIN	5	AGLC	H2	HAS	0.900000E-01	1.00800	0
95	MAIN	5	AGLC	O2	OHS	-0.660000	15.9994	0
96	MAIN	5	AGLC	HO2	HOS	0.430000	1.00800	0
97	MAIN	5	AGLC	C3	CTS	0.140000	12.0110	0
98	MAIN	5	AGLC	H3	HAS	0.900000E-01	1.00800	0
99	MAIN	5	AGLC	O3	OHS	-0.660000	15.9994	0
100	MAIN	5	AGLC	HO3	HOS	0.430000	1.00800	0
101	MAIN	5	AGLC	C4	CTS	0.100000	12.0110	0
102	MAIN	5	AGLC	H4	HAS	0.100000	1.00800	0
103	MAIN	5	AGLC	C6	CPS	0.500000E-01	12.0110	0
104	MAIN	5	AGLC	H61	HAS	0.900000E-01	1.00800	0
105	MAIN	5	AGLC	H62	HAS	0.900000E-01	1.00800	0
106	MAIN	5	AGLC	O6	OHS	-0.660000	15.9994	0
107	MAIN	5	AGLC	HO6	HOS	0.430000	1.00800	0
108	MAIN	6	AGLC	C1	CTS	0.300000	12.0110	0
109	MAIN	6	AGLC	H1	HAS	0.100000	1.00800	0
110	MAIN	6	AGLC	O1	OES	-0.400000	15.9994	0
111	MAIN	6	AGLC	C5	CTS	0.100000	12.0110	0
112	MAIN	6	AGLC	H5	HAS	0.100000	1.00800	0
113	MAIN	6	AGLC	O5	OES	-0.400000	15.9994	0
114	MAIN	6	AGLC	C2	CTS	0.140000	12.0110	0
115	MAIN	6	AGLC	H2	HAS	0.900000E-01	1.00800	0
116	MAIN	6	AGLC	O2	OHS	-0.660000	15.9994	0
117	MAIN	6	AGLC	HO2	HOS	0.430000	1.00800	0
118	MAIN	6	AGLC	C3	CTS	0.140000	12.0110	0
119	MAIN	6	AGLC	H3	HAS	0.900000E-01	1.00800	0
120	MAIN	6	AGLC	O3	OHS	-0.660000	15.9994	0
121	MAIN	6	AGLC	HO3	HOS	0.430000	1.00800	0
122	MAIN	6	AGLC	C4	CTS	0.100000	12.0110	0
123	MAIN	6	AGLC	H4	HAS	0.100000	1.00800	0
124	MAIN	6	AGLC	C6	CPS	0.500000E-01	12.0110	0
125	MAIN	6	AGLC	H61	HAS	0.900000E-01	1.00800	0
126	MAIN	6	AGLC	H62	HAS	0.900000E-01	1.00800	0
127	MAIN	6	AGLC	O6	OHS	-0.660000	15.9994	0
128	MAIN	6	AGLC	HO6	HOS	0.430000	1.00800	0
129	MAIN	7	AGLC	C1	CTS	0.300000	12.0110	0
130	MAIN	7	AGLC	H1	HAS	0.100000	1.00800	0
131	MAIN	7	AGLC	O1	OES	-0.400000	15.9994	0
132	MAIN	7	AGLC	C5	CTS	0.100000	12.0110	0
133	MAIN	7	AGLC	H5	HAS	0.100000	1.00800	0
134	MAIN	7	AGLC	O5	OES	-0.400000	15.9994	0
135	MAIN	7	AGLC	C2	CTS	0.140000	12.0110	0
136	MAIN	7	AGLC	H2	HAS	0.900000E-01	1.00800	0
137	MAIN	7	AGLC	O2	OHS	-0.660000	15.9994	0
138	MAIN	7	AGLC	HO2	HOS	0.430000	1.00800	0
139	MAIN	7	AGLC	C3	CTS	0.140000	12.0110	0
140	MAIN	7	AGLC	H3	HAS	0.900000E-01	1.00800	0
141	MAIN	7	AGLC	O3	OHS	-0.660000	15.9994	0
142	MAIN	7	AGLC	HO3	HOS	0.430000	1.00800	0
143	MAIN	7	AGLC	C4	CTS	0.100000	12.0110	0
144	MAIN	7	AGLC	H4	HAS	0.100000	1.00800	0
145	MAIN	7	AGLC	C6	CPS	0.500000E-01	12.0110	0
146	MAIN	7	AGLC	H61	HAS	0.900000E-01	1.00800	0
147	MAIN	7	AGLC	H62	HAS	0.900000E-01	1.00800	0
148	MAIN	7	AGLC	O6	OHS	-0.660000	15.9994	0
149	MAIN	7	AGLC	HO6	HOS	0.430000	1.00800	0
150	MAIN	8	AGLC	C1	CBS	0.200000	12.0110	0

151	MAIN	8	AGLC	H1	HAS	0.900000E-01	1.00800	0
152	MAIN	8	AGLC	O1	OHS	-0.660000	15.9994	0
153	MAIN	8	AGLC	HO1	HOS	0.430000	1.00800	0
154	MAIN	8	AGLC	C5	CTS	0.250000	12.0110	0
155	MAIN	8	AGLC	H5	HAS	0.900000E-01	1.00800	0
156	MAIN	8	AGLC	O5	OES	-0.400000	15.9994	0
157	MAIN	8	AGLC	C2	CTS	0.140000	12.0110	0
158	MAIN	8	AGLC	H2	HAS	0.900000E-01	1.00800	0
159	MAIN	8	AGLC	O2	OHS	-0.660000	15.9994	0
160	MAIN	8	AGLC	HO2	HOS	0.430000	1.00800	0
161	MAIN	8	AGLC	C3	CTS	0.140000	12.0110	0
162	MAIN	8	AGLC	H3	HAS	0.900000E-01	1.00800	0
163	MAIN	8	AGLC	O3	OHS	-0.660000	15.9994	0
164	MAIN	8	AGLC	HO3	HOS	0.430000	1.00800	0
165	MAIN	8	AGLC	C4	CTS	0.100000	12.0110	0
166	MAIN	8	AGLC	H4	HAS	0.100000	1.00800	0
167	MAIN	8	AGLC	C6	CPS	0.500000E-01	12.0110	0
168	MAIN	8	AGLC	H61	HAS	0.900000E-01	1.00800	0
169	MAIN	8	AGLC	H62	HAS	0.900000E-01	1.00800	0
170	MAIN	8	AGLC	O6	OHS	-0.660000	15.9994	0
171	MAIN	8	AGLC	HO6	HOS	0.430000	1.00800	0

178 !NBOND: bonds

1	3	1	2	1	6	1	7
7	8	7	9	9	10	7	11
11	12	11	13	13	14	11	15
15	16	15	17	17	18	15	4
4	5	4	19	19	20	19	21
19	22	22	23	4	6	24	26
24	25	24	29	24	30	30	31
30	32	32	33	30	34	34	35
34	36	36	37	34	38	38	39
38	27	27	28	27	40	40	41
40	42	40	43	43	44	27	29
45	47	45	46	45	50	45	51
51	52	51	53	53	54	51	55
55	56	55	57	57	58	55	59
59	60	59	48	48	49	48	61
61	62	61	63	61	64	64	65
48	50	66	68	66	67	66	71
66	72	72	73	72	74	74	75
72	76	76	77	76	78	78	79
76	80	80	81	80	69	69	70
69	82	82	83	82	84	82	85
85	86	69	71	87	89	87	88
87	92	87	93	93	94	93	95
95	96	93	97	97	98	97	99
99	100	97	101	101	102	101	90
90	91	90	103	103	104	103	105
103	106	106	107	90	92	108	110
108	109	108	113	108	114	114	115
114	116	116	117	114	118	118	119
118	120	120	121	118	122	122	123
122	111	111	112	111	124	124	125
124	126	124	127	127	128	111	113
129	131	129	130	129	134	129	135
135	136	135	137	137	138	135	139

139	140	139	141	141	142	139	143
143	144	143	132	132	133	132	145
145	146	145	147	145	148	148	149
132	134	150	152	150	151	152	153
150	156	150	157	157	158	157	159
159	160	157	161	161	162	161	163
163	164	161	165	165	166	165	154
154	155	154	167	167	168	167	169
167	170	170	171	154	156	3	38
26	59	47	80	68	101	89	122
110	143	131	165				

329 !NTHETA: angles

2	1	3	2	1	6	2	1	7
3	1	6	3	1	7	6	1	7
1	3	38	5	4	6	5	4	15
5	4	19	6	4	15	6	4	19
15	4	19	1	6	4	1	7	8
1	7	9	1	7	11	8	7	9
8	7	11	9	7	11	7	9	10
7	11	12	7	11	13	7	11	15
12	11	13	12	11	15	13	11	15
11	13	14	4	15	11	4	15	16
4	15	17	11	15	16	11	15	17
16	15	17	15	17	18	4	19	20
4	19	21	4	19	22	20	19	21
20	19	22	21	19	22	19	22	23
25	24	26	25	24	29	25	24	30
26	24	29	26	24	30	29	24	30
24	26	59	28	27	29	28	27	38
28	27	40	29	27	38	29	27	40
38	27	40	24	29	27	24	30	31
24	30	32	24	30	34	31	30	32
31	30	34	32	30	34	30	32	33
30	34	35	30	34	36	30	34	38
35	34	36	35	34	38	36	34	38
34	36	37	3	38	27	3	38	34
3	38	39	27	38	34	27	38	39
34	38	39	27	40	41	27	40	42
27	40	43	41	40	42	41	40	43
42	40	43	40	43	44	46	45	47
46	45	50	46	45	51	47	45	50
47	45	51	50	45	51	45	47	80
49	48	50	49	48	59	49	48	61
50	48	59	50	48	61	59	48	61
45	50	48	45	51	52	45	51	53
45	51	55	52	51	53	52	51	55
53	51	55	51	53	54	51	55	56
51	55	57	51	55	59	56	55	57
56	55	59	57	55	59	55	57	58
26	59	48	26	59	55	26	59	60
48	59	55	48	59	60	55	59	60
48	61	62	48	61	63	48	61	64
62	61	63	62	61	64	63	61	64
61	64	65	67	66	68	67	66	71
67	66	72	68	66	71	68	66	72
71	66	72	66	68	101	70	69	71

70	69	80	70	69	82	71	69	80
71	69	82	80	69	82	66	71	69
66	72	73	66	72	74	66	72	76
73	72	74	73	72	76	74	72	76
72	74	75	72	76	77	72	76	78
72	76	80	77	76	78	77	76	80
78	76	80	76	78	79	47	80	69
47	80	76	47	80	81	69	80	76
69	80	81	76	80	81	69	82	83
69	82	84	69	82	85	83	82	84
83	82	85	84	82	85	82	85	86
88	87	89	88	87	92	88	87	93
89	87	92	89	87	93	92	87	93
87	89	122	91	90	92	91	90	101
91	90	103	92	90	101	92	90	103
101	90	103	87	92	90	87	93	94
87	93	95	87	93	97	94	93	95
94	93	97	95	93	97	93	95	96
93	97	98	93	97	99	93	97	101
98	97	99	98	97	101	99	97	101
97	99	100	68	101	90	68	101	97
68	101	102	90	101	97	90	101	102
97	101	102	90	103	104	90	103	105
90	103	106	104	103	105	104	103	106
105	103	106	103	106	107	109	108	110
109	108	113	109	108	114	110	108	113
110	108	114	113	108	114	108	110	143
112	111	113	112	111	122	112	111	124
113	111	122	113	111	124	122	111	124
108	113	111	108	114	115	108	114	116
108	114	118	115	114	116	115	114	118
116	114	118	114	116	117	114	118	119
114	118	120	114	118	122	119	118	120
119	118	122	120	118	122	118	120	121
89	122	111	89	122	118	89	122	123
111	122	118	111	122	123	118	122	123
111	124	125	111	124	126	111	124	127
125	124	126	125	124	127	126	124	127
124	127	128	130	129	131	130	129	134
130	129	135	131	129	134	131	129	135
134	129	135	129	131	165	133	132	134
133	132	143	133	132	145	134	132	143
134	132	145	143	132	145	129	134	132
129	135	136	129	135	137	129	135	139
136	135	137	136	135	139	137	135	139
135	137	138	135	139	140	135	139	141
135	139	143	140	139	141	140	139	143
141	139	143	139	141	142	110	143	132
110	143	139	110	143	144	132	143	139
132	143	144	139	143	144	132	145	146
132	145	147	132	145	148	146	145	147
146	145	148	147	145	148	145	148	149
151	150	152	151	150	156	151	150	157
152	150	156	152	150	157	156	150	157
150	152	153	155	154	156	155	154	165
155	154	167	156	154	165	156	154	167
165	154	167	150	156	154	150	157	158

150	157	159	150	157	161	158	157	159
158	157	161	159	157	161	157	159	160
157	161	162	157	161	163	157	161	165
162	161	163	162	161	165	163	161	165
161	163	164	131	165	154	131	165	161
131	165	166	154	165	161	154	165	166
161	165	166	154	167	168	154	167	169
154	167	170	168	167	169	168	167	170
169	167	170	167	170	171			

528 !NPHI: dihedrals

1	6	4	5	1	6	4	15	
1	6	4	19	1	7	9	10	
1	7	11	12	1	7	11	13	
1	7	11	15	2	1	6	4	
2	1	7	8	2	1	7	9	
2	1	7	11	3	1	6	4	
3	1	7	8	3	1	7	9	
3	1	7	11	4	6	1	7	
4	15	11	7	4	15	11	12	
4	15	11	13	4	15	17	18	
4	19	22	23	5	4	15	11	
5	4	15	16	5	4	15	17	
5	4	19	20	5	4	19	21	
5	4	19	22	6	1	7	8	
6	1	7	9	6	1	7	11	
6	4	15	11	6	4	15	16	
6	4	15	17	6	4	19	20	
6	4	19	21	6	4	19	22	
7	11	13	14	7	11	15	16	
7	11	15	17	8	7	9	10	
8	7	11	12	8	7	11	13	
8	7	11	15	9	7	11	12	
9	7	11	13	9	7	11	15	
10	9	7	11	11	15	4	19	
11	15	17	18	12	11	13	14	
12	11	15	16	12	11	15	17	
13	11	15	16	13	11	15	17	
14	13	11	15	15	4	19	20	
15	4	19	21	15	4	19	22	
16	15	4	19	16	15	17	18	
17	15	4	19	20	19	22	23	
21	19	22	23	24	29	27	28	
24	29	27	38	24	29	27	40	
24	30	32	33	24	30	34	35	
24	30	34	36	24	30	34	38	
25	24	29	27	25	24	30	31	
25	24	30	32	25	24	30	34	
26	24	29	27	26	24	30	31	
26	24	30	32	26	24	30	34	
27	29	24	30	27	38	34	30	
27	38	34	35	27	38	34	36	
27	40	43	44	28	27	38	34	
28	27	38	39	28	27	40	41	
28	27	40	42	28	27	40	43	
29	24	30	31	29	24	30	32	29
24	30	34	29	27	38	34		

29	27	38	39	29	27	40	41
29	27	40	42	29	27	40	43
30	34	36	37	30	34	38	39
31	30	32	33	31	30	34	35
31	30	34	36	31	30	34	38
32	30	34	35	32	30	34	36
32	30	34	38	33	32	30	34
34	38	27	40	35	34	36	37
35	34	38	39	36	34	38	39
37	36	34	38	38	27	40	41
38	27	40	42	38	27	40	43
39	38	27	40	41	40	43	44
42	40	43	44	45	50	48	49
45	50	48	59	45	50	48	61
45	51	53	54	45	51	55	56
45	51	55	57	45	51	55	59
46	45	50	48	46	45	51	52
46	45	51	53	46	45	51	55
47	45	50	48	47	45	51	52
47	45	51	53	47	45	51	55
48	50	45	51	48	59	55	51
48	59	55	56	48	59	55	57
48	61	64	65	49	48	59	55
49	48	59	60	49	48	61	62
49	48	61	63	49	48	61	64
50	45	51	52	50	45	51	53
50	45	51	55	50	48	59	55
50	48	59	60	50	48	61	62
50	48	61	63	50	48	61	64
51	55	57	58	51	55	59	60
52	51	53	54	52	51	55	56
52	51	55	57	52	51	55	59
53	51	55	56	53	51	55	57
53	51	55	59	54	53	51	55
55	59	48	61	56	55	57	58
56	55	59	60	57	55	59	60
58	57	55	59	59	48	61	62
59	48	61	63	59	48	61	64
60	59	48	61	62	61	64	65
63	61	64	65	66	71	69	70
66	71	69	80	66	71	69	82
66	72	74	75	66	72	76	77
66	72	76	78	66	72	76	80
67	66	71	69	67	66	72	73
67	66	72	74	67	66	72	76
68	66	71	69	68	66	72	73
68	66	72	74	68	66	72	76
69	71	66	72	69	80	76	72
69	80	76	77	69	80	76	78
69	82	85	86	70	69	80	76
70	69	80	81	70	69	82	83
70	69	82	84	70	69	82	85
71	66	72	73	71	66	72	74
71	66	72	76	71	69	80	76
71	69	80	81	71	69	82	83
71	69	82	84	71	69	82	85
72	76	78	79	72	76	80	81

73	72	74	75	73	72	76	77
73	72	76	78	73	72	76	80
74	72	76	77	74	72	76	78
74	72	76	80	75	74	72	76
76	80	69	82	77	76	78	79
77	76	80	81	78	76	80	81
79	78	76	80	80	69	82	83
80	69	82	84	80	69	82	85
81	80	69	82	83	82	85	86
84	82	85	86	87	92	90	91
87	92	90	101	87	92	90	103
87	93	95	96	87	93	97	98
87	93	97	99	87	93	97	101
88	87	92	90	88	87	93	94
88	87	93	95	88	87	93	97
89	87	92	90	89	87	93	94
89	87	93	95	89	87	93	97
90	92	87	93	90	101	97	93
90	101	97	98	90	101	97	99
90	103	106	107	91	90	101	97
91	90	101	102	91	90	103	104
91	90	103	105	91	90	103	106
92	87	93	94	92	87	93	95
92	87	93	97	92	90	101	97
92	90	101	102	92	90	103	104
92	90	103	105	92	90	103	106
93	97	99	100	93	97	101	102
94	93	95	96	94	93	97	98
94	93	97	99	94	93	97	101
95	93	97	98	95	93	97	99
95	93	97	101	96	95	93	97
97	101	90	103	98	97	99	100
98	97	101	102	99	97	101	102
100	99	97	101	101	90	103	104
101	90	103	105	101	90	103	106
102	101	90	103	104	103	106	107
105	103	106	107	108	113	111	112
108	113	111	122	108	113	111	124
108	114	116	117	108	114	118	119
108	114	118	120	108	114	118	122
109	108	113	111	109	108	114	115
109	108	114	116	109	108	114	118
110	108	113	111	110	108	114	115
110	108	114	116	110	108	114	118
111	113	108	114	111	122	118	114
111	122	118	119	111	122	118	120
111	124	127	128	112	111	122	118
112	111	122	123	112	111	124	125
112	111	124	126	112	111	124	127
113	108	114	115	113	108	114	116
113	108	114	118	113	111	122	118
113	111	122	123	113	111	124	125
113	111	124	126	113	111	124	127
114	118	120	121	114	118	122	123
115	114	116	117	115	114	118	119
115	114	118	120	115	114	118	122
116	114	118	119	116	114	118	120

116	114	118	122	117	116	114	118
118	122	111	124	119	118	120	121
119	118	122	123	120	118	122	123
121	120	118	122	122	111	124	125
122	111	124	126	122	111	124	127
123	122	111	124	125	124	127	128
126	124	127	128	129	134	132	133
129	134	132	143	129	134	132	145
129	135	137	138	129	135	139	140
129	135	139	141	129	135	139	143
130	129	134	132	130	129	135	136
130	129	135	137	130	129	135	139
131	129	134	132	131	129	135	136
131	129	135	137	131	129	135	139
132	134	129	135	132	143	139	135
132	143	139	140	132	143	139	141
132	145	148	149	133	132	143	139
133	132	143	144	133	132	145	146
133	132	145	147	133	132	145	148
134	129	135	136	134	129	135	137
134	129	135	139	134	132	143	139
134	132	143	144	134	132	145	146
134	132	145	147	134	132	145	148
135	139	141	142	135	139	143	144
136	135	137	138	136	135	139	140
136	135	139	141	136	135	139	143
137	135	139	140	137	135	139	141
137	135	139	143	138	137	135	139
139	143	132	145	140	139	141	142
140	139	143	144	141	139	143	144
142	141	139	143	143	132	145	146
143	132	145	147	143	132	145	148
144	143	132	145	146	145	148	149
147	145	148	149	150	156	154	155
150	156	154	165	150	156	154	167
150	157	159	160	150	157	161	162
150	157	161	163	150	157	161	165
151	150	152	153	151	150	156	154
151	150	157	158	151	150	157	159
151	150	157	161	152	150	156	154
152	150	157	158	152	150	157	159
152	150	157	161	153	152	150	156
153	152	150	157	154	156	150	157
154	165	161	157	154	165	161	162
154	165	161	163	154	167	170	171
155	154	165	161	155	154	165	166
155	154	167	168	155	154	167	169
155	154	167	170	156	150	157	158
156	150	157	159	156	150	157	161
156	154	165	161	156	154	165	166
156	154	167	168	156	154	167	169
156	154	167	170	157	161	163	164
157	161	165	166	158	157	159	160
158	157	161	162	158	157	161	163
158	157	161	165	159	157	161	162
159	157	161	163	159	157	161	165
160	159	157	161	161	165	154	167

162	161	163	164	162	161	165	166
163	161	165	166	164	163	161	165
165	154	167	168	165	154	167	169
165	154	167	170	166	165	154	167
168	167	170	171	169	167	170	171
6	1	3	38	1	3	38	27
38	3	1	7	1	3	38	34
2	1	3	38	1	3	38	39
3	38	27	40	3	38	27	28
3	38	27	29	3	38	34	30
3	38	34	35	3	38	34	36
29	24	26	59	24	26	59	48
59	26	24	30	24	26	59	55
25	24	26	59	24	26	59	60
26	59	48	61	26	59	48	49
26	59	48	50	26	59	55	51
26	59	55	56	26	59	55	57
50	45	47	80	45	47	80	69
80	47	45	51	45	47	80	76
46	45	47	80	45	47	80	81
47	80	69	82	47	80	69	70
47	80	69	71	47	80	76	72
47	80	76	77	47	80	76	78
71	66	68	101	66	68	101	90
101	68	66	72	66	68	101	97
67	66	68	101	66	68	101	102
68	101	90	103	68	101	90	91
68	101	90	92	68	101	97	93
68	101	97	98	68	101	97	99
92	87	89	122	87	89	122	111
122	89	87	93	87	89	122	118
88	87	89	122	87	89	122	123
89	122	111	124	89	122	111	112
89	122	111	113	89	122	118	114
89	122	118	119	89	122	118	120
113	108	110	143	108	110	143	132
143	110	108	114	108	110	143	139
109	108	110	143	108	110	143	144
110	143	132	145	110	143	132	133
110	143	132	134	110	143	139	135
110	143	139	140	110	143	139	141
134	129	131	165	129	131	165	154
165	131	129	135	129	131	165	161
130	129	131	165	129	131	165	166
131	165	154	167	131	165	154	155
131	165	154	156	131	165	161	157
131	165	161	162	131	165	161	163

0 !NIMPHI: impropers

26	!NDON: donors						
9	10	13	14	17	18	22	23
32	33	36	37	43	44	53	54
57	58	64	65	74	75	78	79
85	86	95	96	99	100	106	107
116	117	120	121	127	128	137	138

13. Appendix G

NAMD SMD Fixed Atoms (REF) File

NAMD uses a column of the REF file to determine which atoms will be fixed and which atoms will be pulled. In addition, another three columns are used to specify the direction of the constant force that will be applied to the SMD atom.

The following file is the REF file used for simulations performed on an 8 unit amylase molecule. The highlighted rows contain the fixed atom and coordinate information.

```
CRYST1      0.000      0.000      0.000  90.00  90.00  90.00 P 1      1
ATOM      1  C1  AGLCM  1      -0.901  0.420 -0.683  0.00  0.00      MAIN
ATOM      2  H1  AGLCM  1      -1.474 -0.430 -1.083  0.00  0.00      MAIN
ATOM      3  O1  AGLCM  1      -1.281  0.650  0.677  0.00  0.00      MAIN
ATOM      4  C5  AGLCM  1      -0.663  2.788 -1.059  0.00  0.00      MAIN
ATOM      5  H5  AGLCM  1      -0.876  2.962  0.009  0.00  0.00      MAIN
ATOM      6  O5  AGLCM  1      -1.298  1.560 -1.445  0.00  0.00      MAIN
ATOM      7  C2  AGLCM  1      0.614  0.213 -0.805  0.00  0.00      MAIN
ATOM      8  H2  AGLCM  1      0.828 -0.041 -1.855  0.00  0.00      MAIN
ATOM      9  O2  AGLCM  1      1.072 -0.849  0.036  0.00  0.00      MAIN
ATOM     10  HO2  AGLCM  1      2.037 -0.887 -0.063  0.00  0.00      MAIN
ATOM     11  C3  AGLCM  1      1.371  1.486 -0.464  0.00  0.00      MAIN
ATOM     12  H3  AGLCM  1      1.227  1.702  0.608  0.00  0.00      MAIN
ATOM     13  O3  AGLCM  1      2.759  1.307 -0.735  0.00  0.00      MAIN
ATOM     14  HO3  AGLCM  1      3.197  2.148 -0.537  0.00  0.00      MAIN
ATOM     15  C4  AGLCM  1      0.834  2.661 -1.268  0.00  0.00      MAIN
ATOM     16  H4  AGLCM  1      1.036  2.478 -2.336  0.00  0.00      MAIN
ATOM     17  O4  AGLCM  1      1.488  3.856 -0.846  0.00  1.00      MAIN
ATOM     18  HO4  AGLCM  1      1.275  4.590 -1.433  0.00  0.00      MAIN
ATOM     19  C6  AGLCM  1      -1.261  3.942 -1.852  0.00  0.00      MAIN
ATOM     20  H61  AGLCM  1      -0.740  4.884 -1.622  0.00  0.00      MAIN
ATOM     21  H62  AGLCM  1      -1.145  3.775 -2.935  0.00  0.00      MAIN
ATOM     22  O6  AGLCM  1      -2.630  4.087 -1.516  0.00  0.00      MAIN
ATOM     23  HO6  AGLCM  1      -3.120  3.263 -1.688  0.00  0.00      MAIN
ATOM     24  C1  AGLCM  2      -3.673 -0.908  3.637  0.00  0.00      MAIN
ATOM     25  H1  AGLCM  2      -4.370 -1.547  4.201  0.00  0.00      MAIN
ATOM     26  O1  AGLCM  2      -3.742  0.433  4.142  0.00  0.00      MAIN
ATOM     27  C5  AGLCM  2      -3.468 -0.097  1.382  0.00  0.00      MAIN
ATOM     28  H5  AGLCM  2      -3.621  0.935  1.737  0.00  0.00      MAIN
ATOM     29  O5  AGLCM  2      -4.153 -0.956  2.304  0.00  0.00      MAIN
ATOM     30  C2  AGLCM  2      -2.240 -1.414  3.648  0.00  0.00      MAIN
ATOM     31  H2  AGLCM  2      -2.244 -2.445  3.257  0.00  0.00      MAIN
ATOM     32  O2  AGLCM  2      -1.689 -1.413  4.967  0.00  0.00      MAIN
ATOM     33  HO2  AGLCM  2      -0.759 -1.678  4.874  0.00  0.00      MAIN
ATOM     34  C3  AGLCM  2      -1.369 -0.561  2.742  0.00  0.00      MAIN
ATOM     35  H3  AGLCM  2      -1.277  0.441  3.194  0.00  0.00      MAIN
ATOM     36  O3  AGLCM  2      -0.083 -1.167  2.639  0.00  0.00      MAIN
```

ATOM	37	HO3	AGLCM	2	0.352	-0.861	1.818	0.00	0.00	MAIN
ATOM	38	C4	AGLCM	2	-1.970	-0.418	1.346	0.00	0.00	MAIN
ATOM	39	H4	AGLCM	2	-1.793	-1.358	0.801	0.00	0.00	MAIN
ATOM	40	C6	AGLCM	2	-4.097	-0.201	-0.009	0.00	0.00	MAIN
ATOM	41	H61	AGLCM	2	-3.671	0.572	-0.663	0.00	0.00	MAIN
ATOM	42	H62	AGLCM	2	-3.839	-1.171	-0.462	0.00	0.00	MAIN
ATOM	43	O6	AGLCM	2	-5.510	-0.062	0.032	0.00	0.00	MAIN
ATOM	44	HO6	AGLCM	2	-5.840	0.031	-0.884	0.00	0.00	MAIN
ATOM	45	C1	AGLCM	3	-5.613	2.478	7.254	0.00	0.00	MAIN
ATOM	46	H1	AGLCM	3	-6.260	2.620	8.132	0.00	0.00	MAIN
ATOM	47	O1	AGLCM	3	-5.461	3.733	6.574	0.00	0.00	MAIN
ATOM	48	C5	AGLCM	3	-5.750	1.255	5.187	0.00	0.00	MAIN
ATOM	49	H5	AGLCM	3	-5.619	2.208	4.650	0.00	0.00	MAIN
ATOM	50	O5	AGLCM	3	-6.353	1.568	6.449	0.00	0.00	MAIN
ATOM	51	C2	AGLCM	3	-4.253	1.864	7.577	0.00	0.00	MAIN
ATOM	52	H2	AGLCM	3	-4.436	0.950	8.164	0.00	0.00	MAIN
ATOM	53	O2	AGLCM	3	-3.435	2.753	8.342	0.00	0.00	MAIN
ATOM	54	HO2	AGLCM	3	-2.567	2.322	8.417	0.00	0.00	MAIN
ATOM	55	C3	AGLCM	3	-3.514	1.467	6.307	0.00	0.00	MAIN
ATOM	56	H3	AGLCM	3	-3.233	2.382	5.759	0.00	0.00	MAIN
ATOM	57	O3	AGLCM	3	-2.344	0.740	6.678	0.00	0.00	MAIN
ATOM	58	HO3	AGLCM	3	-2.071	0.159	5.938	0.00	0.00	MAIN
ATOM	59	C4	AGLCM	3	-4.392	0.602	5.411	0.00	0.00	MAIN
ATOM	60	H4	AGLCM	3	-4.475	-0.378	5.906	0.00	0.00	MAIN
ATOM	61	C6	AGLCM	3	-6.681	0.385	4.338	0.00	0.00	MAIN
ATOM	62	H61	AGLCM	3	-6.289	0.314	3.309	0.00	0.00	MAIN
ATOM	63	H62	AGLCM	3	-6.694	-0.640	4.739	0.00	0.00	MAIN
ATOM	64	O6	AGLCM	3	-8.004	0.908	4.323	0.00	0.00	MAIN
ATOM	65	HO6	AGLCM	3	-8.502	0.526	3.592	0.00	0.00	MAIN
ATOM	66	C1	AGLCM	4	-6.648	7.692	7.203	0.00	0.00	MAIN
ATOM	67	H1	AGLCM	4	-7.171	8.515	7.714	0.00	0.00	MAIN
ATOM	68	O1	AGLCM	4	-6.460	8.040	5.823	0.00	0.00	MAIN
ATOM	69	C5	AGLCM	4	-7.191	5.407	6.679	0.00	0.00	MAIN
ATOM	70	H5	AGLCM	4	-7.024	5.643	5.616	0.00	0.00	MAIN
ATOM	71	O5	AGLCM	4	-7.581	6.626	7.320	0.00	0.00	MAIN
ATOM	72	C2	AGLCM	4	-5.325	7.274	7.844	0.00	0.00	MAIN
ATOM	73	H2	AGLCM	4	-5.518	7.110	8.916	0.00	0.00	MAIN
ATOM	74	O2	AGLCM	4	-4.319	8.279	7.700	0.00	0.00	MAIN
ATOM	75	HO2	AGLCM	4	-3.498	7.887	8.041	0.00	0.00	MAIN
ATOM	76	C3	AGLCM	4	-4.817	5.963	7.254	0.00	0.00	MAIN
ATOM	77	H3	AGLCM	4	-4.523	6.133	6.204	0.00	0.00	MAIN
ATOM	78	O3	AGLCM	4	-3.689	5.538	8.017	0.00	0.00	MAIN
ATOM	79	HO3	AGLCM	4	-3.562	4.573	7.907	0.00	0.00	MAIN
ATOM	80	C4	AGLCM	4	-5.900	4.893	7.300	0.00	0.00	MAIN
ATOM	81	H4	AGLCM	4	-6.020	4.629	8.363	0.00	0.00	MAIN
ATOM	82	C6	AGLCM	4	-8.319	4.373	6.740	0.00	0.00	MAIN
ATOM	83	H61	AGLCM	4	-8.084	3.525	6.076	0.00	0.00	MAIN
ATOM	84	H62	AGLCM	4	-8.387	3.962	7.759	0.00	0.00	MAIN
ATOM	85	O6	AGLCM	4	-9.569	4.948	6.374	0.00	0.00	MAIN
ATOM	86	HO6	AGLCM	4	-10.206	4.252	6.180	0.00	0.00	MAIN
ATOM	87	C1	AGLCM	5	-7.216	11.340	3.373	0.00	0.00	MAIN
ATOM	88	H1	AGLCM	5	-7.649	12.316	3.108	0.00	0.00	MAIN
ATOM	89	O1	AGLCM	5	-7.048	10.558	2.183	0.00	0.00	MAIN
ATOM	90	C5	AGLCM	5	-8.010	9.451	4.640	0.00	0.00	MAIN
ATOM	91	H5	AGLCM	5	-7.881	8.825	3.743	0.00	0.00	MAIN
ATOM	92	O5	AGLCM	5	-8.245	10.787	4.184	0.00	0.00	MAIN
ATOM	93	C2	AGLCM	5	-5.917	11.381	4.176	0.00	0.00	MAIN

ATOM	94	H2	AGLCM	5	-6.080	12.053	5.034	0.00	0.00	MAIN
ATOM	95	O2	AGLCM	5	-4.824	11.876	3.399	0.00	0.00	MAIN
ATOM	96	HO2	AGLCM	5	-4.031	11.759	3.949	0.00	0.00	MAIN
ATOM	97	C3	AGLCM	5	-5.566	9.999	4.717	0.00	0.00	MAIN
ATOM	98	H3	AGLCM	5	-5.314	9.336	3.872	0.00	0.00	MAIN
ATOM	99	O3	AGLCM	5	-4.446	10.132	5.590	0.00	0.00	MAIN
ATOM	100	HO3	AGLCM	5	-4.380	9.341	6.166	0.00	0.00	MAIN
ATOM	101	C4	AGLCM	5	-6.743	9.407	5.482	0.00	0.00	MAIN
ATOM	102	H4	AGLCM	5	-6.815	10.005	6.404	0.00	0.00	MAIN
ATOM	103	C6	AGLCM	5	-9.229	8.912	5.395	0.00	0.00	MAIN
ATOM	104	H61	AGLCM	5	-9.109	7.831	5.575	0.00	0.00	MAIN
ATOM	105	H62	AGLCM	5	-9.287	9.388	6.386	0.00	0.00	MAIN
ATOM	106	O6	AGLCM	5	-10.432	9.154	4.675	0.00	0.00	MAIN
ATOM	107	HO6	AGLCM	5	-11.158	8.666	5.077	0.00	0.00	MAIN
ATOM	108	C1	AGLCM	6	-7.551	10.933	-1.925	0.00	0.00	MAIN
ATOM	109	H1	AGLCM	6	-7.927	11.331	-2.880	0.00	0.00	MAIN
ATOM	110	O1	AGLCM	6	-7.327	9.524	-2.051	0.00	0.00	MAIN
ATOM	111	C5	AGLCM	6	-8.506	10.676	0.277	0.00	0.00	MAIN
ATOM	112	H5	AGLCM	6	-8.403	9.582	0.185	0.00	0.00	MAIN
ATOM	113	O5	AGLCM	6	-8.648	11.185	-1.056	0.00	0.00	MAIN
ATOM	114	C2	AGLCM	6	-6.312	11.608	-1.349	0.00	0.00	MAIN
ATOM	115	H2	AGLCM	6	-6.518	12.689	-1.282	0.00	0.00	MAIN
ATOM	116	O2	AGLCM	6	-5.161	11.403	-2.172	0.00	0.00	MAIN
ATOM	117	HO2	AGLCM	6	-4.409	11.757	-1.668	0.00	0.00	MAIN
ATOM	118	C3	AGLCM	6	-6.031	11.084	0.053	0.00	0.00	MAIN
ATOM	119	H3	AGLCM	6	-5.769	10.014	-0.008	0.00	0.00	MAIN
ATOM	120	O3	AGLCM	6	-4.941	11.822	0.602	0.00	0.00	MAIN
ATOM	121	HO3	AGLCM	6	-4.883	11.659	1.568	0.00	0.00	MAIN
ATOM	122	C4	AGLCM	6	-7.259	11.249	0.941	0.00	0.00	MAIN
ATOM	123	H4	AGLCM	6	-7.308	12.334	1.127	0.00	0.00	MAIN
ATOM	124	C6	AGLCM	6	-9.769	10.943	1.100	0.00	0.00	MAIN
ATOM	125	H61	AGLCM	6	-9.723	10.381	2.048	0.00	0.00	MAIN
ATOM	126	H62	AGLCM	6	-9.808	12.009	1.375	0.00	0.00	MAIN
ATOM	127	O6	AGLCM	6	-10.944	10.590	0.379	0.00	0.00	MAIN
ATOM	128	HO6	AGLCM	6	-11.709	10.625	0.963	0.00	0.00	MAIN
ATOM	129	C1	AGLCM	7	-7.396	6.452	-4.807	0.00	0.00	MAIN
ATOM	130	H1	AGLCM	7	-7.634	5.851	-5.698	0.00	0.00	MAIN
ATOM	131	O1	AGLCM	7	-7.143	5.582	-3.696	0.00	0.00	MAIN
ATOM	132	C5	AGLCM	7	-8.599	8.000	-3.398	0.00	0.00	MAIN
ATOM	133	H5	AGLCM	7	-8.512	7.300	-2.552	0.00	0.00	MAIN
ATOM	134	O5	AGLCM	7	-8.587	7.197	-4.590	0.00	0.00	MAIN
ATOM	135	C2	AGLCM	7	-6.246	7.434	-4.967	0.00	0.00	MAIN
ATOM	136	H2	AGLCM	7	-6.485	8.104	-5.809	0.00	0.00	MAIN
ATOM	137	O2	AGLCM	7	-5.010	6.771	-5.237	0.00	0.00	MAIN
ATOM	138	HO2	AGLCM	7	-4.326	7.460	-5.193	0.00	0.00	MAIN
ATOM	139	C3	AGLCM	7	-6.103	8.273	-3.708	0.00	0.00	MAIN
ATOM	140	H3	AGLCM	7	-5.814	7.617	-2.869	0.00	0.00	MAIN
ATOM	141	O3	AGLCM	7	-5.086	9.250	-3.929	0.00	0.00	MAIN
ATOM	142	HO3	AGLCM	7	-5.094	9.907	-3.199	0.00	0.00	MAIN
ATOM	143	C4	AGLCM	7	-7.418	8.971	-3.372	0.00	0.00	MAIN
ATOM	144	H4	AGLCM	7	-7.470	9.784	-4.112	0.00	0.00	MAIN
ATOM	145	C6	AGLCM	7	-9.935	8.728	-3.243	0.00	0.00	MAIN
ATOM	146	H61	AGLCM	7	-9.988	9.205	-2.250	0.00	0.00	MAIN
ATOM	147	H62	AGLCM	7	-9.997	9.542	-3.982	0.00	0.00	MAIN
ATOM	148	O6	AGLCM	7	-11.029	7.835	-3.417	0.00	0.00	MAIN
ATOM	149	HO6	AGLCM	7	-11.844	8.253	-3.120	0.00	0.00	MAIN
ATOM	150	C1	AGLCM	8	-6.736	1.658	-2.610	0.00	0.00	MAIN

ATOM	151	H1	AGLCM	8	-6.821	2.066	-1.582	0.00	0.00	MAIN
ATOM	152	O1	AGLCM	8	-0.899	-0.393	-0.192	0.40	0.00	MAIN
ATOM	153	HO1	AGLCM	8	-7.622	-0.004	-2.438	0.00	0.00	MAIN
ATOM	154	C5	AGLCM	8	-8.143	3.425	-3.337	0.00	0.00	MAIN
ATOM	155	H5	AGLCM	8	-8.234	3.715	-2.279	0.00	0.00	MAIN
ATOM	156	O5	AGLCM	8	-7.893	2.015	-3.340	0.00	0.00	MAIN
ATOM	157	C2	AGLCM	8	-5.521	2.227	-3.332	0.00	0.00	MAIN
ATOM	158	H2	AGLCM	8	-5.516	1.805	-4.351	0.00	0.00	MAIN
ATOM	159	O2	AGLCM	8	-4.296	1.887	-2.680	0.00	0.00	MAIN
ATOM	160	HO2	AGLCM	8	-3.591	2.099	-3.306	0.00	0.00	MAIN
ATOM	161	C3	AGLCM	8	-5.624	3.739	-3.431	0.00	0.00	MAIN
ATOM	162	H3	AGLCM	8	-5.483	4.159	-2.420	0.00	0.00	MAIN
ATOM	163	O3	AGLCM	8	-4.591	4.202	-4.299	0.00	0.00	MAIN
ATOM	164	HO3	AGLCM	8	-4.708	5.161	-4.468	0.00	0.00	MAIN
ATOM	165	C4	AGLCM	8	-6.980	4.183	-3.978	0.00	0.00	MAIN
ATOM	166	H4	AGLCM	8	-6.886	4.033	-5.065	0.00	0.00	MAIN
ATOM	167	C6	AGLCM	8	-9.472	3.745	-4.028	0.00	0.00	MAIN
ATOM	168	H61	AGLCM	8	-9.712	4.813	-3.894	0.00	0.00	MAIN
ATOM	169	H62	AGLCM	8	-9.365	3.583	-5.112	0.00	0.00	MAIN
ATOM	170	O6	AGLCM	8	-10.533	2.939	-3.524	0.00	0.00	MAIN
ATOM	171	HO6	AGLCM	8	-11.376	3.211	-3.900	0.00	0.00	MAIN
END										